University of Alberta

CFD Modeling of Flow Patterns and Hydraulics of Commercial-Scale Sieve Trays

by

Getye Gesit

©

A thesis submitted to the Faculty of Graduate Studies and Research in partial fulfilment of the requirements for the degree of Master of Science

in

Chemical Engineering

Department of Chemical and Materials Engineering

Edmonton, Alberta

Fall 2004

Library and Archives Canada

Published Heritage Branch

395 Wellington Street
Ottawa ON K1A 0N4
Canada

Bibliothèque et Archives Canada

Direction du Patrimoine de l'édition

395, rue Wellington
Ottawa ON K1A 0N4
Canada

Your file Votre référence
ISBN: 0-612-95751-9
Our file Notre référence
ISBN: 0-612-95751-9

The author has granted a non-exclusive license allowing the Library and Archives Canada to reproduce, loan, distribute or sell copies of this thesis in microform, paper or electronic formats.

The author retains ownership of the copyright in this thesis. Neither the thesis nor substantial extracts from it may be printed or otherwise reproduced without the author's permission.

L'auteur a accordé une licence non exclusive permettant à la Bibliothèque et Archives Canada de reproduire, prêter, distribuer ou vendre des copies de cette thèse sous la forme de microfiche/film, de reproduction sur papier ou sur format électronique.

L'auteur conserve la propriété du droit d'auteur qui protège cette thèse. Ni la thèse ni des extraits substantiels de celle-ci ne doivent être imprimés ou aturement reproduits sans son autorisation.

In compliance with the Canadian Privacy Act some supporting forms may have been removed from this thesis.

While these forms may be included in the document page count, their removal does not represent any loss of content from the thesis.

Conformément à la loi canadienne sur la protection de la vie privée, quelques formulaires secondaires ont été enlevés de cette thèse.

Bien que ces formulaires aient inclus dans la pagination, il n'y aura aucun contenu manquant.

Canada

Acknowledgment

The author gratefully thanks all those who helped. Dr. K. Nandakumar and Dr. K. T. Chuang are gratefully acknowledged for giving me guidance and support. Without the help of Mebrate W. Deres, this thesis would have been impossible. A number of friends have been influential in several ways. Thank you all.

Table of Contents

Chapter 1 Introduction 1

Chapter 2 Literature Review – Sieve Trays 3

2.1 Introduction 3

2.2 Performance Parameters 3

2.3 Flow Regimes 4

2.4 Tray Capacity Limits (Operating Region) 5

2.5 Tray Hydraulics 6

2.5.1 Clear Liquid Height 6

2.5.2 Froth Height 7

2.5.3 Average Liquid Holdup Fraction in Froth 7

2.5.4 Tray Pressure Drop 7

2.6 Mass Transfer and Tray Efficiency 8

2.7 Flow Patterns and Flow Maldistributions 10

2.8 Conclusion 12

Chapter 3 Literature Review – Fluid Mechanics 14

3.1 Introduction 14

3.2 Conservation Equations 14

3.3 Turbulence Modeling 16

3.4 Multiphase Modeling 18

3.5 Turbulent Multiphase Flow 20

3.6 Computational Fluid Dynamics (CFD) 21

3.6.1 Grid Generation 22

3.6.2 Interpolation and Differencing Schemes 23

3.6.3 Solution of Algebraic System of Equations 23

3.7 Attempts Made to Model Sieve Tray Hydrodynamics using CFD 24

3.8 Conclusion 25

Chapter 4 Two-Phase Flow Model 26

4.1 Introduction 26

4.2 Experimental Basis of the Model 26

4.3 Model Assumptions 26

4.4 Model Equations 27

4.5 Flow Geometry 30

4.6 Boundary and Initial Conditions 33
4.6.1 Boundary Conditions 33
4.6.2 Flow Field Initialization 35
4.7 Conclusion 36
Chapter 5 Simulation Results and Discussion 38
5.1 Introduction 38
5.2 Solution Algorithms 38
5.3 Grid Size Sensitivities 39
5.4 Velocity Distributions 40
5.5 Clear Liquid Height, Froth Height, and Average Liquid Holdup Fraction in Froth 44
5.6 Conclusion 47
Chapter 6 Further Work 70
6.1 Mass Transfer Modeling and Prediction of Sieve Tray Efficiency 70
6.2 Prediction of Residence Time Distributions 70
6.3 Using CFD in Tray Design Studies 71
Bibliography 72
Appendix A CFX-4.4 Code 78
CFX-4.4 Sample Command File 78
CFX-4.4 Sample Fortran User Subroutines 82
Appendix B CFX-5.4 Code 103
CFX-5.4 Sample Command File 103

List of Figures

Figure 4.1 Flow geometry and boundaries 32

Figure 5.1 Transient simulation convergence as indicated by a plot of clear liquid height versus time. A transient simulation is assumed to have converged whenever the clear liquid height does not appreciably change with time. 49

Figure 5.2 Sensitivity of the clear liquid height prediction to grid spacing, and hole number and size, $Q_L = 6.94 \times 10^{-3} m^3/s$, $F_s = 0.462$ (CFX4.4) 50

Figure 5.3 Sensitivity of the liquid velocity profile prediction to grid spacing, and hole number and size (CFX4.4), $Q_L = 17.8 \times 10^{-3} m^3/s$, $F_s = 0.462$.(a) Upstream profile, (b) downstream profile. 51

Figure 5.4 Experimental probe positions of Solari and Bell (1986). All measurements are in meters. The plane of the probes is at an elevation of 0.038m above the tray floor. 52

Figure 5.5 Liquid velocity profile, $Q_L = 17.8 \times 10^{-3} m^3/s$, $F_s = 0.462$ (CFX5.4) (a) Upstream profile, (b) downstream profile. 53

Figure 5.6 Liquid velocity profile, $Q_L = 17.8 \times 10^{-3} m^3/s$, $F_s = 0.801$. (CFX5.4). (a) Upstream profile, (b) downstream profile. 54

Figure 5.7 Liquid velocity profile, $Q_L = 6.94 \times 10^{-3} m^3/s$, $F_s = 1.015$. (CFX5.4) (a) Upstream profile, (b) downstream profile 55

Figure 5.8 Liquid velocity profile, $Q_L = 6.94 \times 10^{-3} m^3/s$, $F_s = 1.464$, with a flat inlet profile (CFX5.4) (a) Upstream profile, (b) downstream profile 56

Figure 5.9 Liquid velocity vector plots on the plane of the experimental probes. A modified liquid velocity vector, which is a product of the liquid velocity vector and the liquid volume fraction, was used in obtaining the magnitudes of the velocity vectors shown. 57

Figure 5.10 Selected streamline profiles of liquid (in black) and gas (in white). 58

Figure 5.11 (a) to (c) Gas V velocity profiles at different elevations above tray floor. (d) Gas V velocity profiles in the longitudinal direction to the liquid flow.. 59

Figure 5.12 Average liquid U velocity profiles at different elevations above tray floor. Average taken between x = 0.209 m and x = 0.438 m, $Q_L = 17.8 \times 10^{-3} m^3/s$, $F_s = 0.801$ (from CFX4.4- 32,784 cells and 45 holes). 60

Figure 5.13 Average gas and liquid U velocity profiles at different elevations above tray floor. Averages taken between x = 0.209 m and x = 0.438 m, $Q_L = 17.8x10^{-3}m^3/s$, $F_s = 0.801$ (from CFX4.4-32,784 cells and 45 holes). .. 61

Figure 5.14 Sensitivity of the liquid velocity profile prediction to turbulence intensity at liquid inlet (CFX4.4), $Q_L = 17.8x10^{-3}m^3/s$, $F_s = 0.462$.(a) Upstream profile, (b) downstream profile. 62

Figure 5.15 Clear liquid height as a function of F-factor F_s, $Q_L=17.8x10^{-3}m^3/s$..... 63

Figure 5.16 Clear liquid height as a function of liquid rate Q_L, Fs = 0.462 64

Figure 5.17 Average liquid holdup fraction in froth α as a function of F-factor F_s, $Q_L = 17.8x10^{-3}\ m^3/s$ 65

Figure 5.18 Average froth height h_F as a function of F-factor F_s, $Q_L = 0.0178\ m^3/s$ 66

Figure 5.19 Liquid volume fraction profiles on a vertical section 0.01m from the tray centre (a) $Q_L = 17.8x10^{-3}m^3/s$, $F_s = 0.462$ (40,000 nodes with 45 holes) (b) $Q_L = 6.94x10^{-3}m^3/s$, $F_s = 0.462$ (40,000 nodes with 45 holes) (c) $Q_L = 17.8x10^{-3}m^3/s$, $F_s = 0.462$ (90,000 nodes with actual number of holes) (d) $Q_L = 6.94x10^{-3}m^3/s$, $F_s = 1.464$ (40,000 nodes with 45 holes) 67

Figure 5.20 Dispersion height versus liquid dispersion density profile, $Q_L = 6.94x10^{-3}\ m^3/s$ 68

Figure 5.21 Clear liquid height profiles in longitudinal and transverse directions to liquid flow, $Q_L = 6.94x10^{-3}m^3/s$. (a) averaged in the y and z directions. (b) averaged in the x and y directions 69

Nomenclature

A_B	tray bubbling area [m^2]
A_H	total area of holes [m^2]
C_D	drag coefficient
d_G	bubble diameter [m]
$\boldsymbol{f}$	body force vector per unit mass [m s^{-2}]
F_{LV}	flow parameter $= \frac{L}{G}\sqrt{\frac{\rho_G}{\rho_L}}$,
	L, G = liquid, gas mass flow rate, respectively [kg/s]
F_S	F-factor $= V_S\sqrt{\rho_G}$
$\mathbf{g}$	gravitational acceleration vector [m s^{-2}]
h_F	froth height [m]
h_L	clear liquid height [m]
h_w	weir height [m]
k	specific turbulent kinetic energy [m^2 s^{-2}]
k_α	specific turbulent kinetic energy of phase α [m^2 s^{-2}]
L_w	weir length [m]
$\mathbf{M}_{GL}$	interphase momentum transfer vector [kg m^{-2} s^{-2}]
p	pressure [N m^{-2}]
p_G	gas phase pressure [N m^{-2}]
P_k	turbulence production rate [kg m^{-1} s^{-3}]
$P_{k,\alpha}$	turbulence production rate of phase α [kg m^{-1} s^{-3}]

p_L	liquid phase pressure [N m^{-2}]
Q_L	liquid volumetric flow rate [m^3/s]
R	tray radius [m]
r_G	gas phase volume fraction
$r_G^{average}$	average gas holdup fraction in froth
r_L	liquid phase volume fraction
r_α	volume fraction of phase α
T	temperature [K]
U	x-component of velocity [m/s]
V	y-component of velocity [m/s]
$\mathbf{V}$	velocity vector [m/s]
$\mathbf{V}'$	fluctuating part of velocity vector [m/s]
$\mathbf{V}_G$	gas phase velocity vector [m/s]
$\mathbf{V}_L$	liquid phase velocity vector [m/s]
V_S	gas phase superficial velocity based on bubbling area [m/s]
V_{slip}	slip velocity [m/s]
$\mathbf{V}_\alpha$	velocity vector of phase α [m/s]
W	z-component of velocity [m/s]
x	coordinate position in the direction of liquid flow across tray [m]
y	coordinate position in the direction of vapour flow [m]
z	coordinate position in the transverse direction to liquid flow across tray [m]

Greek Letters

α	average liquid holdup fraction in froth
δ	identity tensor
ε	turbulent kinetic energy dissipation rate [$m^2\ s^{-3}$]
ε_α	turbulent kinetic energy dissipation rate of phase α [$m^2\ s^{-3}$]
κ	bulk viscosity [$kg\ m^{-1}\ s^{-1}$]
μ	molecular viscosity [$kg\ m^{-1}\ s^{-1}$]
$\mu_{eff,G}$	effective viscosity of gas [$kg\ m^{-1}\ s^{-1}$]
$\mu_{eff,L}$	effective viscosity of liquid [$kg\ m^{-1}\ s^{-1}$]
μ_{eff}	effective viscosity [$kg\ m^{-1}\ s^{-1}$]
μ_t	turbulent viscosity [$kg\ m^{-1}\ s^{-1}$]
$\mu_{t\alpha}$	turbulent viscosity of phase α [$kg\ m^{-1}\ s^{-1}$]
μ_α	molecular viscosity of phase α [$kg\ m^{-1}\ s^{-1}$]
$\mu_{\alpha,eff}$	effective viscosity of phase α [$kg\ m^{-1}\ s^{-1}$]
ρ	density [kg/m^3]
ρ_G	gas phase density [kg/m^3]
ρ_L	liquid phase density [kg/m^3]
ρ_α	density of phase α [kg/m^3]
τ	stress tensor [$N\ m^{-2}$]

Chapter 1 Introduction*

Sieve trays are widely used as phase contacting devices in distillation, absorption, and stripping columns. An impasse that has hindered the further improvement of these devices is the fact that little is known about the flow phenomena prevailing inside a tray for given geometry and operating conditions. The main reason for this is the poor understanding of the complex behaviours of the multiphase flow inside the tray. As a result, current design and analysis of trays are based on experience and empirical correlations. These practices do not often take into account the actual fluid flow patterns. For example, the well-known AIChE (1958) tray design procedure assumes a uniform rectilinear velocity field with a superimposed backmixing. However, experimental studies (Bell, 1972a,b; Weiler et al., 1973; Sohlo and Kinnunen, 1977; Solari et al., 1982; Solari and Bell, 1986) have shown that actual flow patterns found on industrial trays include flow maldistributions such as channelling, recirculation, stagnant zones, and non-uniform velocity distributions. Except for the few case reports, little is known about what flow configuration to expect for given tray geometry and operating conditions. Mathematical models such as those of Porter et al. (1972), and Bell and Solari (1974) show that flow maldistributions can reduce tray efficiency. Only two attempts (Solari et al., 1982; Solari and Bell, 1986) have been made to relate model parameters to tray geometry and fluid rates and it is not known if these model parameters could be extended to other tray geometries and fluid systems. Very little experimental work has been done to assess the effect of flow maldistributions on tray efficiency.

Therefore, there are two major unresolved problems facing the current practice of tray design and analysis. The first one is what flow patterns to expect for given geometry and operating conditions. The second problem is how to relate these flow patterns to tray performance parameters such as tray efficiency and pressure drop. Once a method or methods are devised to accomplish these two tasks, it will be possible to design trays having desired flow patterns that give rise to the best performance. Over the past years, only experimental methods could be thought of to solve the problems mentioned. Although experimental predictions are generally expected to give reliable data, the

* A version of this thesis has been published: Gesit et al., AIChE Journal, Volume 49, Pages 910-924.

chaotic, three-dimensional and multiphase behaviours of the flow inside a tray severely limit the use of these methods and the amount of data they can give.

Recently, the development of powerful computers, advances in numerical methods, and improvements in multiphase flow models permit the investigation of complex flow problems (Mehta et al., 1998). The technique that combines these is computational fluid dynamics (CFD), a technique that is emerging as an important predictive and design tool for flows in process equipment. Compared to experimental methods, it gives complete information, and has relatively low cost and fast speed. A further major advantage of CFD over experimental methods is its flexibility as it typically enables changing flow geometry and system conditions without incurring appreciable cost. An important step should, however, accompany the first time use of CFD; its extent of applicability has to be validated using experimental data mainly to cater for uncertainties involved in mathematically and numerically modeling complex flow phenomena such as turbulence and multiphase interactions.

In this work, a CFD model has been developed to simulate the hydrodynamics of a commercial scale sieve tray. The predictions of the fluid flow patterns and hydraulics of the sieve tray are given with a modeling of the downcomer region provided. Tray geometry and fluids were based on the experimental work of Solari and Bell (1986) that was carried out in a 1.22 m diameter air-water sieve tray simulator. The CFD simulation results are in good agreement with the experimental results of these authors. The objective of the work is finding out the extent to which CFD can be used as a design and prediction tool for industrial trays. Specifically, the goal of the work is establishing CFD as a prediction and analysis tool for the hydrodynamics of sieve trays. From the results of this work, it can be concluded that CFD can be used as an invaluable tool in tray design and analysis.

Chapter 2 Literature Review – Sieve Trays

2.1 Introduction

Sieve trays are widely used as phase contacting devices. They are predominantly applied in distillation that is the dominant separation process of the chemical processing industries. They are also used in the closely related mass transfer operations of absorption and stripping. Low cost, high separation efficiency, simplicity of fabrication and non-proprietary nature are some of the reasons that make sieve trays the first choice and standard column internals. Sieve tray design information may also be extended to the design of other type of trays.

There is a vast amount of literature on sieve trays. The text by Lockett (1986) is the best in clearly showing the origins and limitations of the current analysis and design of trays. Kister (1990, 1992) is a good source. Stichlmair and Fair (1998) give another perspective. This chapter reviews the literature on tray performance and design

2.2 Performance Parameters

To the sieve tray designer, the three parameters of interest are tray capacity, pressure drop, and mass transfer efficiency. In analysis mode, the geometry and internal details of the tray are known and the interest lies in determining for given fluids the allowable minimum and maximum vapour and liquid loads (tray capacity), the resulting pressure drop, and the mass transfer efficiency. In design mode, the geometry and internal details of the tray are determined so as to achieve specified values of the performance parameters. Whereas the performance analysis is straightforward, the design mode generally involves a trial-and-error procedure.

2.3 Flow Regimes

The presence of different phases implies the possibility and need of accounting for the structure of a multiphase system. The concept of flow regime refers to the nature of the multiphase system. The study of flow regimes is important for two reasons (Lockett 1986). One is that tray performance depends on the structure of the multiphase system. For example, Zuiderweg (1982, 1986) gives different correlations for different flow regimes. The second reason is that certain regimes are worth avoiding while some regimes are worth having.

For a given tray geometry and column pressure, depending on liquid and vapour rates, one of the following flow regimes may prevail on the tray: bubble, foam, froth, spray, or emulsion regime (Lockett, 1986; Kister, 1992). In the bubble regime, discrete noncoalescing bubble swarms rise through a fairly calm liquid. This regime occurs in small columns at low vapour rates and when using tall weirs. In the foam regime, bubbles grow in size limiting the liquid presence to a thin film. The bubbles formed at holes rise unbroken. The foam regime occurs at low vapour rates and in small columns. In the froth (mixed) regime, gas passes through the liquid as jets and bubbles of ill-defined and rapidly changing shape and varying velocities. This is the most commonly encountered regime. In the spray (drop) regime, the vapour is the continuous phase. The liquid is projected and torn up by gas jets to form small drops. This regime occurs at high vapour rates and is favoured by large holes, low fractional hole area, and low column pressure. Finally, the emulsion regime occurs at high liquid rates and relatively low vapour rates in high-pressure columns. The high velocity liquid bends and tears off the vapour bubbles and jets. Most of the gas will then be emulsified within the liquid forming almost a homogeneous phase.

Of the five regimes, the froth, spray and emulsion regimes are common in industrial trays.

2.4 Tray Capacity Limits (Operating Region)

Trays may not handle arbitrary rates of vapour and liquid. Rather, trays operate satisfactorily only within a limited region of vapour and liquid rate combination. The maximum limit is set by flooding whereas the minimum limit is set by excessive entrainment and weeping.

Flooding is excessive accumulation of liquid inside the tray column. It can result from either entrainment flooding or downcomer flooding. Entrainment flooding occurs at low to moderate liquid rates as vapour rate is increased. At low liquid rates and relatively high vapour rates, the tray operates in the spray regime where the liquid is present in the form of droplets. As vapour rate is increased, a limit is reached where the liquid droplets are excessively carried to the tray above. This results in the accumulation of liquid on the tray above and in a reduction in tray efficiency since less volatile material rich liquid is moving in an undesired direction. At low liquid rate as vapour rate is increased, the limit of excessive entrainment is reached. At high liquid rates, dowmncomer flooding is the common mechanism of flooding, which may be due to either downcomer backup or downcomer choke flooding. Kister (1992) gives details.

Weeping is the flow of liquid through the tray holes at low vapour rates. A further reduction in vapour rate beyond the weep point leads to excessive weeping. Weeping of liquid implies liquid bypassing or short-circuiting. Hence weeping results in a reduction in tray efficiency. Dumping is the condition at which all of the liquid weeps with no liquid reaching the downcomer region.

2.5 Tray Hydraulics

2.5.1 Clear Liquid Height

Clear liquid height is defined as the height of liquid that would exist in the tray in the absence of both weeping and vapour flow. For trays operating in the froth regime, the correlation of Colwell (1979) is recommended for the prediction of clear liquid height, h_L.

$$h_L = \alpha\left[h_w + \frac{0.7301}{C_d^{2/3}}\left(\frac{Q_L}{\alpha L_w}\right)^{2/3}\right] \tag{2.1}$$

where

$$\alpha = \frac{1}{1+12.6\left(\frac{\rho_G}{\rho_L-\rho_G}\frac{V_S^2}{gh_L}\right)^{0.4}\left(\frac{A_B}{A_H}\right)^{0.25}} \tag{2.2}$$

$$C_d = 0.61+0.08\frac{h_{ow}}{h_w},\ \text{if } \frac{h_{ow}}{h_w} \le 8.14$$
$$C_d = 1.06\left(1+\frac{h_{ow}}{h_w}\right)^{1.5},\ \text{if } \frac{h_{ow}}{h_w} > 8.14 \tag{2.3}$$

$$h_{ow} = \frac{h_L}{\alpha} - h_w \tag{2.4}$$

The correlation of Bennett et al. (1983) has also been reported to give reasonable prediction.

$$h_L = \alpha\left[h_w + C\left(\frac{Q_L}{\alpha L_w}\right)^{2/3}\right] \tag{2.5}$$

where

$$\alpha = \exp\left[-12.55\left(V_S\sqrt{\frac{\rho_G}{\rho_L - \rho_G}}\right)^{0.91}\right] \tag{2.6}$$

$$C = 0.50 + 0.438\exp(-137.8h_w). \tag{2.7}$$

Clear liquid height is one of the most extensively used hydraulic parameters used in correlations for sieve tray performance prediction.

2.5.2 Froth Height

Froth height is defined as the height of the two-phase mixture whose liquid holdup fraction is above a specified value. Lockett (1986) specifies a liquid holdup fraction of 0.1 for the froth regime, and 0.01 for the spray regime. In conventional tray deign and analysis, froth height has exclusively been calculated as the ratio of clear liquid height to average liquid holdup fraction in froth.

2.5.3 Average Liquid Holdup Fraction in Froth

Average liquid holdup fraction in froth (also sometimes known as froth density or dispersion density) is defined as the average value of the liquid phase holdup fraction in the froth. For the froth regime, the correlation of Colwell (1979), Equation (2.2), has been recommended for the prediction of this parameter. For trays operating in the spray regime, Lockett (1986) recommends the correlation of Stichlmair (1978).

2.5.4 Tray Pressure Drop

The drop in pressure across the tray occurs because of (Bennett et al., 1983): the liquid inventory on the tray, the passage of the vapour through perforations, and formation of vapour bubbles. Thus, the total pressure drop is the sum of the contributions from these. The correlation of Bennett et al. (1983) has been reported to give a reasonably accurate estimate of tray pressure drop. Alternative procedures are suggested by Kister (1992) and Lockett (1986).

2.6 Mass Transfer and Tray Efficiency

The sole purpose of using column internals such as sieve trays is to maximize mass transfer speed and efficiency while operating the internals within allowable limits of fluid loading and pressure drop. The speed of transfer is related to the maximum amounts of vapour and liquid that can be handled per unit time. So, speed of transfer limit is set by contact time requirements, tray capacity limits and upstream process requirements. The efficiency of transfer is a measure of the effectiveness of mass transfer compared to a thermodynamically set limit, i.e., approach to equilibrium.

Tray efficiency is required in the conversion of theoretical number of stages into real number of stages. The efficiency prediction starts with prediction of point efficiency. It then proceeds with the conversion of the point efficiency into overall tray efficiency. From there, section or column efficiency is computed. It should be stated that methods (Krishnamurthy and Taylor, 1985a,b) have emerged that override the need for the use of stage efficiency; these methods are particularly suited for multicomponent systems where the use and definition of efficiency are cumbersome. These methods are known as rate-based or non-equilibrium stage models, in contrast to equilibrium stage models that use tray efficiency to account for deviations from equilibrium.

Prediction of Efficiency

Point Efficiency

The first comprehensive tray efficiency estimation procedure was published by the American Institute of Chemical Engineers (AIChE) (Bubble-Tray Design Manual, 1958). The AIChE method is based on the two-resistance mass transfer model. Vapour- and liquid-phase mass transfer were expressed in terms of transfer units for each resistance. Correlations were given for the number of transfer units in each phase in terms of operating and geometry parameters. Large errors have been reported for the AIChE method by several authors. Yet, only little progress has been made in terms of point efficiency prediction since the AIChE method was published.

Most point efficiency prediction methods, the AIChE method included, are empirical or semi-empirical correlations. Zuiderweg (1982) gives different correlations for mass transfer coefficients of the spray, and froth and emulsion flow regimes. The correlations are based on a relatively small database from Fractionation Research Inc. Chan and Fair (1984) give correlations for the individual vapour- and liquid-phase transfer units. For the liquid-phase transfer unit, they use the same correlation as that of the AIChE. A new correlation is proposed for the vapour-phase transfer unit that implicitly takes care of weeping and entrainment via a fractional approach to flooding. Reviews by Lockett (1986), Kister (1992) and Korchinsky et al. (1994) recommend this Chan and Fair method compared to other available methods. This is partly due to the extensive database on which the correlation is based. The fact that the same liquid-phase transfer unit correlation as that of the AIChE method is used is believed to be the source of weakness of the Chan and Fair method. Chen and Chuang (1993) propose a semi-empirical model for the prediction of number of transfer units and hence point efficiency. The database used was however relatively small. Bennett et al. (1997) developed correlations for efficiency and entrainment. The point efficiency correlation is reported to correlate point efficiency to within 6.4%.

Some attempts have been made recently to predict point efficiency from a mechanistic modeling of the two-phase flow. Prado and Fair (1990) present a mechanistic model of point efficiency that considers a modeling of the structure of the two-phase mixture. The model was, however, limited to air-water system. Garcia and Fair (2000b) extended the Prado and Fair model to non-aqueous systems. Taylor and Krishna (1993) give a fundamental model of efficiency that has attempted to take care of two-phase structure modeling. But the model does not give relationships for several of the parameters involved in the two-phase structure modeling, such as jet or bubble diameter, height of jet, rise velocities, etc.

Tray Efficiency

Once the point efficiency is predicted, the next step is the conversion of the point efficiency to tray efficiency. In converting point efficiency to tray efficiency, almost all available methods use the mixing model of the AIChE method. The AIChE method assumes plug flow of liquid with a superimposed backmixing. However, experimental studies (discussed in the next section) have shown that actual flow patterns found on industrial trays include flow maldistributions such as channelling, recirculation, stagnant zones, and non-uniform velocity distributions.

2.7 Flow Patterns and Flow Maldistributions

In this section, the literature on the nature and effect of flow patterns and flow maldistribution is briefly reviewed.

Bell (1972a) was the first to come with a useful result of residence time distribution measurements on sieve trays. A fibre optic technique was used to measure liquid phase point residence times on commercial scale sieve trays. The fibre optic technique was demonstrated to have sufficient resolution to yield residence time profiles in the tray. The results from experiments on a 1.22 m diameter sieve tray showed that the assumption of plug flow of liquid is inaccurate. The data showed a region of short residence times along the tray centreline and long ones near the tray wall. In another work (Bell, 1972b), residence time profiles measured using the fibre optic technique in a 2.44 m diameter sieve tray are reported. The results of the study demonstrated the presence of circulating flow patterns with a retrograde component near the tray wall.

Sohlo and Kinnunen (1977) measured liquid velocities by floating cork balls. The velocity profiles indicated that deviations from ideal plug flow occur.

Solari et al. (1982) carried out experiments on a 1.25 m diameter sieve tray column to measure liquid velocity distributions. They found that the size of the non-uniform flow region ranges from 5 to 60% of the bubbling area. At low gas rates, the bubbling action was found to be localized in those regions of the tray characterized as dead zones or

zones of retrograde flow. As the tray approaches flooding due to increase in gas rate, the gas is reported to be more or less equally distributed. But over a wide range of gas and liquid flow rates, most of the gas was found contacting liquid that had the longest residence time while a large fraction of the liquid was not in contact with the gas. This condition clearly reduces tray efficiency. High gas rates are reported to reduce both the retrograde flow and the non-uniform velocity distribution.

Solari and Bell (1986) used the fibre optic technique to measure detailed liquid residence time and velocity distributions on a commercial-scale sieve tray. The residence time distributions were found to be strongly affected by the gas rate and showed extended residence times near the tray wall and relatively shorter residence times near the tray centreline. Results qualitatively identical to the Bell (1972b) results are reported. Variance distributions are reported showing the existence of zones of different degrees of lateral mixing. Strong evidence of flow recirculation was found in the absence of gas flow. The velocity profiles at low gas rates showed severe flow non-uniformities, characterized by a high velocity at the centreline and a stagnant zone close to the wall. At higher gas rates, the velocity distribution was found to be relatively mild.

Effect of Flow Maldistributions on Tray Performance

Experimental Studies

Only a very few number of experimental studies have been done to assess the effects of flow maldistributions. Weiler et al. (1973) compared the performances of slotted and unslotted 7.62 m diameter sieve trays. The directionally slotted tray is reported to perform better than the unslotted one. Yanagi and Scott (1973) performed experiments on two sets of 1.22 and 2.44 m diameter single-pass cross flow sieve trays. In one set of trays, a uniform liquid flow pattern was achieved by modifying the inlet downcomer baffle and the outlet weir sections of conventionally designed trays. The second set of trays had conventional design. Severe liquid flow non-uniformity was observed for the second set of trays. The efficiency measurements showed almost no difference for the two cases. Lockett and Safekourdi (Lockett 1986; Lockett and Safekourdi, 1976) and Solari and Bell (1986) argued, based on their models, that the

Yanagi and Scott test conditions were such that liquid flow maldistribution should not have had a noticeable effect on efficiency (Kister, 1992).

Theoretical Studies

Porter et al. (1972) proposed a model that considered uniform flow of liquid along the centreline with stagnant zones near the tray wall. The uniform flow region was taken to be as wide as the weir length. The theoretical study showed that liquid channelling might produce significant deleterious effects on large diameter columns that are absent in small columns and thus are not capable of investigation in a laboratory.

Bell and Solari (1974) proposed a theory that considered a non-uniform liquid flow distribution without transverse mixing. The liquid flow distribution was modeled as characterized by the fraction of the bubbling area carrying the flow in the flow direction, and a fraction of the net flow to the tray that appeared in retrograde flow. The study showed that the presence of non-uniform velocity distributions or retrograde flow could substantially reduce the efficiency of distillation trays.

Solari and Bell (1978) extended the retrograde flow model for the case of partial transverse mixing and found that a high degree of transverse mixing is required to overcome the unfavourable effect of velocity gradients on tray efficiency.

2.8 Conclusion

What is clear from the literature and current practice is that the further performance improvement of sieve trays has stood still. The principal reason for this is the poor knowledge of the complex behaviours of the multiphase transport processes inside the tray. The spatial details of the multiphase flow field are lacking and the designer relies heavily on gross oversimplifications. Experience and empirical correlations are heavily used.

Except for the few experimental case reports, little is known about what flow patterns to expect for given tray geometry and operating conditions. The cited theoretical

models provide useful insight as to what happens in the case of the prevalence of flow patterns or flow maldistributions used by the models. The models are limited since they are at most two-dimensional and/or consider only one of the phases present; they do not consider the chaotic, three-dimensional and multiphase nature of the problem. Besides, model parameters have not been related to geometry, operating conditions and system variables. In general, both the equilibrium and nonequilibrium stage models of tray design are concerned with what happens for the overall tray or stage rather than dealing with what happens inside the tray spatially.

In conclusion, there are two major unresolved problems facing the current practice of tray design and analysis. The first one is what flow patterns to expect for given geometry and operating conditions. The second problem is how to relate these flow patterns to tray performance parameters such as tray efficiency and pressure drop. Once a method or methods are devised to accomplish the two tasks, it will be possible to design trays that have desired flow patterns that give rise to the best performance. This work proposes computational fluid dynamics as an elegant method to solve the problems posed.

Chapter 3 Literature Review – Fluid Mechanics

3.1 Introduction

In recent years, there has been a growing interest and progress in the development of mathematical models for complex flow phenomena such as turbulent and multiphase flows. This has been paralleled by the advent of high-speed and large-memory computers, and by the evolution of precise mathematical theories of numerical algorithm and grid generation. The technique that exploits these developments is computational fluid dynamics (CFD). CFD has now reached a level of sophistication such that it is possible to investigate flows of industrial interest be they laminar or turbulent, reacting or non-reacting, single-phase or multiphase.

This chapter reviews the mathematical and numerical modeling aspects of fluid flow.

3.2 Conservation Equations

The fact that mass, momentum and energy are conserved is utilized in the development of mathematical models of fluid flow and heat transfer. Any textbook of fluid mechanics or transport phenomena (e.g., Bird et al., 1960) may be consulted for the derivation of the conservation equations. The interest of this work is limited to the hydrodynamic behaviour of sieve trays. Hence, an isothermal flow system is assumed. Thus only the continuity and momentum equations are considered. These equations for the flow of a single-phase fluid are:

Continuity Equation

$$\frac{\partial \rho}{\partial t} + \nabla.(\rho \mathbf{V}) = 0 \tag{3.1}$$

Momentum Equations

$$\frac{\partial}{\partial t}(\rho \mathbf{V}) + \nabla.(\rho \mathbf{V}\mathbf{V}) = -\nabla p + \nabla.\boldsymbol{\tau} + \rho \boldsymbol{f} \tag{3.2}$$

Closure Relationships

Equations (3.1) and (3.2) represent four transport equations with five unknowns (three velocity components (U, V, W), ρ, and p). On top of that, the stress tensor $\boldsymbol{\tau}$ has six unknown components. The body force $\boldsymbol{f}$ is assumed to be given. For closure, two more equations are required. One equation comes from an equation of state:

$$p = p(\rho, T). \tag{3.3}$$

The second equation is a relationship for the viscous stress tensor $\boldsymbol{\tau}$. For a Newtonian fluid, $\boldsymbol{\tau}$ is related to fluid properties and velocity as:

$$\boldsymbol{\tau} = \mu\left(\nabla \mathbf{V} + (\nabla \mathbf{V})^T\right) + \left(\kappa - \frac{2}{3}\mu\right)\nabla.\mathbf{V}\boldsymbol{\delta} \tag{3.4}$$

where μ is molecular viscosity, $\boldsymbol{\delta}$ is identity tensor, κ is bulk viscosity, and $(\nabla \mathbf{V})^T$ is the transpose of $(\nabla \mathbf{V})$. Often times, the last term on the right hand side of this expression drops out because $\nabla.\mathbf{V}$ is usually small. For an incompressible fluid, it is identically zero. For constant density and viscosity for a Newtonian fluid with gravity as the only body force, Equation (3.2) reduces to:

$$\frac{\partial}{\partial t}(\rho \mathbf{V}) + \nabla.(\rho \mathbf{V}\mathbf{V}) = -\nabla p + \mu \nabla^2 \mathbf{V} + \rho \boldsymbol{g} \tag{3.5}$$

which is the *Navier-Stokes* equation. It has been customary to refer to the general continuity, momentum and energy equations as the Navier-Stokes system of equations (e.g., Chung, 2002).

3.3 Turbulence Modeling

Turbulence consists of random fluctuations of the various flow quantities. It is three-dimensional, chaotic, and is characterized by a large range of excited time and length scales. The flow field variables in turbulent flow vary significantly and irregularly both in time and position.

The same equations that govern laminar flows are applicable to turbulent flows. However, for turbulent flows, an enormous amount of information is contained in the equations. Turbulent flows contain time and length scales much smaller than the smallest possible grid size. Thus the direct numerical simulation of these flows would require computing speed and memory that are many orders of magnitude higher than available in the foreseeable future.

In order to be able to predict the effects of turbulence, *turbulence models* are used. The most popular approach is to follow the procedure introduced by Reynolds (1895). In this approach, all quantities are expressed as the sum of mean and fluctuating components. And then the common step is to time average the Navier-Stokes equations obtaining the Reynolds-Averaged Navier-Stokes (RANS) equations. For an incompressible flow, Reynolds averaging of the Navier-Stokes equations gives:

$$\frac{\partial}{\partial t}(\rho \mathbf{V}) + \nabla.(\rho \mathbf{V}\mathbf{V}) = -\nabla p + \nabla.\boldsymbol{\tau} - \nabla.\rho\overline{V'V'} + \rho \boldsymbol{g} \tag{3.6}$$

where $\mathbf{V}$, p, and $\boldsymbol{\tau}$ are time-averaged mean quantities and V' is the fluctuating part of the velocity vector. The continuity equation is unchanged except that velocity is now a mean quantity. For compressible flows, density weighted Favre (1965) averaging is the preferred approach.

Closure Relationships

We see that the statistical approach (Reynolds averaging) has led to the appearance of a new quantity, $-\rho\overline{V'V'}$, known as Reynolds stress. This is a second order symmetric

tensor. Six more unknowns have been introduced. For closure, we must relate these unknowns to the mean flow variables. Various models for the Reynolds or turbulent stress have been proposed. The models can be broadly classified into two: eddy-viscosity models and Reynolds stress models (Pope, 2000; Wilcox, 1993). The most widely used is the k-epsilon (k-ε) model (Jones and Launder, 1972), which is based on the eddy-viscosity hypothesis. The eddy-viscosity hypothesis assumes that

$$-\rho\overline{\mathbf{V}'\mathbf{V}'} = -\frac{2}{3}\mu_t \rho k \boldsymbol{\delta} - \frac{2}{3}\mu_t \nabla.\mathbf{V}\boldsymbol{\delta} + \mu_t\left(\nabla\mathbf{V} + (\nabla\mathbf{V})^T\right) \tag{3.7}$$

where μ_t is the turbulent viscosity and k is the turbulent kinetic energy. In the k-ε model, the turbulent viscosity is computed from

$$\mu_t = C_\mu \rho \frac{k^2}{\varepsilon} \tag{3.8}$$

Transport equations are used and solved for the turbulent kinetic energy k and turbulent kinetic energy dissipation rate ε.

$$\frac{\partial}{\partial t}(\rho k) + \nabla.(\rho \mathbf{V} k) = \nabla.(\frac{\mu_{eff}}{\sigma_k}\nabla k) + P_k - \rho\varepsilon \tag{3.9}$$

$$\frac{\partial}{\partial t}(\rho \varepsilon) + \nabla.(\rho \mathbf{V} \varepsilon) = \nabla.(\frac{\mu_{eff}}{\sigma_\varepsilon}\nabla \varepsilon) + \frac{\varepsilon}{k}(C_{\varepsilon 1}P_k - C_{\varepsilon 2}\rho\varepsilon) \tag{3.10}$$

where

$$\mu_{eff} = \mu + \mu_t. \tag{3.11}$$

The standard values of the closure coefficients are (Launder and Sharma, 1974):

$$C_\mu = 0.09, C_{\varepsilon 1} = 1.44, C_{\varepsilon 2} = 1.92, \sigma_k = 1.0, \text{ and } \sigma_\varepsilon = 1.3. \tag{3.12}$$

Turbulence modeling is well treated in the literature (Wilcox, 1993; Libby, 1998; Salas et al., 1999; Pope, 2000).

3.4 Multiphase Modeling

A multiphase flow system contains a mixture of phases that may have different flow fields; i.e., different velocity, temperature, pressure etc. fields. The phases in multiphase flow are assumed to be mixed at scales much larger than the molecular scale. But they are also assumed to be mixed at scales much smaller than the scale of the overall system or problem. Examples of multiphase flow systems are bubbles in a liquid, droplets in a gas, and solid particles in a fluid.

The ideal analysis of a multiphase flow would be to solve the single-phase governing equations for each phase by accounting for interactions between particles in each phase in the flow field. For example, for a dispersed phase flow this would mean solving the single-phase governing equations for the continuous phase by accounting for the effects of each and every individual dispersed phase particle. Obviously such an analysis is impractical. Computationally, this would require a grid dimension at least as small as the smallest fluid or solid particle in the field (Crowe et al., 1998). This is beyond current computer capability.

A way out of this problem has been through multiphase modeling, which has been accomplished using local volume averaging. In the averaging approach, the governing equations are expressed based on average properties. One considers the average properties in a volume containing many particles and ascribes the average values to a point in the flow enclosed by the volume (Crowe et al., 1998). Volume averaging is carried out by averaging properties at an instant in time over a volume and ascribing the average values to a point in the flow. The single-phase flow conservation governing equations are volume averaged resulting in equations that are expressed in terms of volume-averaged flow variables for the multiphase flow.

Multi-fluid model

The Eulerain-Eulerain multi-fluid model is a popular multiphase model. In the multi-fluid modeling approach, each phase possesses its own flow field; i.e., each phase has its own velocity, temperature, etc. field. The phases are considered as interpenetrating continua; i.e., each point in the mixture is occupied simultaneously (in variable proportions) by each phase (Lakehal, 2002). Each phase is governed by its own conservation and constitutive equations; these are then coupled through interphase transfer or interaction terms.

The continuity and momentum equations after volume averaging become:

Continuity equation for phase α

$$\frac{\partial}{\partial t}(r_\alpha \rho_\alpha) + \nabla.(r_\alpha \rho_\alpha \mathrm{V}_\alpha) = S_{\alpha,mass} \tag{3.13}$$

$S_{\alpha,mass}$ is mass source or sink because of interphase mass transfer. r_α is volume fraction of phase α in the averaging (arbitrary but well-defined) volume.

Momentum equations for phase α

$$\begin{aligned}&\frac{\partial}{\partial t}(r_\alpha \rho_\alpha \mathrm{V}_\alpha) + \nabla.(r_\alpha \rho_\alpha \mathrm{V}_\alpha \mathrm{V}_\alpha) \\ &= -r_\alpha \nabla p_\alpha + \nabla.\left[r_\alpha \mu_\alpha \left(\nabla \mathrm{V}_\alpha + (\nabla \mathrm{V}_\alpha)^T\right)\right] + r_\alpha \rho_\alpha \mathrm{g} + S_{\alpha,mom} + \mathrm{F}_\alpha\end{aligned} \tag{3.14}$$

$S_{\alpha,mom}$ represents momentum source due to external body forces other than gravity. F_α represents interphase momentum transfer due to fluid-fluid and/or fluid-solid interactions. The volume fractions summation constraint adds one more equation:

$$\sum_{\alpha=1}^{N_p} r_\alpha = 1 \tag{3.15}$$

where N_P is the total number of phases.

Jakobsen et al. (1997) have considered the derivation of the multiphase flow transport equations. The monographs by Gidaspow (1994) and Crowe et al. (1998) present a critical view of the multiphase flow models.

The current philosophy of the mathematical modeling of multiphase flows is (volume) averaging. However, yet there is no agreement on the governing equations of multiphase flows (Crowe et al., 1998; Van Wachem and Almstedt, 2003).

Closure Relationships

We see that in order to solve for volume fraction, velocity and pressure fields, we need to specify the interphase interaction terms in terms of the volume-averaged flow variables. There are no generalized models for these terms. The terms are flow-problem dependent.

3.5 Turbulent Multiphase Flow

Yet another stage of modeling involves turbulence in multiphase flow. This is an area that is underdeveloped. What is being done currently is to perform turbulence averaging on the already averaged conservation equations. Volume fraction weighted Favre averaging is often given preference in order to eliminate complications arising from correlations of volume fraction with velocity (Lakehal, 2002). The turbulence averaging results in Reynolds stress terms in the momentum equations for each phase. In order to close the system of equations, the Reynolds stresses in each phase have to be expressed in terms of mean flow variables. To achieve this goal, the simplest possible generalizations of the single-phase turbulence models are used. For example, the k-epsilon model may be generalized for a multiphase system. The eddy-viscosity hypothesis is applied to each phase. Like the single-phase case, an effective viscosity is used in the momentum equations.

$$\mu_{\alpha,eff} = \mu_\alpha + \mu_{t\alpha}, \tag{3-16}$$

where for the k-ε model

$$\mu_{t\alpha} = C_\mu \rho_\alpha \frac{k_\alpha^2}{\varepsilon_\alpha}. \tag{3-17}$$

The equations for k_α and ε_α are:

$$\begin{aligned} &\frac{\partial}{\partial t}(r_\alpha \rho_\alpha k_\alpha) + \nabla.(r_\alpha \rho_\alpha V_\alpha k_\alpha) \\ &\quad = \nabla.\left(r_\alpha (\mu_\alpha + \frac{\mu_{t\alpha}}{\sigma_k}) \nabla k_\alpha \right) + r_\alpha (P_{k,\alpha} - \rho_\alpha \varepsilon_\alpha) + T_{\alpha\beta}^{(k)} \end{aligned} \tag{3.18}$$

$$\begin{aligned} &\frac{\partial}{\partial t}(r_\alpha \rho_\alpha \varepsilon_\alpha) + \nabla.(r_\alpha \rho_\alpha V_\alpha \varepsilon_\alpha) \\ &\quad = \nabla.\left(r_\alpha (\mu_\alpha + \frac{\mu_{t\alpha}}{\sigma_\varepsilon}) \nabla \varepsilon_\alpha \right) + r_\alpha \frac{\varepsilon_\alpha}{k_\alpha} (C_{\varepsilon 1} P_{k,\alpha} - C_{\varepsilon 2} \rho_\alpha \varepsilon_\alpha) + T_{\alpha\beta}^{(\varepsilon)} \end{aligned} \tag{3.19}$$

where $T_{\alpha\beta}^{(k)}$ and $T_{\alpha\beta}^{(\varepsilon)}$ are interphase transfer terms that need to be specified, if any exist.

Banerjee (1990) analyzes the modeling considerations for turbulent multiphase flows. Borchers et al. (1999) have assessed the applicability of the k-ε model for gas-liquid flows in bubble columns.

3.6 Computational Fluid Dynamics (CFD)

The differential equations of momentum, mass and energy transfer form a system of coupled non-linear partial differential equations. The equations have no known general analytical solutions. Analytical solutions are possible only for a few simple special cases, for cases where the equations can be made linear through simplifications. The equations can, however, be discretized and solved numerically. Experimental measurement of flow variables is another approach to the problem. Although experimental measurements are generally expected to give reliable data, they give a limited amount of data, and are

costly, time-consuming, and less flexible. The remaining solution is solving the partial differential equations numerically. Compared to experiments, numerical analysis gives a large amount of data, and is cheap, fast, and more flexible.

Computational fluid dynamics (CFD) is concerned with obtaining numerical solutions using the computer. The advent of high-speed, large-memory computers, the evolution of precise numerical algorithms, and developments in complex flow phenomena modeling have enabled CFD to obtain numerical solutions to flows of industrial interest. CFD obtains numerical solutions through three steps: discretization of the flow domain, discretization of the partial differential equations, and solving of an algebraic system of equations that results from the discretization process.

Of the solution methods used in CFD codes, the finite volume method is the most common. It is the method used in the commercial codes CFX-4.4 and CFX-5.4, the packages used for the CFD analysis of this work. Versteeg and Malalasekera (1995) give a good introduction to the finite volume method.

Computational fluid dynamics has been the subject of many authors (Patankar, 1980; Versteeg and Malalasekera, 1995; Anderson, 1995; Ferziger and Perić, 1996; Tannehill et al., 1997, Wesseling, 2001; Chung, 2002).

3.6.1 Grid Generation

In the finite volume method, the flow domain is divided into small subregions known as control (finite) volumes. The grid could be structured or unstructured. In the former case, transformation from physical space into computational space is performed. This will give grid lines that are oriented regularly in three directions so that coordinate transformations of curvilinear lines result in a cube for three-dimensional problems. The partial differential equations are then discretized and solved using the simplified computational space coordinate system. Unlike structured grids, in unstructured grids, coordinate transformation is not performed and as a result they can be used for irregular geometries but at the expense of more complex computer programming. The state of the art of grid generation is discussed by Thompson et al. (1985, 1998).

In CFX-4.4, structured grids were used while in CFX-5.4 unstructured grids were used.

3.6.2 Interpolation and Differencing Schemes

The finite volume method uses the integral form of the conservation equations. Integration is carried out for each finite or control volume (CV). This requires approximations of surface and volume integrals. The surface integration process requires values of variables at one or more faces and/or corners. Since variables are evaluated and stored at the centre of each CV or cell, methods of interpolating values of variables at faces or corners from the CV centres are required. The methods of interpolation are known as differencing schemes. One of the popular ones is upwind differencing, first put forward by Courant et al. (1952). In this scheme, CV face value of a variable is set equal to the CV centre value upstream of the CV face. The scheme is first order accurate. Another popular scheme is the hybrid differencing scheme of Spalding (1972) that uses upwind differencing for local Peclet number greater than two and linear interpolation (central differencing, which is 2^{nd} order accurate) for local Peclet number less than two. A third order scheme is achieved using quadratic upwind interpolation which is the QUICK (Quadratic Upwind Interpolation for Convection Kinematics) scheme made popular by Leonard (1979). Other popular schemes are the MUSCL (Monotone Upstream-Centred Schemes for Conservation Laws) schemes of Van Leer (1979).

In CFX-4.4, hybrid differencing was used for all the equations except for the volume fraction equations where the Min-Mod scheme of Van Leer was used. In CFX-4.4, the pressure-velocity coupling was obtained using the SIMPLEC algorithm (Van Doormal and Raithby, 1984). In CFX-5.4, upwind differencing was used for all equations. But for some cases, the results obtained using the upwind scheme were further run using higher order schemes in order to assess the sensitivity of the simulation results to the accuracy order of the differencing scheme.

3.6.3 Solution of Algebraic System of Equations

Iterative methods are typically used to solve the algebraic system of equations resulting from the discretization process. CFX-4.4 allows the use of different equation

solvers for different variables. The command file in Appendix A gives details of the CFX-4.4 features used in this work. Default settings are used for those not explicitly given. In CFX-5.4, the multigrid method, originally pioneered by Brandt (1972, 1977, 1992), is used together with a coupled solver. The command file in Appendix B gives details of the CFX-5.4 features used in this research work.

3.7 Attempts Made to Model Sieve Tray Hydrodynamics using CFD

About six attempts have been made so far to simulate tray hydrodynamics using CFD. In a previous work (Mehta et al., 1998), liquid velocity distributions were predicted by considering the steady state, three-dimensional flow of the liquid phase. The effects of the vapour flow were taken into account by incorporating additional terms calculated using empirical correlations for sieve tray hydraulics. Fischer and Quarini (1998) modeled the three-dimensional transient gas-liquid tray hydrodynamics by using a drag coefficient with a constant value of 0.44, a value that corresponds to the inertial turbulent regime. Liu et al. (1999) developed a two-dimensional model that simulates the flow of the liquid phase. They have attempted to include the effect of the vapour flow by incorporating additional terms into the liquid phase model equations.

Krishna et al. (1999b) for a rectangular geometry, and van Baten and Krishna (2000) for a circular geometry developed CFD models to simulate the transient, three-dimensional two-phase flow behaviour of a 0.3 m diameter sieve tray. The two phase equations were coupled through an interphase drag term that was estimated using the drag coefficient correlation of Krishna et al. (1999a) and the Bennett et al. (1983) correlation for liquid holdup fraction in froth. The authors reported clear liquid height and dispersion profile predictions, and remarked that the flow inside the tray exhibited a chaotic and three-dimensional behaviour. Krishna and Van Baten (2003) performed transient simulations of sieve trays of 0.3 m and 0.9 m in diameter. The simulations are shown to reveal chaotic three-dimensional flow behaviour with circulation patterns in all three dimensions. Flow pattern studies have been made by means of tracer injection. The

authors underline the limitations of models that are two-dimensional or that consider only one phase.

Two-dimensional models are limited knowing that the flow phenomenon inside the tray is truly chaotic as indicated and hence three-dimensional. With one of the phases missing, models that consider only one phase are not capable of predicting and simulating complete tray behaviour. Van Baten and Krishna (2000) and Krishna and Van Baten (2003) did a pioneering work of using a CFD model to simulate sieve tray hydrodynamics. The authors, however, made no attempt to predict and validate velocity distributions.

3.8 Conclusion

In this chapter, the mathematical and numerical modeling of fluid flow were reviewed with special emphasis given to complex flow phenomena encountered in sieve trays. An overview of the mathematical modeling of fluid flow was given for laminar single-phase flow to turbulent multiphase flow. The problems that give rise to the need for turbulence and multiphase modeling were indicated. The computational methods used in this work were also indicated. CFD modeling attempts made to model sieve tray hydrodynamics were reviewed.

From the literature survey it can be concluded that fundamental modeling of two-phase flow has so far concentrated on pipe flow and bubble columns. Models for flows as complex as those found on sieve trays are lacking. Krishna et al. (1999b) propose a relationship for the interphase drag in sieve trays operating in the bubbly flow regime. Their relation is tested and used in this work.

Chapter 4 Two-Phase Flow Model

4.1 Introduction

The goal of this work is establishing CFD as a prediction tool for sieve tray hydrodynamics. To this end, this thesis proposes a three-dimensional two-phase flow model for the hydrodynamics of a commercial-scale sieve tray. This chapter presents the essential features of the proposed model.

4.2 Experimental Basis of the Model

The geometry and operating conditions of the model are based on the experimental work of Solari and Bell (1986) that was carried out in a 1.22 m diameter sieve tray. In that work, liquid phase residence time and velocity distributions were measured using a fluorometric technique. The fluids used were air and water.

4.3 Model Assumptions

Fluid Properties

The physical properties of air (the gas or vapour phase) and water (the liquid phase) are assumed to be constant. The assumption is reasonable since there are no physical processes that can cause significant variations of fluid properties. Thus, both the liquid and gas (vapour) phases are incompressible fluids.

Mass Transfer

Interphase exchange of mass between the air and water is assumed to have a negligible effect on the tray hydrodynamics. The assumption introduces a saving in computational load as one mass transfer equation per phase is not being solved.

Energy Transfer

Isothermal conditions are assumed. The energy transfer on a single tray basis is assumed to have a negligible effect on the tray hydrodynamics. Since fluid flow is incompressible, the hydrodynamics can be investigated independent of the energy transfer. By assuming isothermal flow, a saving in computational load is made since one energy equation per phase is not being solved

4.4 Model Equations

The model considers the flow of gas and liquid in the Eulerian-Eulerian framework in which each phase is treated as an interpenetrating continuum having separate transport equations. With the model focusing on the froth region of the sieve tray, the gas phase has been taken as the dispersed phase while the liquid phase has formed the continuous phase. Since the focus is on the hydrodynamic behaviour of sieve trays, energy and interphase mass transfers have not been considered in this work. Thus for each phase the time and volume averaged continuity and momentum equations are numerically solved.

Continuity Equations

Gas phase

$$\frac{\partial(r_G \rho_G)}{\partial t} + \nabla.(r_G \rho_G \mathbf{V}_G) = 0 \tag{4.1}$$

Liquid phase

$$\frac{\partial(r_L \rho_L)}{\partial t} + \nabla.(r_L \rho_L \mathbf{V}_L) = 0 \tag{4.2}$$

Momentum Equations

Gas phase

$$\frac{\partial}{\partial t}(r_G \rho_G \mathbf{V}_G) + \nabla.(r_G(\rho_G \mathbf{V}_G \mathbf{V}_G)) = -r_G \nabla p_G + \nabla.(r_G \mu_{eff,G}(\nabla \mathbf{V}_G + (\nabla \mathbf{V}_G)^T)) + r_G \rho_G \boldsymbol{g} - \mathbf{M}_{GL} \tag{4.3}$$

Liquid phase

$$\frac{\partial}{\partial t}(r_L \rho_L \mathbf{V}_L) + \nabla.(r_L(\rho_L \mathbf{V}_L \mathbf{V}_L)) = -r_L \nabla p_L + \nabla.(r_L \mu_{eff,L}(\nabla \mathbf{V}_L + (\nabla \mathbf{V}_L)^T)) + r_L \rho_L \mathbf{g} + \mathbf{M}_{GL} \tag{4.4}$$

The gas and liquid volume fractions, r_G and r_L, are related by the summation constraint.

$$r_G + r_L = 1 \tag{4.5}$$

The same pressure field has been assumed for both phases, i.e.,

$$p_G = p_L. \tag{4.6}$$

$\mu_{eff,G}$ and $\mu_{eff,L}$ are the effective viscosities of the gas and liquid phases, respectively.

$$\mu_{eff,G} = \mu_{laminar,G} + \mu_{turbulent,G} \tag{4.7}$$

$$\mu_{eff,L} = \mu_{laminar,L} + \mu_{turbulent,L} \tag{4.8}$$

The term $\mathbf{M}_{GL}$ in the momentum equations represents interphase momentum transfer between the two phases.

Closure Relationships

In order to solve Equations (4.1) to (4.8) for velocities, pressure and volume fractions, we need additional equations that relate the interphase momentum transfer term

$\mathbf{M}_{GL}$ and the turbulent viscosities to the mean flow variables. The interphase momentum transfer term $\mathbf{M}_{GL}$ is basically interphase drag force per unit volume. With the gas as the disperse phase, the equation for $\mathbf{M}_{GL}$ is

$$\mathbf{M}_{GL} = \frac{3}{4}\frac{C_D}{d_G} r_G \rho_L |\mathbf{V}_G - \mathbf{V}_L|(\mathbf{V}_G - \mathbf{V}_L) \tag{4.9}$$

The drag coefficient C_D has been estimated using the drag correlation of Krishna et al. (1999a), a relation proposed for the rise of a swarm of large bubbles in the churn turbulent regime.

$$C_D = \frac{4}{3}\frac{\rho_L - \rho_G}{\rho_L} g d_G \frac{1}{V_{slip}^2} \tag{4.10}$$

where the slip velocity $V_{slip} = |\mathbf{V}_G - \mathbf{V}_L|$ is estimated from the gas superficial velocity V_S and the average gas holdup fraction in the froth region as

$$V_{slip} = \frac{V_S}{r_G^{average}} \tag{4.11}$$

For the average gas holdup fraction, two correlations were considered. One was the correlation of Bennett et al. (1983).

$$r_G^{average} = 1 - \alpha, \text{ where } \alpha \text{ is given by Equation (2.6)} \tag{4.12}$$

The second one was that of Colwell's (1979).

$$r_G^{average} = 1 - \alpha, \text{ where } \alpha \text{ is given by Equation (2.2)} \tag{4.13}$$

Substituting and simplifying, the interphase momentum transfer term as a function of local variables and constant coefficients put in a form suitable for the CFD use becomes (Van Baten and Krishna, 2000):

$$\mathbf{M}_{GL} = \frac{(r_G^{average})^2}{(1.0 - r_G^{average}) V_s^{\,2}} g(\rho_L - \rho_G) r_G r_L |\mathbf{V}_G - \mathbf{V}_L| (\mathbf{V}_G - \mathbf{V}_L) \qquad (4.14)$$

Interestingly this relation is independent of bubble diameter. This obviates the need for its input that could have been difficult.

The turbulence viscosities were related to the mean flow variables by using the standard k-ε turbulence model with default model coefficients. No turbulence models were used for the gas phase.

4.5 Flow Geometry

The model geometry and boundaries are shown in Figure 4.1. The tray has a diameter of 1.22 m, a 13% downcomer area, a weir height of 0.05 m, a downcomer clearance of 0.038 m, and a 5% hole area with 0.0127 m diameter holes arranged in a 0.05 m triangular pitch. Solari et al. (1982) and Solari and Bell (1986) found symmetric flow fields about the tray centre. Making use of their observations, only half of the tray was modeled so as to save computational time and machine memory. The model includes the downcomer region. Liquid enters the tray through the downcomer clearance area, labelled Liquid Inlet, and leaves the flow geometry through the downcomer clearance area that leads to the tray below, labelled Liquid Outlet. Gas enters through holes at the bottom of the tray, labelled Vapour inlet holes, and leaves through holes at the top, labelled Vapour outlet holes.

One of the geometry modeling problems faced was specifying the tray holes. Because of the relatively large tray diameter, working with the actual number of holes proved to be computationally demanding. Hence in several simulations a smaller number

of holes were used, the total area of which equals that of the total area of the actual number of holes. But in few simulations (using CFX-5.4 which uses unstructured grid and a coupled solver) the actual number of holes were used and flow predictions were compared on both the macro (like clear liquid height) and micro (velocity distributions) scales. In some simulations, the holes were entirely removed and a uniform vapour velocity specified at the bottom vapour inlet, but it proved to be unsatisfactory.

The whole tray spacing (0.61 m) was considered in the simulation, even though the primary focus is in the froth region (about 0.20 m above the tray floor). This resulted in better numerical convergence, as well as provided with an ability to assess the froth height from the simulations.

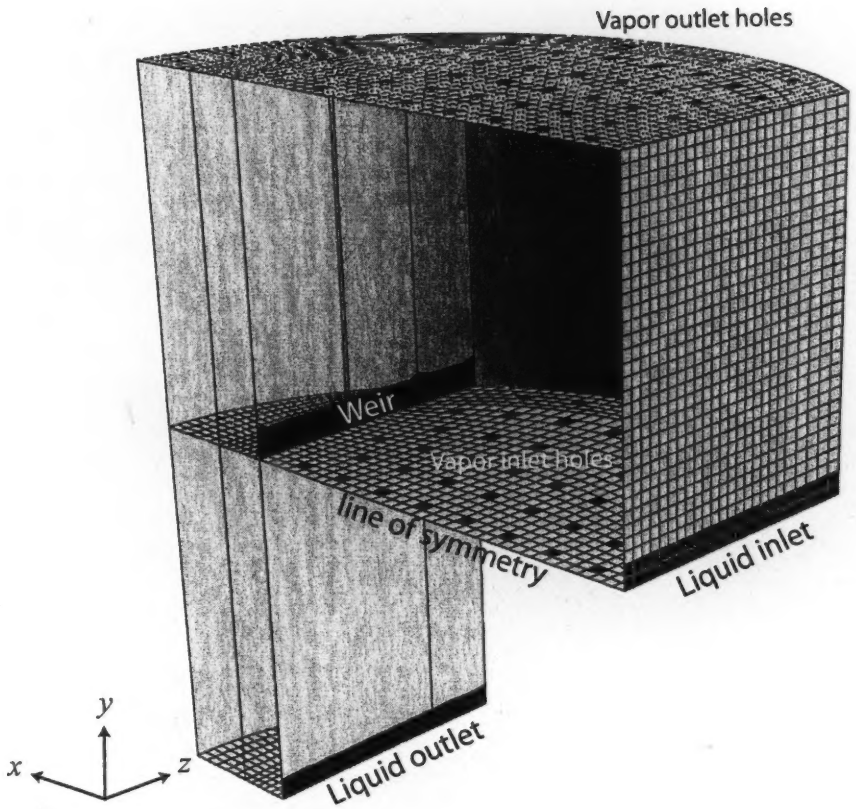

Figure 4.1 Flow geometry and boundaries

4.6 Boundary and Initial Conditions

4.6.1 Boundary Conditions

To solve the continuity and momentum equations, appropriate boundary conditions must be specified at all external boundaries plus at any specific internal boundaries of the flow geometry. Unfortunately, there is a lack of information about the inlet flow conditions in the sieve tray literature; only average quantities like flow rate are measured while the simulation requires detailed velocity profile as input. Intuition and experience were used as guides in specifying the boundary conditions. In some cases, an iterative procedure was followed where the results of a specified boundary profile were compared against the experimental data for the interior points of the tray.

Liquid Inlet

The velocity profile at the liquid inlet was found to have a significant effect on the liquid velocity distribution inside the tray. In the single-phase modeling work (Mehta et al., 1998), a uniform liquid inlet velocity profile was recommended for low values of flow parameter F_{LV} ($F_{LV} < 0.25$). That was found to be an important recommendation. Equations (4.15) and (4.16) give the two liquid inlet velocity profiles tested and used in this work.

Uniform Liquid Inlet Velocity Profile

$$U_{L,in} = \frac{Q_L}{A_{CL}} \tag{4.15}$$

Parabolic Liquid Inlet Velocity Profile

$$U_{L,in} = \frac{1.5Q_L}{A_{CL}}\left[1-\left(\frac{2z}{L_W}\right)^2\right] \tag{4.16}$$

with $A_{CL} = h_{ap} L_W$, where h_{ap} is the downcomer clearance and L_W is the weir length. The liquid volume fraction at the liquid inlet was taken to be unity assuming that only liquid enters through the downcomer clearance.

Vapour Inlet

A concern here was achieving uniform gas bubbling. That was possible for the unstructured meshes. For the structured grid, the gas inlet and outlet holes of the model are individual cell faces at the bottom and top of the tray. Because of the cylindrical geometry of the tray and the tapering at the weir location, the structured grid gives cell faces that differ in areas. The gas velocity at an inlet hole was calculated such that the same mass flow rate enters through each hole.

$$V_{hole,i} = \left(\frac{V_S A_B}{2 N_H} \right) \frac{1}{A_{hole,i}} \tag{4.17}$$

where N_H is the number of holes in the model geometry (half of the full tray). The gas hole velocity thus depends on the size and number of holes although their products make less sensitive the changes in the hole velocity values. Another way of specifying the gas hole velocities is to specify the same gas hole velocity for the inlet holes.

$$V_{hole} = \frac{V_S A_B}{2 \sum_{i=1}^{N_H} A_{hole,i}} \tag{4.18}$$

For a given inlet hole, the ratio of the gas momentum calculated using Equation (4.17) to that calculated using Equation (4.18) will be:

$$\left(\frac{V_{hole,i}}{V_{hole}} \right)^2 = \left(\frac{\sum_{i=1}^{N_H} A_{hole,i}}{N_H A_{hole,i}} \right)^2 . \tag{4.19}$$

The closer to one another the hole area values are, the more uniform the gas bubbling becomes. For the structured grid, neither of the equations for the gas hole velocity assures uniform gas bubbling. The gas volume fraction at the inlet holes was specified to be unity.

Liquid and Vapour Outlets

The liquid and vapour outlet boundaries were specified as mass flow boundaries with fractional mass flux specifications. At the liquid outlet, only liquid was assumed to leave the flow geometry and only gas was assumed to exit through the vapour outlet. These specifications will be in agreement with the specifications at the gas inlet and liquid inlet where only one fluid was assumed to enter.

Wall and Symmetry Boundary Conditions

A no-slip wall boundary condition was specified for the liquid phase and a free slip wall boundary condition was used for the gas phase. At the plane of symmetry, the normal component of velocity is zero and the gradients of the other variables in the transverse coordinate direction are taken to be zero.

4.6.2 Flow Field Initialization

Good initial guesses of the flow variables are important not only to avoid a significantly longer computational time but also in some cases to avoid numerical divergence. Water and air at room temperature and atmospheric pressure were the fluids used in the simulation. Initially, the tray was filled with water and air having volume fractions that varied in the vertical direction. In order to shorten the time needed to reach convergence, volume fractions were estimated using functions the parameters of which were determined using sieve tray hydraulics correlations. For both the regions above the bubbling area of the tray and the downcomer, functions of the following form were employed.

$$r_{L1} = r_0 \quad \text{if} \quad y \le h_L \tag{4.20}$$

$$r_{L2} = a + by^c \quad \text{if} \quad y \geq h_L \tag{4.21}$$

where r_0 is a constant value set slightly greater than the average liquid holdup fraction in the froth region calculated using the Bennett et al. (1983) correlation. Typically values ranging from 0.80 to 0.90 were used depending on the liquid and gas rates. The constants a, b and c were determined by requiring the equation to satisfy three conditions. One was the equation should return $r_L = r_0$ at $y = h_L$. This was done to avoid sudden localized jumps in the volume fraction values. The second one was the equation should return $r_L = 0.10$ at $y = h_F$. The last requirement was that the following integral sum should hold

$$T_S\left[\frac{1}{h_L}\int_0^{h_L} r_{L1}(y)dy + \frac{1}{(T_S - h_L)}\int_{h_L}^{T_S} r_{L2}(y)dy\right] = h_L \tag{4.22}$$

For the downcomer region, the clear liquid height is equal to the downcomer backup and a value of 0.99 was used for r_0.

The superficial gas velocity based on the bubbling area was used as an initial guess for the vertical component of the gas velocity throughout the flow region. The other components of the gas velocity were set to zero. For the liquid phase, a uniform horizontal velocity distribution that is equal to the flat liquid inlet velocity value was specified for all the cells in the froth region. A small negative value was set for the vertical component of the liquid velocity in the froth region. In the downcomer region, the downcomer velocity of the liquid was specified for the vertical component of the liquid velocity.

4.7 Conclusion

In this chapter, the essential features of a two-phase flow model were given. The model typically uses the interphase drag relationship of Krishna et al. (1999b). The main idea of the whole project is checking if any one of the existing interphase drag relations

can be used to predict the velocity distribution measured by Solari and Bell (1986). To achieve that goal, appropriate physical models, flow geometry, and boundary and initial conditions are given. The data given by Solari and Bell (1986) are the most comprehensive and more or less reproducible and free of errors. Thus, the proposed model differs from that of Van Baten and Krishna (2000) in the set-up of boundary conditions and in the type of data used for model validation.

Chapter 5 Simulation Results and Discussion

5.1 Introduction

In this chapter, the ability of the CFD model to predict and simulate sieve tray hydrodynamics is checked in many ways using quantities computed from the velocity and volume fraction solution fields.

One set of quantities computed is velocity distributions. Predicted liquid velocity distributions are compared with the experimental data of Solari and Bell (1986) for several combinations of liquid and gas rates. The model predictions are in good agreement with the experimental data of these authors. Possible factors that can affect the predicted velocity distributions are pointed out.

The other set of quantities calculated from the simulation results is the computation of averages from the volume fraction field. Clear liquid height, froth height and liquid holdup fraction in froth are most widely used in conventional sieve tray design and analysis. Predictions of these quantities are made and the prediction results compared with values calculated from correlations that have been accepted to give accurate predictions. The physical and numerical factors that can affect the prediction results are indicated.

After validating the simulation results, the use of the CFD as an insight tool is demonstrated in several ways. Parametric studies and their generalizations, characterization of the gas and liquid flows using various flow visualization techniques such as vector plots, streamlines, and shaded contour plots are made.

5.2 Solution Algorithms

This section provides information on top of that given in section 3.6.

The CFD analysis was carried out using the commercial packages CFX-5.4 and CFX-4.4 of AEA Technology. Transient simulations were conducted in CFX-4.4 while those of the CFX-5.4 were steady state ones.

In CFX-4.4, for the time term, implicit first order backward time differencing was used with fixed time steps that varied from 5.0×10^{-4} to 5.0×10^{-3} seconds. It was found necessary to run simulations with small underrelaxation factors generally less than 0.5. Most of the transient simulations were conducted using eight SGI R10000 195 MHz processors run in parallel. Better transient simulation convergence was observed when starting with lower gas rates. Tray hydraulics parameters such as clear liquid height and froth height were calculated at each time step. A transient simulation was deemed to have converged whenever the clear liquid height value shows no appreciable change with time (♣Figure 5.1).

Several types of simulations were conducted with CPU time per CFD simulation for convergence varying from as low as half a day to about a week.

5.3 Grid Size Sensitivities

Grid convergence requires that after a certain grid size the numerical results do not change significantly as the grid size is further decreased. Because of the relatively large tray diameter used, it was necessary to work with relatively coarse meshes having a small number of vapour inlet holes. The sensitivities of the simulation results to grid size, the number of holes and their size have been checked for both the structured (CFX-4.4) and the unstructured (CFX-5.4) meshes. For the CFX-4.4 simulations, an eight-block grid structure was constructed to get finite volume cells having higher orthogonalities. Test simulations were run with a coarse grid of 10,692 cells having 18 holes. The sensitivity of the simulation results was checked by comparing the results for 10,692, 32,784, and 42,716 cells (Figures 5.2 and 5.3). Figure 5.2 shows a macroscopic quantity, viz. clear

♣ Figures for this chapter are given starting on Page 49.

liquid height for three different grid sizes, while Figure 5.3 shows detailed velocity variation along two locations in the tray.

Figure 5.3 also includes the experimental data points as measured by Solari and Bell (1986). The authors made linear liquid velocity measurements along two lines perpendicular to the liquid flow direction on a plane 0.038 m above the tray floor. The probe positions are shown in Figure 5.4. Average linear liquid velocities were calculated by dividing the distance between two rows of probes by the time elapsed for the dye to cover this distance. In the model geometry, probes 5 to 8 lie on x = 0.209 m and probes 9 to 12 lie on x = 0.438 m. In order to compare the experimental measurements with the CFD predictions, line integrals of the horizontal component of the liquid velocity were taken on the plane y = 0.038 m between x = 0.209 m and x = 0.438 m. The resulting velocity profiles have been referred to as upstream profiles. Similarly, line integrals were taken between x = 0.438 m and x = 0.667 m for the measurements made between the middle of the tray and the outlet weir with the resulting velocity profiles designated as downstream profiles. From Figure 5.3, it is clear that no significant improvements are observed in the simulation results as the number of cells and holes are increased.

Using CFX-5.4, where the mesh was unstructured, it was possible to get results for the actual number of holes. As shown in Figure 5.5, the liquid velocity profile curves are closer to the experimental values for the finer mesh with the actual number of holes although the improvements are not very significant. Not unexpectedly, both CFX-4.4 and CFX-5.4 predict similar liquid velocity profiles. The physical models are exactly the same in both versions of the simulator.

5.4 Velocity Distributions

In Figures 5.5 to 5.8, liquid horizontal velocities predicted by the CFD simulations are compared against the experimental data of Solari and Bell (1986) for a range of operating conditions. Since the inlet velocity profiles were not characterized in their experiments, a few alternate specifications are considered for the inlet velocity profile. A parabolic liquid inlet velocity profile was used for most of the simulations while a flat

profile was used in few cases to assess the sensitivity of the flow profiles to the inlet conditions. The predictions are generally in good agreement with the experimental data. It has been observed that (Kister, 1992) at very low liquid rates, the liquid inlet velocity profile has a strong influence on the liquid flow profile within the tray. In the single-phase modeling work, a flat inlet profile was recommended for low values of the flow parameter F_{LV} ($F_{LV} < 0.25$). As Figure 5.7 shows, the parabolic and flat inlet profiles give comparable results at $F_S = 1.015$ for which the flow parameter ($F_{LV} = 0.25$) is on the borderline of the above recommendation. A flat inlet profile was used for the gas and liquid loads where $F_{LV} < 0.25$. In general, it can be concluded that the liquid *inlet velocity profile* should be a function of the liquid and gas flow rates and that it should have significant effect in the evolution of the flow in the interior of the tray. The uncertainties in the specification of this inlet boundary condition (which are often not well characterized in experiments) might be one of the reasons for some of the discrepancies observed between the CFD predictions and the experimental data. The liquid velocity profiles will be affected by the average liquid holdup fraction and drag coefficient correlations used in estimating the interphase drag term. Another source of error but a less significant one is the grid resolution and the number and size of holes (as shown in Figures 5.3 and 5.5). Overall, the model predictions are not far from the experimental errors. The slight oscillations observed in the lower liquid rate velocity profiles are caused by a high rate gas rising through a small number of holes.

From the experimental studies that have been conducted so far, particularly from the works of Solari et al. (1982) and Solari and Bell (1986), a general understanding of the liquid flow pattern inside trays has been developed as summarized in Chapter 2 and by Kister (1992). An assessment of the ability of the CFD model to predict the observations that have been made can be obtained with help of the liquid velocity profiles along specific lines as presented earlier; a more complete picture emerges with the liquid velocity vector plots shown in Figure 5.9. It should be noted that the liquid (or gas) velocity vector alone could be large even in zones where the corresponding liquid volume fraction is zero. Hence the product of the liquid velocity vector with the local liquid volume fraction is plotted, since it gives a true measure of local liquid flow rates. A non-

uniform liquid velocity distribution is observed in all cases. The liquid velocity decreases as one moves from the tray centre towards the tray wall. Solari and Bell (1986) made similar observations. As Solari and Bell (1986) remarked, the gas rate plays an important role in determining the liquid velocity distribution. The degrees of recirculation, channelling or stagnant zones that prevail depend on the gas rate. Having a fewer holes (Figure 5.9b) results in more uneven liquid distribution as compared to having more number of holes (Figure 5.9a). The liquid velocity distribution in the transverse direction is more uniform at higher gas rates (compare Figures 5.9c and 5.9d) as the increased gas rate helps to distribute the liquid more evenly. The non-uniform liquid velocity distribution in the transverse direction is more vivid at higher liquid rate (Figure 5.9a). This is expected since the given gas rate ($F_S = 0.462$) is high enough to shape the velocity distribution of the lower liquid rate as Solari et al. (1982) observed. At low gas rate and high liquid rate (corresponding to Figure 5.9a), the two-phase model for the CFX4.4 simulation with 42176 cells (not shown) tended to predict backward flow of liquid near the tray wall although it was weak. Finer resolution of the grid spacing near the tray wall provided by the CFX5.4 mesh eliminated the backward flow replacing it with a stagnant zone as seen in Figure 5.9a. Solari and Bell concluded this region to be a stagnant region after performing additional dye injection tests. The single-phase model at the given liquid and gas rate combination also predicted a stagnant zone. Comparing the vector plots for lower and higher liquid flow rates, the extent of liquid over shoot over the weir can be seen to be captured in a realistic manner in the simulations. For example in Figure 5.9c, the velocity vector head is pointed downwards immediately past the weir, whereas in Figure 5.9a, the inertia at the higher liquid flow rates carries the fluid into the central zone of the downcomer.

Additional insight into the gas and liquid flow behaviour predicted by the CFD model can be gained with the aid of streamlines. In Figure 5.10 are shown liquid and gas phase streamlines for three different combinations of gas and liquid loads giving a picture of how selected liquid and gas phase fluid particles flow from inlet to outlet. Turbulence and agitation by the gas phase (which is stronger at high gas rates, Figure 5.10b) force the liquid particles to follow wobbling paths. There is a noticeable circulation of liquid in the

downcomer. The free falling liquid impinging on the downcomer pool of liquid and floor, the narrow space in the downcomer, and the resistance to liquid flow caused by the narrow downcomer clearance are expected to cause this circulation. The downcomer circulation is in agreement with commonly observed liquid flow behaviour in single-pass cross flow sieve trays as described by Lockett (1986). The effect of the liquid flow on the gas phase streamlines is apparent from the bending of the gas phase streamlines in the direction of the liquid flow. The bending is more intense near the outlet weir because of increased liquid velocities as liquid starts to fall down from the weir. At low liquid rate (Figure 5.10c), the gas encounters almost no sideways push and it appears to flow in a straight path. Like wise, small or no vertical displacements of the liquid streamlines are seen at lower gas rates (Figure 5.10a) whereas at higher gas rates (Figure 5.10b) the liquid is pushed up significantly. These figures also confirm the path of the liquid flow in the downcomer zone with varying liquid flow rates. At low liquid rates, the weir crest is smaller and the liquid flows nearer to the downcomer wall. With increasing gas and liquid rates, the liquid trajectory shows a clear overshoot in the downcomer zone.

A major advantage of the extension to the two-phase modeling is the availability of the gas phase flow profiles. This is needed not only to get a measure of uniformity of the gas phase flow profile, but also in simulating the interphase mass transfer and thus calculating the Murphree tray efficiency, which is the next logical step in carrying out such detailed simulations. Selected profiles of the gas phase vertical component velocity are shown in Figure 5.11. In Figures 5.11a to 5.11c, the oscillations close to the tray floor correspond to the discrete distribution of holes. The magnitude of these oscillations decreases with increasing heights above the tray floor. As soon as the weir height is crossed, the gas velocity decreases owing to the increase in the cross-sectional area available for gas flow. The profile curves have maximum values directly above the inlet holes. There are four maxima corresponding to the four rows of holes encountered in sweeping from the tray centre to the tray wall at $x = 0.32$ m. The triangular pitch arrangement of the holes results in differences in the number of holes encountered between the tray centre and the tray wall at different values of x.

The longitudinal and transverse variations of the gas V velocity profiles are not significant except for the slightly large values of the velocity at the tray centre (Figure 5.11d). Thus the model did not predict any significant gas phase maldisttribution. Figure 5.12 shows that the variation of the liquid velocity profile, U(z), in the vertical direction is small in the active regions of the froth, i.e. from y = 0.019 m to y = 0.15 m. The two-phase modeling makes it possible to verify a hypothesis made in the single-phase modeling work of Mehta et al. (1998) viz. that the gas and liquid phases move with the same velocities in the longitudinal and transverse directions to liquid flow. As shown in Figure 5.13, the hypothesis is a reasonable one since on average the gas and liquid U component velocities have small differences in the active froth region of the sieve tray (e.g. y = 0.15 m). The differences are more pronounced, of course, close to the tray floor (y = 0.038 m).

The sensitivity of the predicted liquid velocity profile to liquid inlet turbulence intensity was checked. As Figure 5.14 shows, the variation of the predicted liquid velocity profile with liquid inlet turbulence intensity was found to be insignificant.

5.5 Clear Liquid Height, Froth Height, and Average Liquid Holdup Fraction in Froth

Having validated the simulation results against the experimentally measured *liquid velocity distributions*, several macroscopic results such as *clear liquid height, froth height* etc are computed and compared with existing correlations. It is essential that the CFD simulations predict the same trends as existing correlations, which have stood the test of time.

Clear liquid height is defined as the height of liquid that would exist on the tray in the absence of weeping and vapour flow. Using this definition, the clear liquid height has been calculated as the tray spacing multiplied by the volume average of the liquid volume fraction above the bubbling area of the tray floor. In Figures 5.15 and 5.16, predicted values of clear liquid height are compared with values calculated using various

correlations, including that proposed by Solari and Bell (1986). Note that the clear liquid height is predicted to decrease with increasing F-factor at a given liquid flow rate (Figure 5.15) and it is expected to increase with liquid flow rate at a given F-factor (Figure 5.16).

For trays operating in the froth regime, the correlations of Colwell (1979) and Bennett et al. (1983) are both good for clear liquid height prediction. The CFD predictions are slightly larger than the values obtained using the Solari and Bell (1986) proposed correlation. Van Baten and Krishna (2000) also found the CFD to give clear liquid height values that are larger than the experimental ones. They reasoned that this happened because the Bennett et al. correlation used in the interphase momentum drag term ignores coalescence caused by impurities.

It is known that the Bennett et al. (1983) correlation overpredicts the liquid holdup fraction in froth. From equation (4.14), at a given gas flow rate the use of the Bennett et al. (1983) correlation amounts to using a constant multiplier as drag coefficient. This constant factor is inversely proportional to the average liquid holdup fraction but it is proportional to the second power of the average gas holdup fraction. Overpredicting the average liquid holdup fraction results in a *reduction* in the interphase drag term. The gas then does not exert enough drag force on the liquid. This may be thought as if the tray is operating at a slightly lower gas rate than the actual one and hence a larger clear liquid height results. To verify this, we changed the gas holdup fraction correlation to that of Colwell's that is known to work well in the froth region. In Figure 5.16 it is verified that the Bennett et al. correlation does indeed lead to larger clear liquid height values as compared to Colwell's correlation.

Other factors that can lead to the overprediction include insufficient spatial resolution of the flow near the tray floor, use of a small number of holes, and use of large calming zones. Reducing the grid spacing in the vertical direction was not found to result in a significant change in the clear height value (see Figure 5.2). Use of a small number of holes is expected to lead to gas channelling that can result in an increased clear liquid height. Large calming zones have a similar effect as that of the use of a small number of holes.

Froth region is usually defined as the region in which the liquid volume fraction is greater than 10%. The average froth height has been calculated as the area average (over the tray deck-(x,z) plane) of the vertical distance (y) from the tray floor at which the liquid volume fraction starts to fall below 10%. Average liquid holdup fraction in froth is often defined as the ratio of clear liquid height to froth height. In conventional sieve tray design and analysis not all the three parameters-*clear liquid height*, *froth height* and *average liquid holdup fraction*-are independent. Given any two of the three, say clear liquid height and average liquid holdup fraction in froth, the third can be calculated (froth height is the ratio of clear liquid height to average liquid holdup fraction in froth). The CFD simulation allows determining all the three parameters independently, provided one uses a cut-off value of 10% in defining the froth region. For the liquid holdup fraction, two approaches were followed. One was as the ratio of clear liquid height to froth height and the other as the volume average of the liquid volume fraction in froth. In either case, we had to make use of the 10% value as the lower limit for the liquid volume fraction in the froth region. Both approaches gave results that are very close to each other as shown in Figure 5.17. This validates the 10% cut-off value used in defining the froth region.

Predicted values of average liquid holdup fraction in froth are shown in Figure 5.17 compared against correlations recommended for this parameter. The CFD simulation gives values that are very close to the values calculated using the Bennett et al. (1983) correlation. Froth height prediction results are shown in Figure 5.18. Comparisons are made with two correlations. Here again the use of the Bennett et al. correlation is expected to lead to a shorter froth height since the gas is not exerting enough force to expand the liquid as high as it should. Taking into account the many uncertainties involved in the correlations used to estimate these parameters, the CFD predictions are quite acceptable.

More profiles of volume fraction dependent quantities are given in Figures 5.19 to 5.21. Figure 5.19 shows shaded contour plots of liquid volume fraction profiles on a vertical plane 0.01m from the tray centre. Almost all the liquid resides near the tray floor. No weeping is expected since the way the CFD imposes and solves boundary conditions does not allow this. From the weir height up, the liquid presence diminishes rapidly until

it suddenly seems to disappear leaving most of the tray space to be filled with the gas phase. The gas is seen reducing the liquid volume fraction around the gas inlet holes as it finds a way up through the pool of liquid on the tray floor. The dispersion density of the froth is more uniform for the actual number of holes (Figure 5.19c). At high gas rate (Figure 5.19d), the expansion of the froth height and the reduction of the average liquid holdup fraction above the tray floor are more pronounced than those at lower gas rates (Figure 5.19b).

Figure 5.20 shows dispersion height versus liquid dispersion density profiles. For a given liquid rate, the dispersion density decreases while the dispersion height increases as the gas rate is increased. Clear liquid height profiles determined from averages of the liquid volume fraction on vertical slices above the tray floor are shown in Figure 5.21. The clear-liquid heights are larger near the liquid entrance and the outlet weir supporting the explanation made earlier concerning the effect of calming zones. Similarly, larger clear liquid heights are seen at the tray centre and near the tray wall where there are no gas inlet holes.

5.6 Conclusion

This work has attempted to predict the flow patterns and hydraulics of a commercial scale sieve tray by means of computational fluid dynamics (CFD). The flow inside the tray was modeled as a three-dimensional two-phase flow of gas and liquid in the Eulerian-Eulerian framework. The time and volume averaged continuity and momentum equations were numerically solved using the commercial packages CFX-5.4 and CFX-4.4 of AEA Technology. The gas and liquid phase equations were coupled through an interphase momentum transfer term that was estimated locally using the drag coefficient correlation of Krishna et al. (1999a) and the Bennett et al. (1983) liquid holdup fraction correlation. The CFD was used to predict velocity distributions, clear liquid height, froth height, and liquid holdup fraction in froth for various combinations of gas and liquid rates. The simulation results exhibit all of the known features of the two-

phase flow field in sieve trays and are in good agreement with the experimental results of Solari and Bell (1986).

Experiments for trays have proved to be expensive and time consuming. That is why only very few attempts have been made so far to determine fluid flow patterns inside trays. Modeling using CFD overcomes many of the limitations associated with experiments. Of paramount importance are its capability to give complete information and the ease with which one can change tray geometry and operating conditions without incurring appreciable cost. From this work, we conclude that even with a simple interphase transfer model, we were able to get results that closely match the experimental data. With more refined models, such as a more accurate interphase momentum transfer relation and the inclusion of energy and mass transfer, we expect to get more accurate predictions. The results of this work show that CFD can be used as an invaluable tool in the design and analysis of industrial trays.

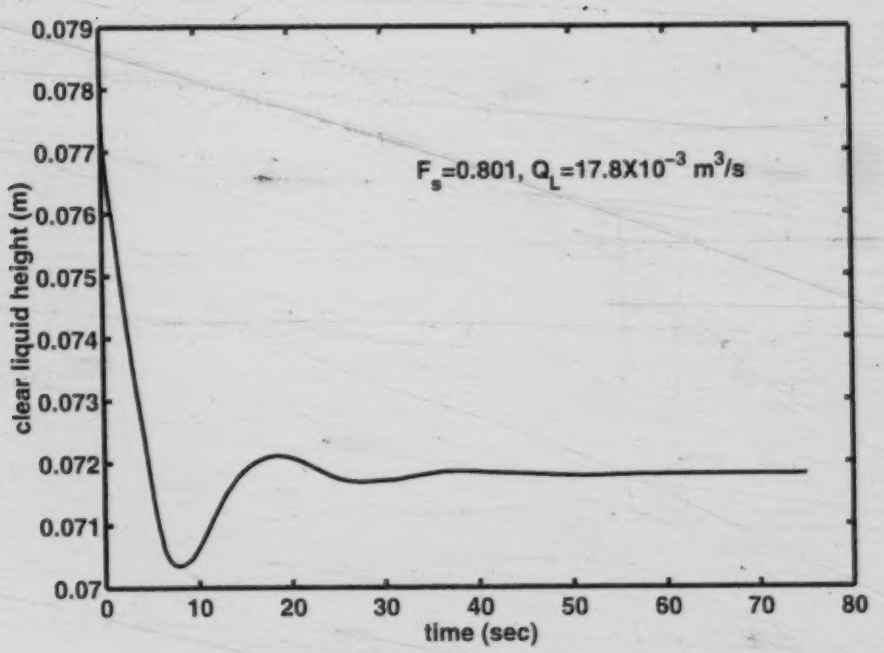

Figure 5.1 Transient simulation convergence as indicated by a plot of clear liquid height versus time. A transient simulation is assumed to have converged whenever the clear liquid height does not appreciably change with time.

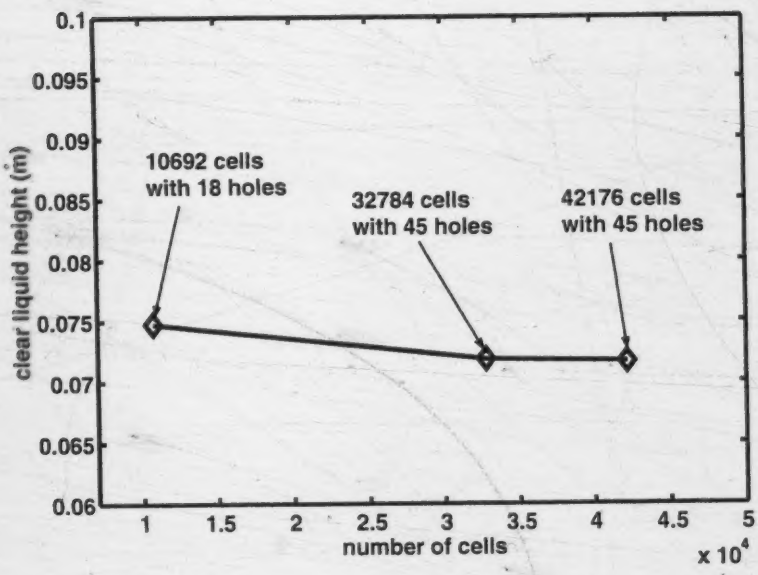

Figure 5.2 Sensitivity of the clear liquid height prediction to grid spacing, and hole number and size, $Q_L = 6.94 \times 10^{-3} m^3/s$, $F_s = 0.462$ (CFX4.4)

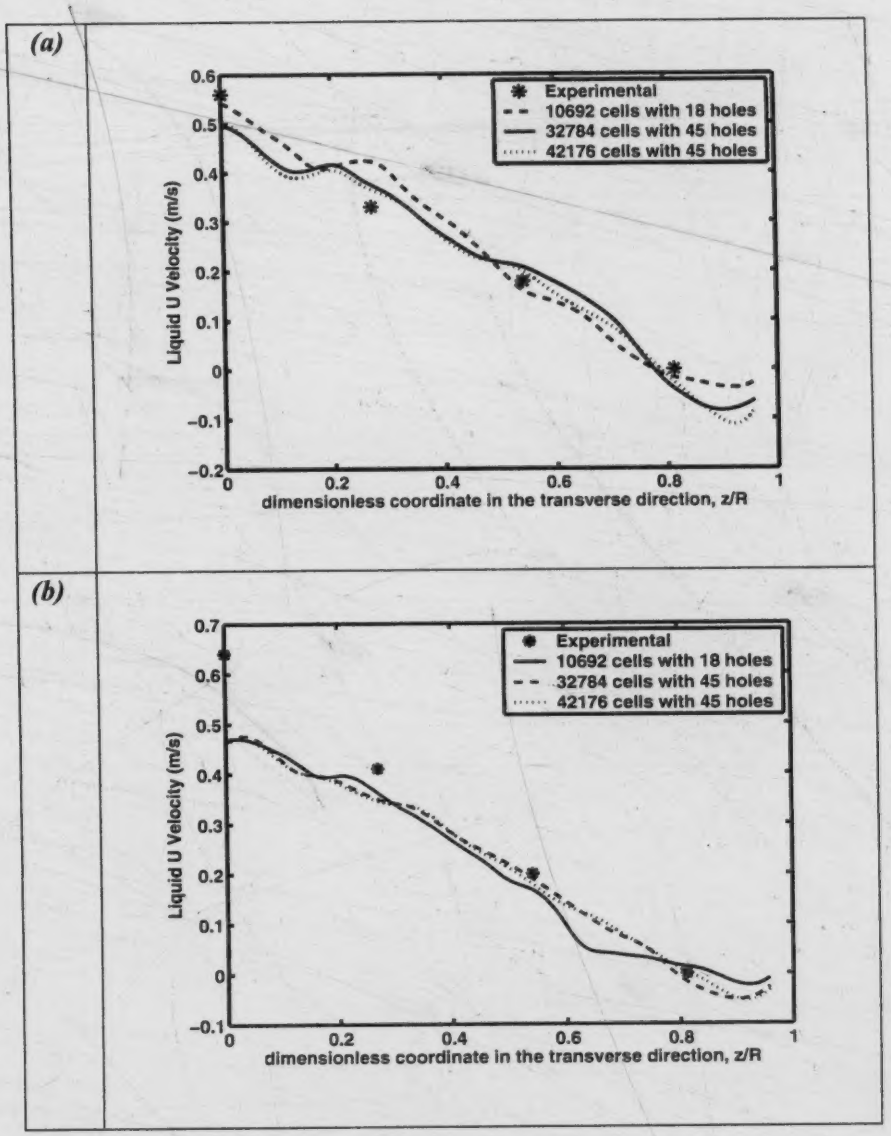
(a)
Experimental
10692 cells with 18 holes
32784 cells with 45 holes
42176 cells with 45 holes
Liquid U Velocity (m/s)
dimensionless coordinate in the transverse direction, z/R
(b)
Experimental
10692 cells with 18 holes
32784 cells with 45 holes
42176 cells with 45 holes
Liquid U Velocity (m/s)
dimensionless coordinate in the transverse direction, z/R

Figure 5.3 Sensitivity of the liquid velocity profile prediction to grid spacing, and hole number and size (CFX4.4), $Q_L = 17.8 \times 10^{-3} m^3/s$, F_s = 0.462. (a) Upstream profile, (b) downstream profile.

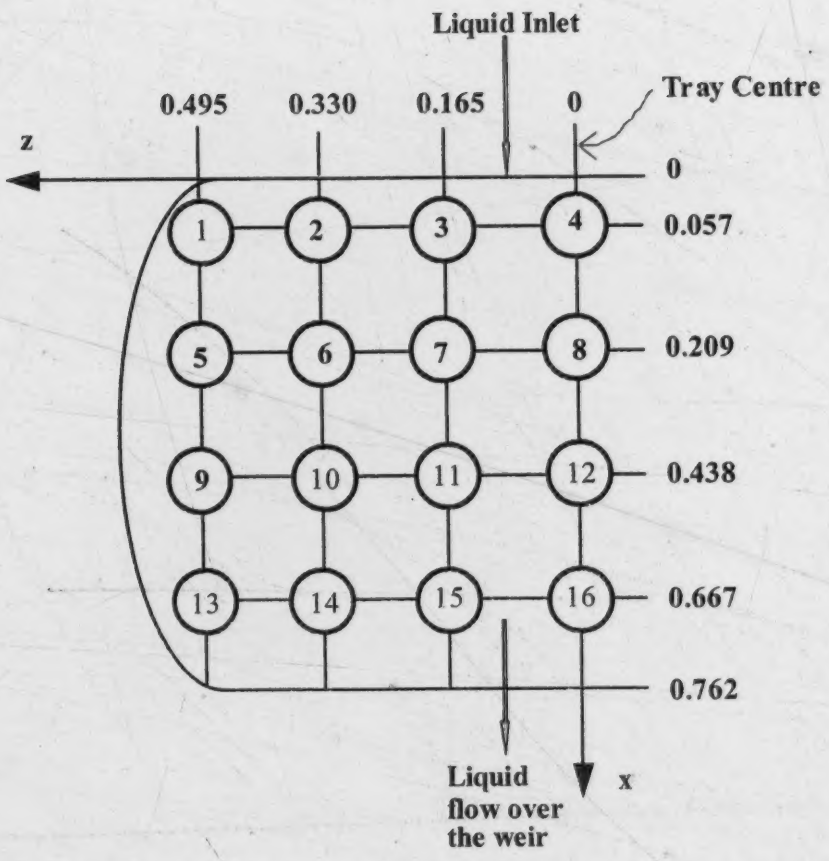

Figure 5.4 Experimental probe positions of Solari and Bell (1986). All measurements are in meters. The plane of the probes is at an elevation of 0.038m above the tray floor.

(a)

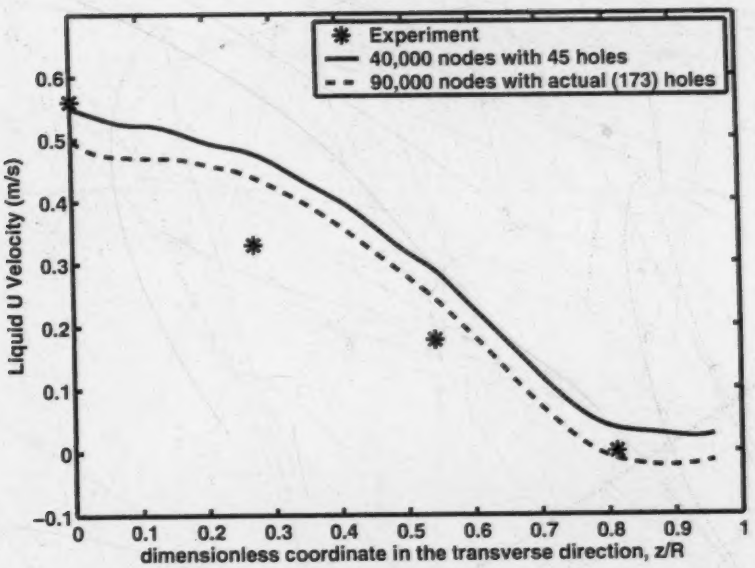
Experiment
40,000 nodes with 45 holes
90,000 nodes with actual (173) holes
Liquid U Velocity (m/s)
dimensionless coordinate in the transverse direction, z/R

(b)

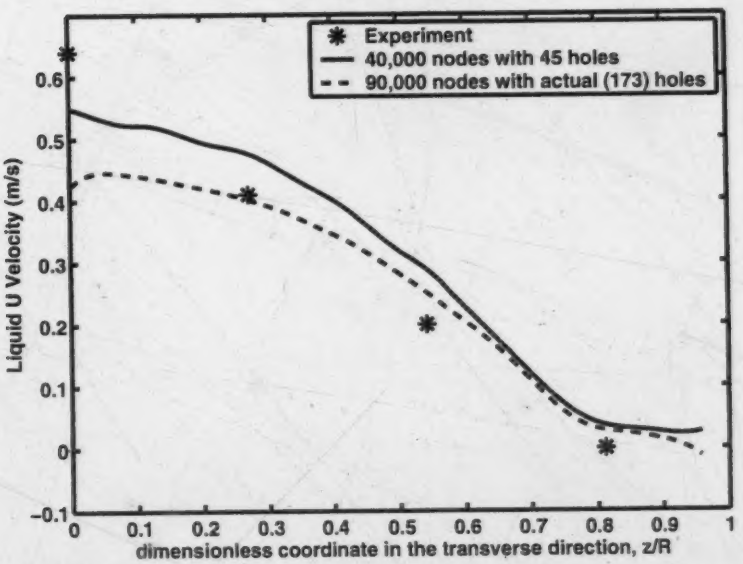
Experiment
40,000 nodes with 45 holes
90,000 nodes with actual (173) holes
Liquid U Velocity (m/s)
dimensionless coordinate in the transverse direction, z/R

Figure 5.5 Liquid velocity profile, $Q_L = 17.8 \times 10^{-3} m^3/s$, $F_s = 0.462$ (CFX5.4) (a) Upstream profile, (b) downstream profile.

(a)

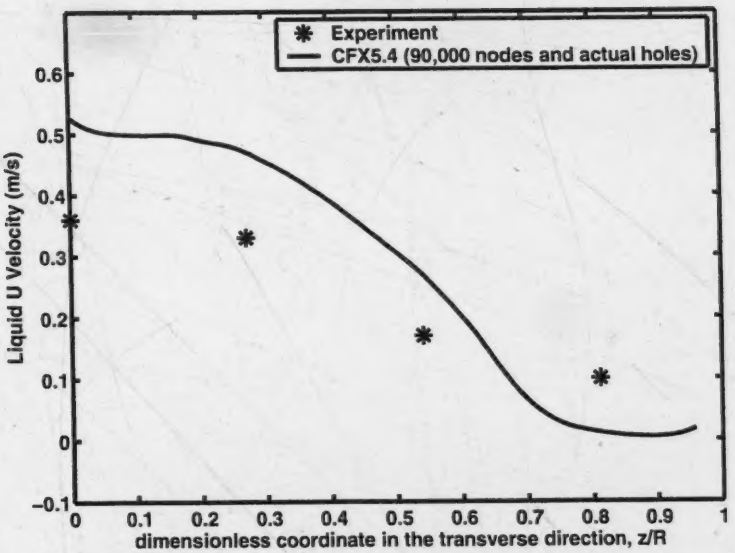
Experiment
CFX5.4 (90,000 nodes and actual holes)
Liquid U Velocity (m/s)
dimensionless coordinate in the transverse direction, z/R

(b)

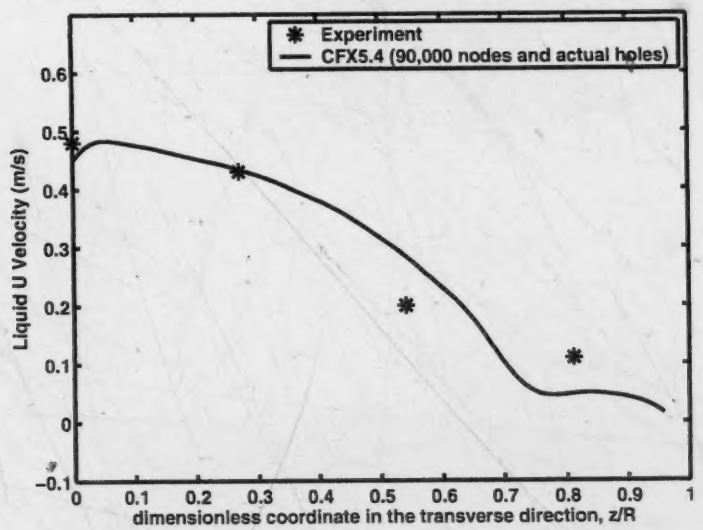
Experiment
CFX5.4 (90,000 nodes and actual holes)
Liquid U Velocity (m/s)
dimensionless coordinate in the transverse direction, z/R

Figure 5.6 Liquid velocity profile, $Q_L = 17.8 \times 10^{-3} m^3/s$, $F_s = 0.801$. (CFX5.4).(a) Upstream profile, (b) downstream profile.

(a)

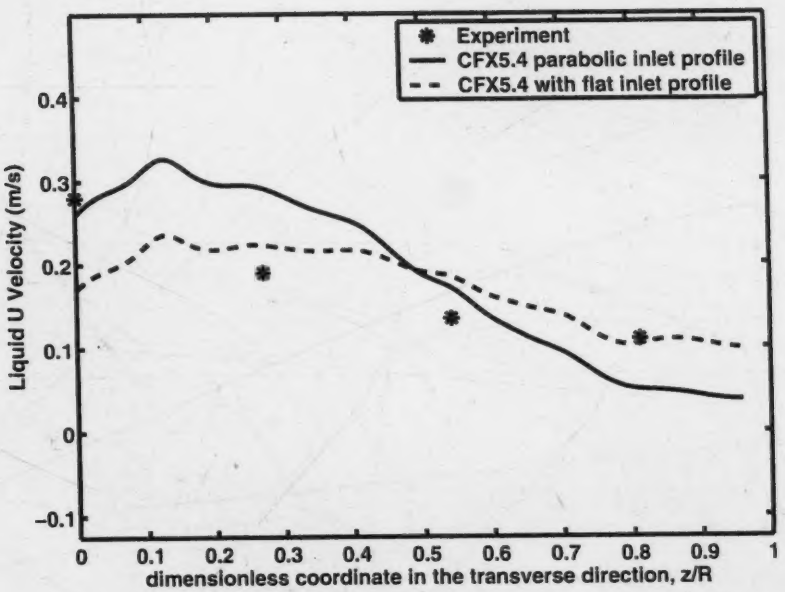

(b)

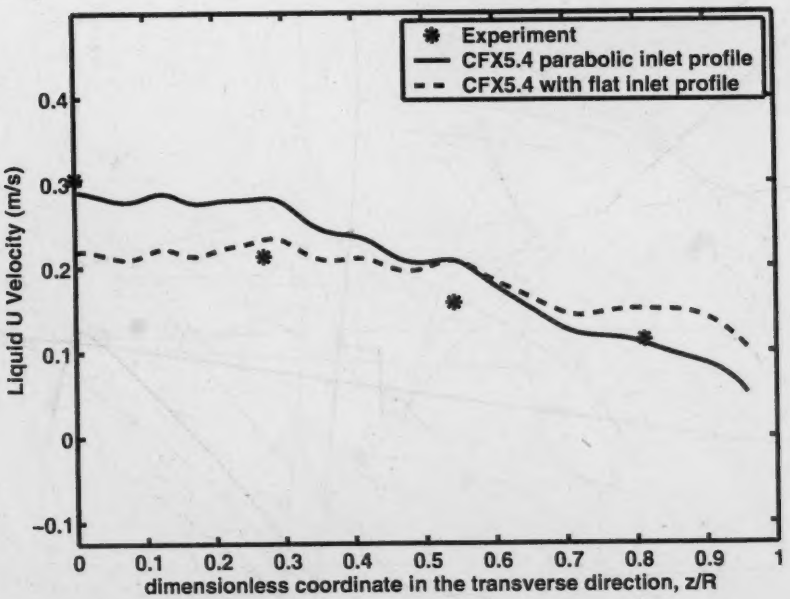

Figure 5.7 Liquid velocity profile, $Q_L = 6.94 \times 10^{-3} m^3/s$, $F_s = 1.015$. (CFX5.4) (a) Upstream profile, (b) downstream profile

(a)

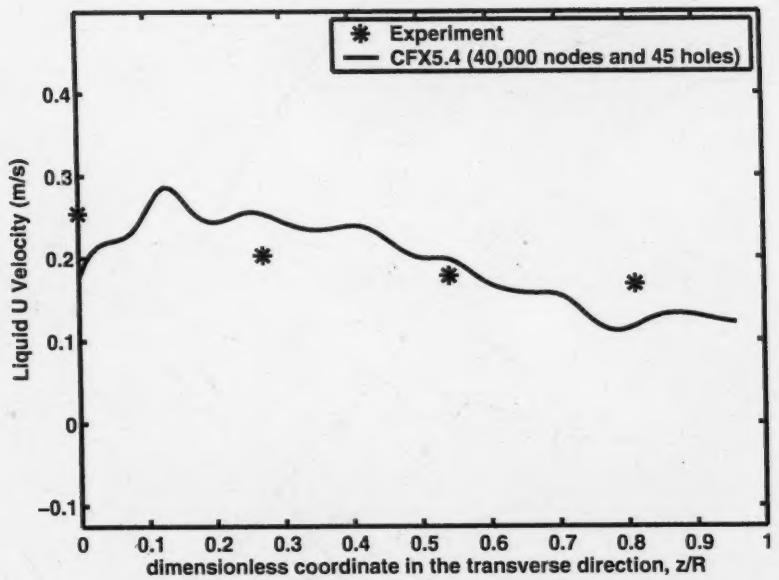

(b)

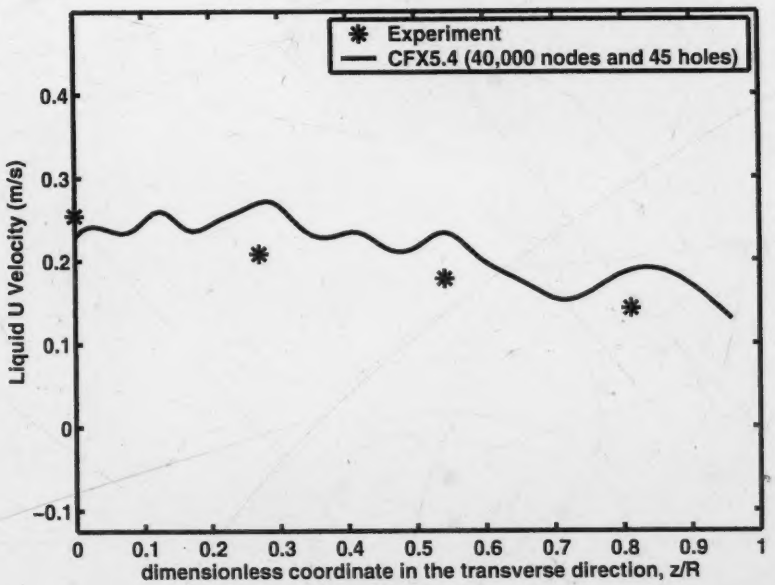

Figure 5.8 Liquid velocity profile, $Q_L = 6.94 \times 10^{-3} m^3/s$, $F_s = 1.464$, with a flat inlet profile (CFX5.4) (a) Upstream profile, (b) downstream profile

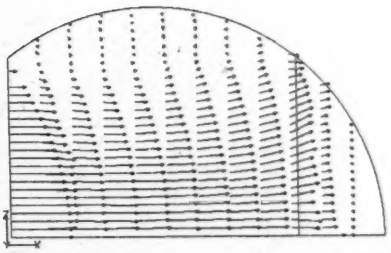

(a) $Q_L = 17.8 \times 10^{-3} m^3/s$, $F_S = 0.462$, Parabolic inlet profile (CFX5.4-90,000 nodes with actual number of holes)

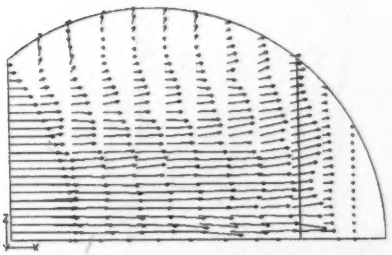

(b) $Q_L = 17.8 \times 10^{-3} m^3/s$, $F_S = 0.462$, Parabolic inlet profile (CFX5.4-40,000 nodes with 45 holes)

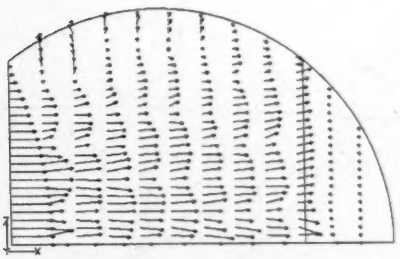

(c) $Q_L = 6.94 \times 10^{-3} m^3/s$, $F_S = 0.462$, Parabolic inlet profile (CFX5.4-40,000 nodes with 45 holes)

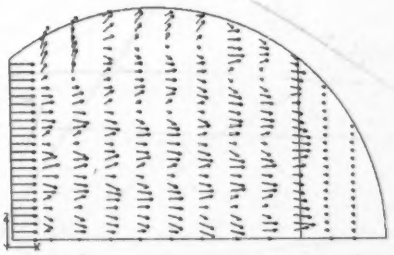

(d) $Q_L = 6.94 \times 10^{-3} m^3/s$, $F_S = 1.464$, Flat inlet profile (CFX5.4-40,000 nodes with 45 holes)

Figure 5.9 Liquid velocity vector plots on the plane of the experimental probes. A modified liquid velocity vector, which is a product of the liquid velocity vector and the liquid volume fraction, was used in obtaining the magnitudes of the velocity vectors shown.

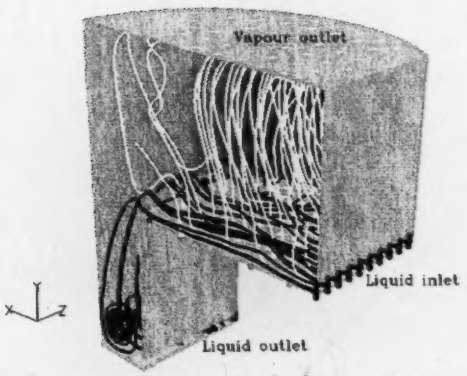

(a) $Q_L = 17.8 \times 10^{-3} m^3/s$, $F_S = 0.462$

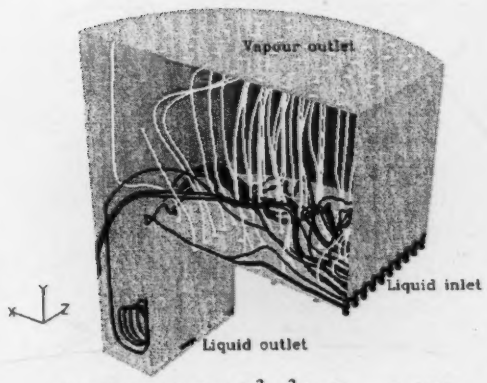

(b) $Q_L = 17.8 \times 10^{-3} m^3/s$, $F_S = 1.464$

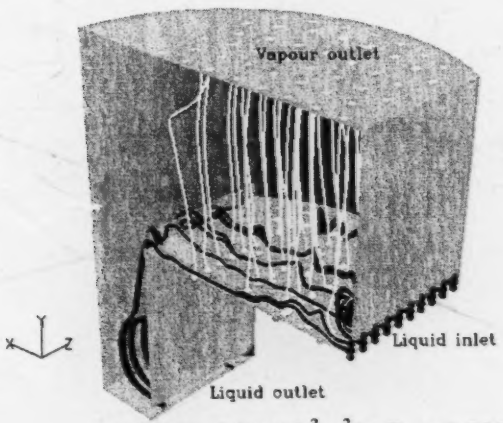

(c) $Q_L = 6.94 \times 10^{-3} m^3/s$, $F_S = 0.801$

Figure 5.10 Selected streamline profiles of liquid (in black) and gas (in white).

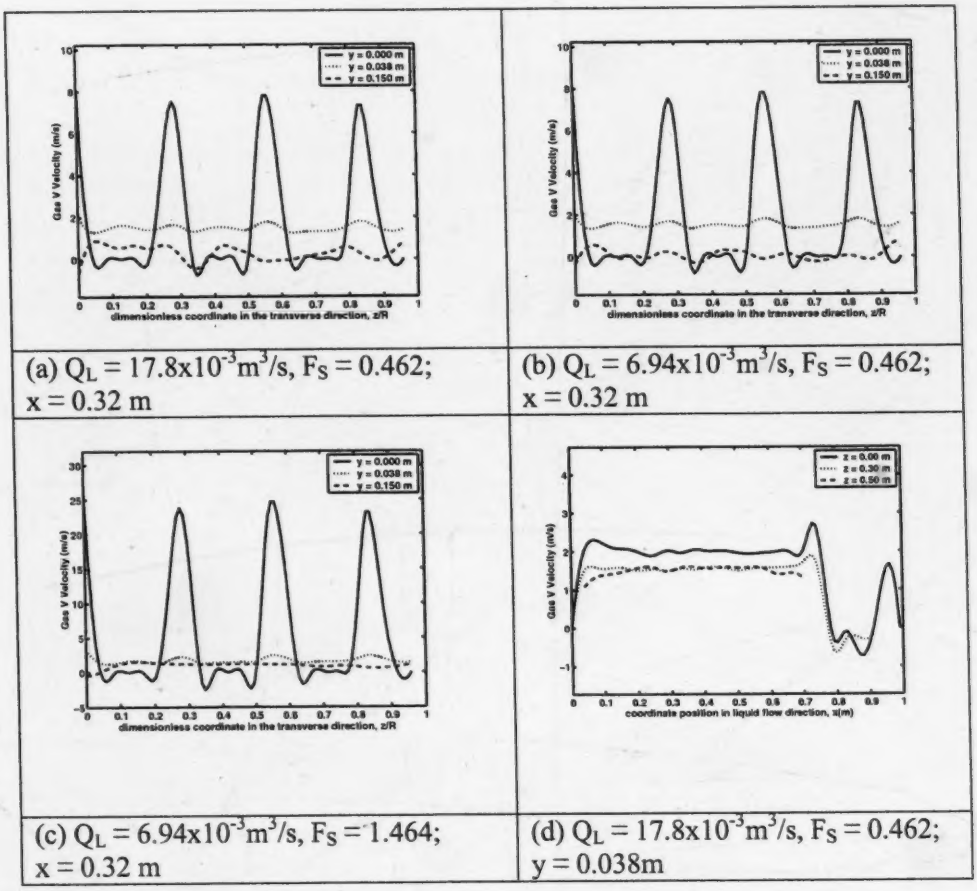
y = 0.000 m
y = 0.038 m
y = 0.150 m
Gas V Velocity (m/s)
dimensionless coordinate in the transverse direction, z/R
z = 0.00 m
z = 0.30 m
z = 0.50 m
coordinate position in liquid flow direction, x(m)

(a) $Q_L = 17.8 \times 10^{-3} m^3/s$, $F_S = 0.462$; $x = 0.32$ m

(b) $Q_L = 6.94 \times 10^{-3} m^3/s$, $F_S = 0.462$; $x = 0.32$ m

(c) $Q_L = 6.94 \times 10^{-3} m^3/s$, $F_S = 1.464$; $x = 0.32$ m

(d) $Q_L = 17.8 \times 10^{-3} m^3/s$, $F_S = 0.462$; $y = 0.038$m

Figure 5.11 (a) to (c) Gas V velocity profiles at different elevations above tray floor. (d) Gas V velocity profiles in the longitudinal direction to the liquid flow.

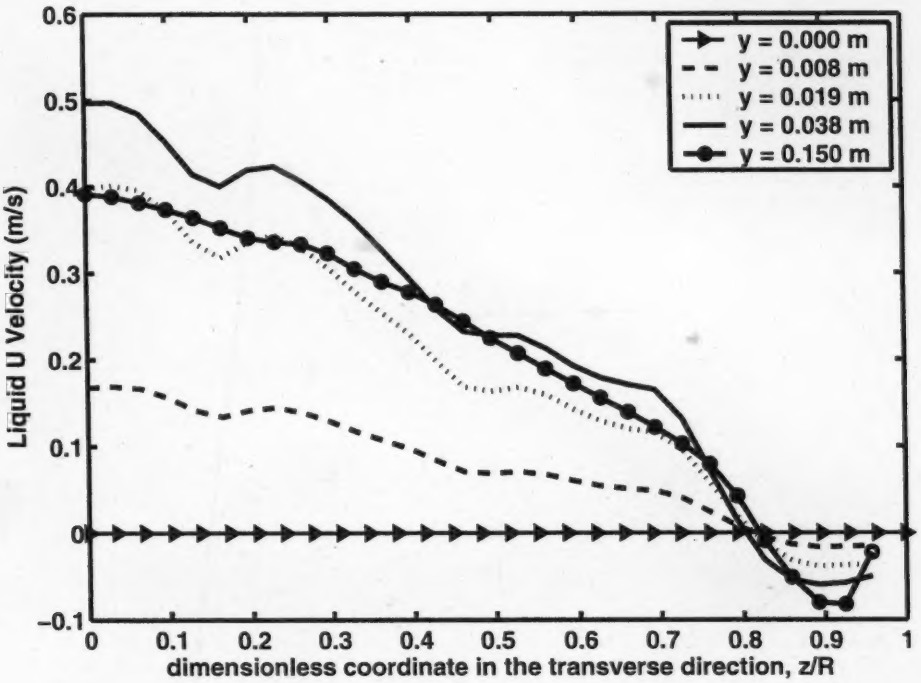

Figure 5.12 Average liquid U velocity profiles at different elevations above tray floor. Average taken between x = 0.209 m and x = 0.438 m, Q_L = $17.8 \times 10^{-3} m^3/s$, F_s = 0.801 (from CFX4.4- 32,784 cells and 45 holes).

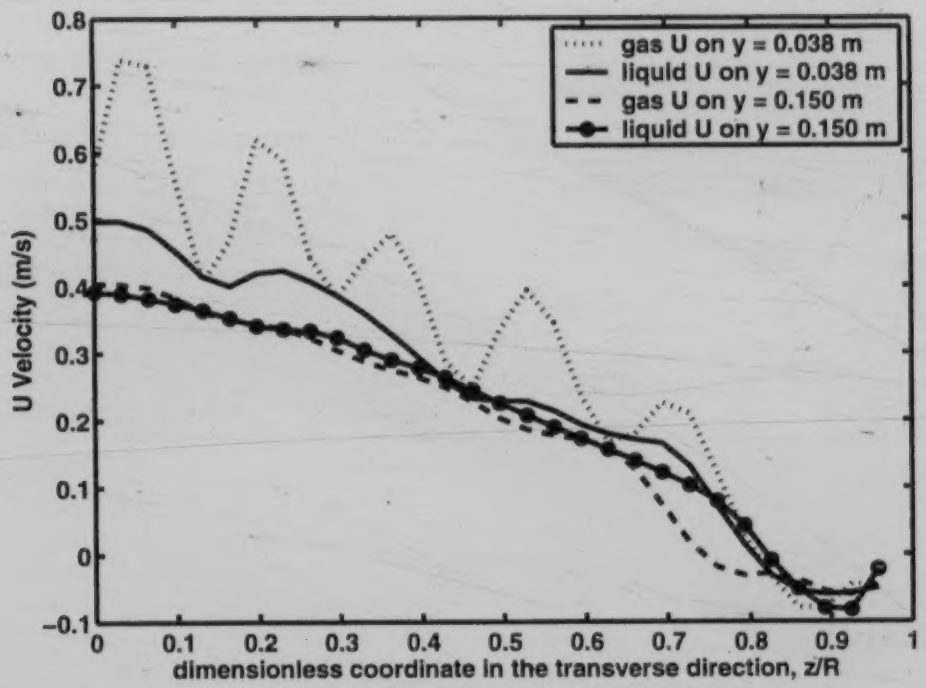

Figure 5.13 Average gas and liquid U velocity profiles at different elevations above tray floor. Averages taken between x = 0.209 m and x = 0.438 m, $Q_L = 17.8 \times 10^{-3} m^3/s$, $F_s = 0.801$ (from CFX4.4-32,784 cells and 45 holes).

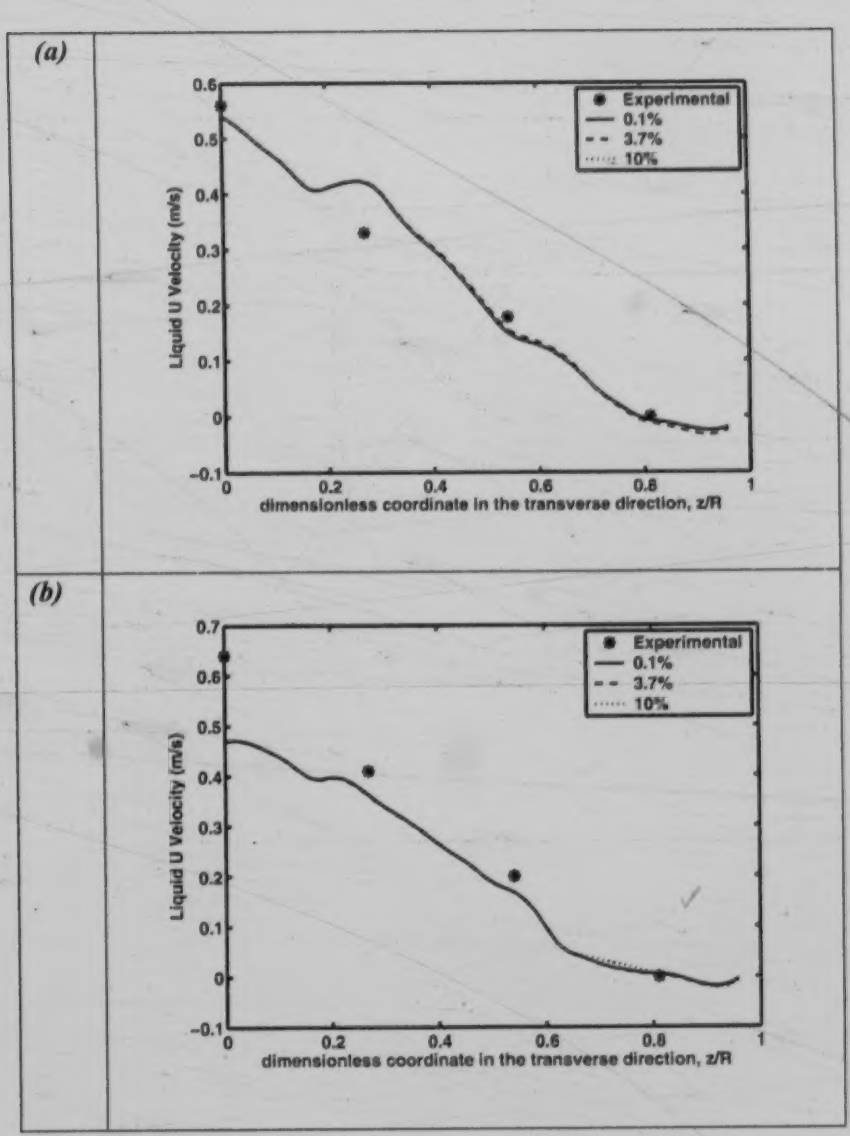

Figure 5.14 Sensitivity of the liquid velocity profile prediction to turbulence intensity at liquid inlet (CFX4.4), $Q_L = 17.8 \times 10^{-3} m^3/s$, F_s = 0.462.(a) Upstream profile, (b) downstream profile.

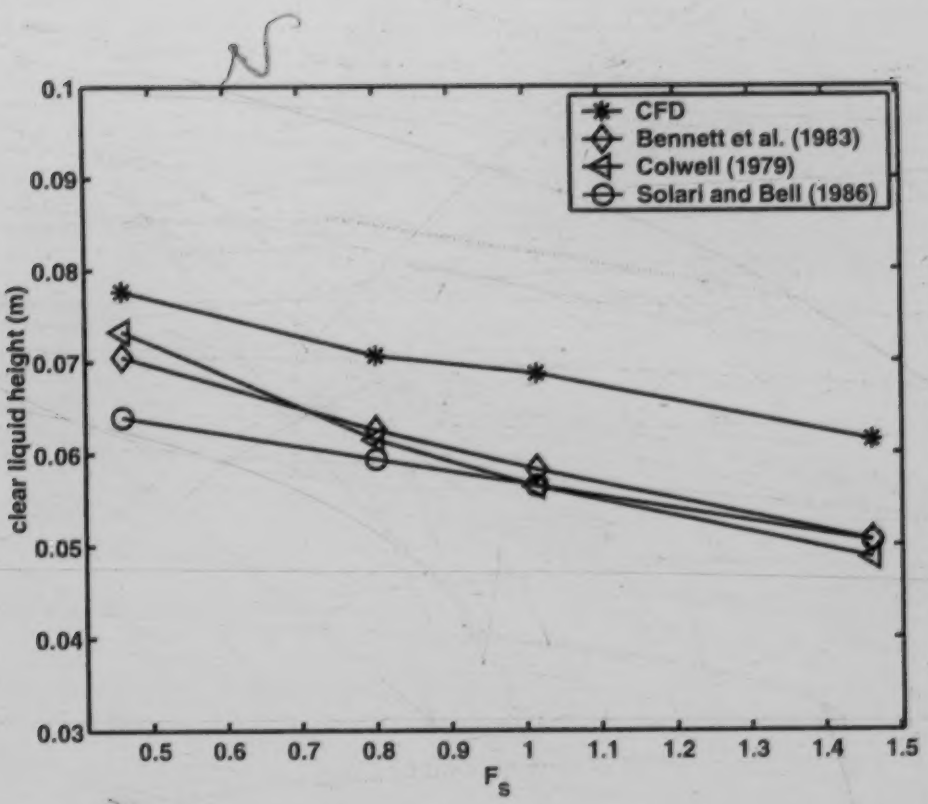

Figure 5.15 Clear liquid height as a function of F-factor F_s, Q_L= 17.8x10^{-3} m^3/s

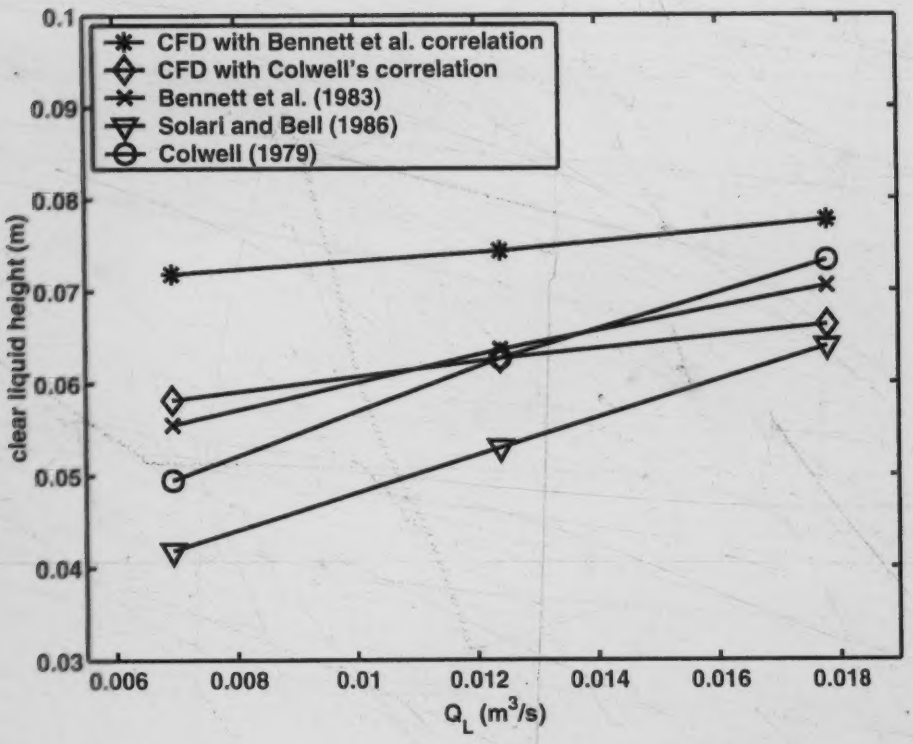

Figure 5.16 Clear liquid height as a function of liquid rate Q_L, Fs = 0.462

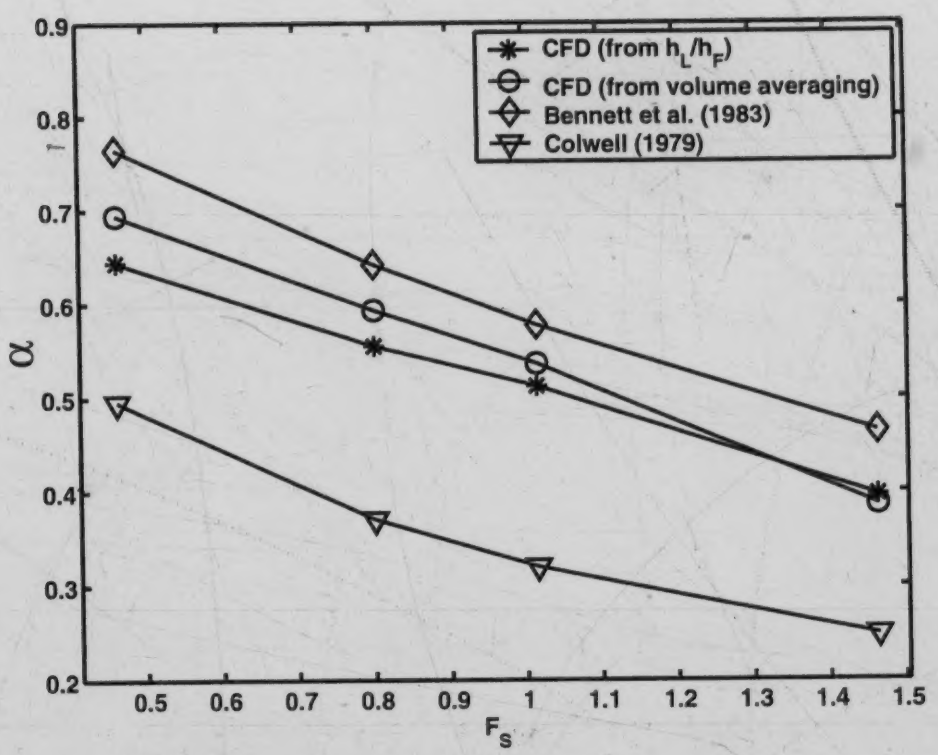

Figure 5.17 Average liquid holdup fraction in froth α as a function of F-factor F_S, $Q_L = 17.8 \times 10^{-3}$ m^3/s

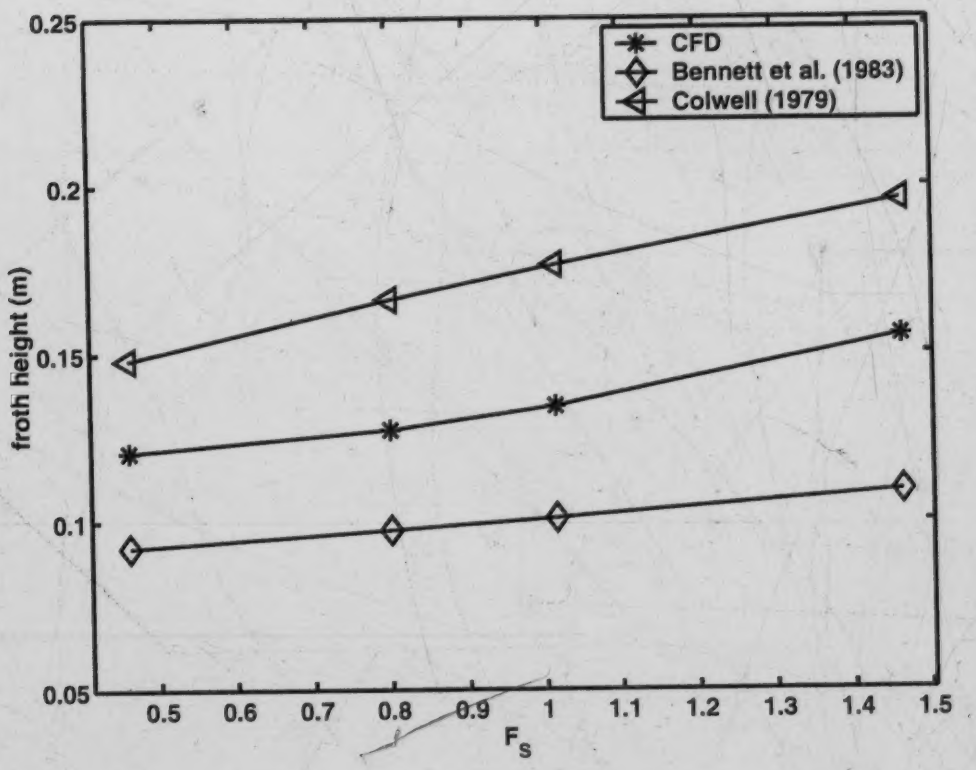

Figure 5.18 Average froth height h_F as a function of F-factor F_S, Q_L = 0.0178 m^3/s

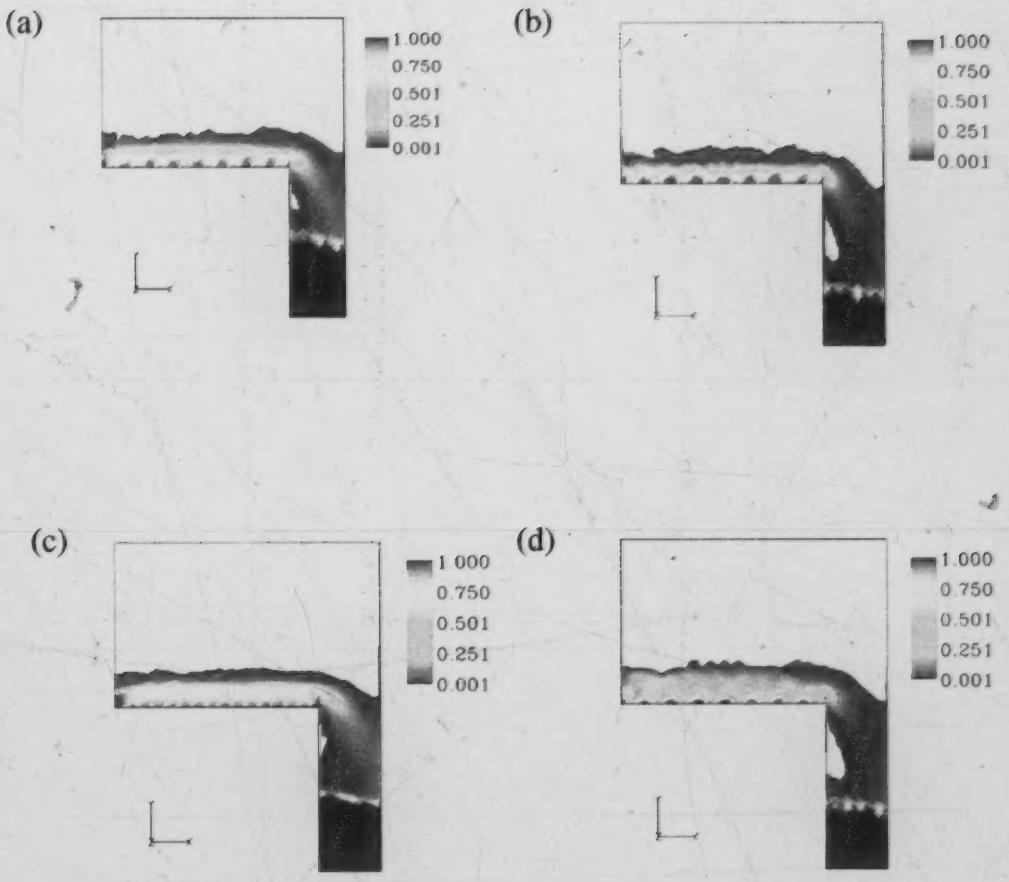

Figure 5.19 Liquid volume fraction profiles on a vertical section 0.01m from the tray centre
(a) $Q_L = 17.8 \times 10^{-3} m^3/s$, $F_S = 0.462$ (40,000 nodes with 45 holes)
(b) $Q_L = 6.94 \times 10^{-3} m^3/s$, $F_S = 0.462$ (40,000 nodes with 45 holes)
(c) $Q_L = 17.8 \times 10^{-3} m^3/s$, $F_S = 0.462$ (90,000 nodes with actual number of holes)
(d) $Q_L = 6.94 \times 10^{-3} m^3/s$, $F_S = 1.464$ (40,000 nodes with 45 holes)

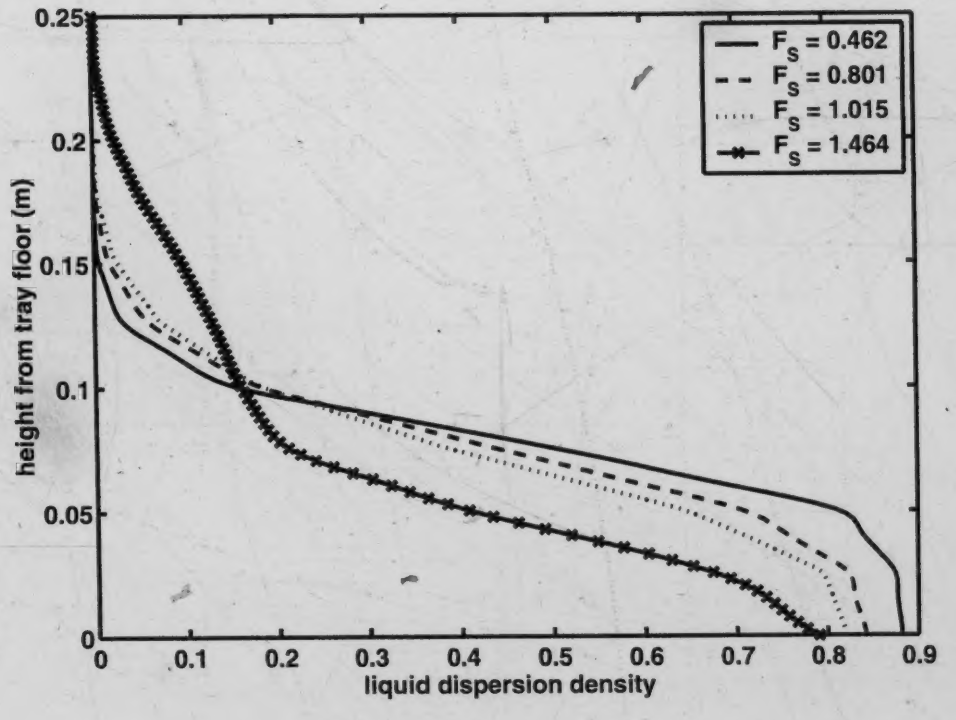

Figure 5.20 Dispersion height vs. liquid dispersion density profile, Q_L = 6.94×10^{-3} m^3/s

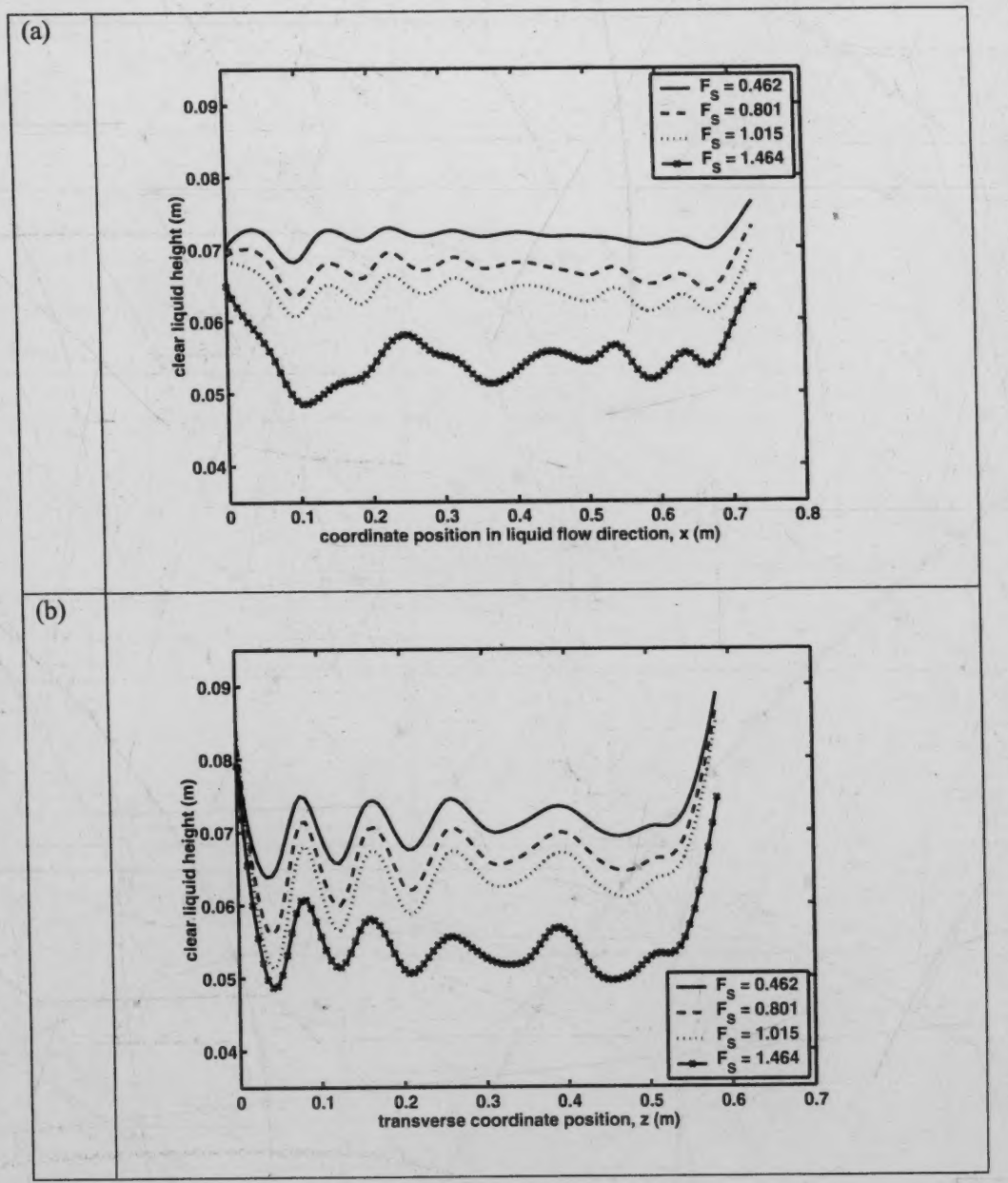

Figure 5.21 Clear liquid height profiles in longitudinal and transverse directions to liquid flow, $Q_L = 6.94 \times 10^{-3} m^3/s$. (a) averaged in the y and z directions. (b) averaged in the x and y directions

Chapter 6 Further Work

6.1 Mass Transfer Modeling and Prediction of Sieve Tray Efficiency

The next most logical step is the modeling of the interphase mass transfer and the prediction of point and average mass transfer efficiencies. After all, all the efforts in the tray design are aimed at the maximization of speed and efficiency of mass transfer. An ultimate goal of the CFD modeling should thus be the modeling of the interphase mass transfer and the prediction of point and average mass transfer efficiencies. Model for the interphase mass transfer needs to be provided. From the numerical solutions of the species conservation equations, point values of the vapour and liquid phase compositions of the light component (assuming a binary mixture) will be available. From these, point and average mass transfer efficiencies of a tray can be computed. The prediction results need to be validated using experimental data. For example, one can use databases used by Bennett et al. (1997), Garcia and Fair (2000a), and Chen and Chuang (1993). Plaka et al. (1989), Korchinsky (1994), and Korchnisky et al. (1994) give additional data.

The success of the tray hydrodynamics simulation means that the mass transfer modeling work is very likely to be successful. Specifically, the hydrodynamics provides velocity and volume fraction fields to the species conservation equations.

6.2 Prediction of Residence Time Distributions

Residence time distribution (RTD) has been extensively used to characterize mixing and flow non-idealities in process vessels. It is a worthwhile effort to investigate the use of CFD as a prediction tool for the residence time distributions of the liquid and gas phase. This will need two inputs. One is the specification of an effective diffusion or dispersion coefficient that is to be used in the equation for the dispersion model of a passive scalar. The second one is validation of the predicted results using experimental data. For the first and the liquid phase, one can, for example, use the correlation of

Zuiderweg (1982) for eddy diffusivity. This correlation has been recommended by Lockett (1986) and Korchinsky (1994) compared to other available correlations.

For the validation of the CFD predictions, the data given by Bell (1972a,b) and Solari and Bell (1986) are the most extensive. Unfortunately, in all the RTD experiments of the authors, tracer was fed to the downcomer leading to the 4^{th} tray whereas measurements were made on the 3^{rd} tray. Thus, the measured RTD included downcomer mixing times. Besides, reported are only the contour plots while validating the CFD predictions requires values of the tracer concentrations at each sampling time at all probes. Except for these works, most of the studies made so far have been to take into account the liquid mixing on the tray by means of dispersion models where diffusion coefficients were extracted and used as measures of the extent of liquid mixing. Therefore, it is suggested that experiments be carried out to avail data not only for the CFD prediction validation but also to distinguish between downcomer and tray mixing effects.

The CFD prediction is expected to be very likely successful because of the success of the hydrodynamics modeling. The hydrodynamics provides velocity and volume fraction fields to the passive scalar (tracer material) transport equations.

6.3 Using CFD in Tray Design Studies

Once CFD is established as a prediction and analysis tool, we will have a powerful tool at our hand for the study of different tray deck designs and contacting mechanisms. For example, one can compare the performance of a normal sieve tray with a slotted one. Others like the use of baffles, flow straighteners, slopped downcomers, etc. can be easily studied. Two practical examples include those of Nutter (1999) and Fair et al. (1999). Nutter compares the MVG^{TM} tray with a sieve tray. Fair et al. propose an ultracapacity tray. In general, one can think of and study all strategies of tray design meant to control the flows and interactions of the vapour and liquid at the boundaries and at points within the tray.

Bibliography

American Institute of Chemical Engineers (AIChE), *Bubble-Tray Design Manual*, New York (1958)

Anderson, J. D., *Computational Fluid Dynamics: The Basics with Applications*, McGraw-Hill, New York (1995)

Banerjee, S., "Modelling Considerations for Turbulent Multiphase Flows," Engineering Turbulence Modelling and Experiments: Proceedings of the International Symposium on Engineering Turbulence Modelling and Measurements held in September 24-28, 1990 Dobrovnik, Yugoslavia/editors, W. Rodi, E. N. Ganic

Bell, R. L., "Experimental Determination of Residence Time Distributions on Commercial Scale Trays using a Fibre Optic Technique", *AIChE Journal*, **18**, 491 (1972a).

Bell, R. L., "Residence Time and Fluid Mixing on Commercial Scale Sieve Trays", *AIChE Journal*, **18**, 498 (1972b).

Bell, R. L., and R. B. Solari, "Effect of Nonuniform Velocity Fields and Retrograde Flow on Distillation Tray Efficiency," *AIChE Journal*, **20**, 688 (1974).

Bennett, D. L., R. Agrawal, and P. J. Cook, "New Pressure Drop Correlation for Sieve Tray Distillation Columns," *AIChE Journal*, **29**, 434 (1983).

Bennett, D. L., D. N. Watson, and M. A. Wiescinski, "New Correlation for Sieve-Tray Point Efficiency, Entrainment and Section Efficiency," *AIChE Journal*, **43**, 1611 (1997).

Bird, R. B., W. E. Stewart, and E. N. Lightfoot, *Transport Phenomena*, Wiley, New York (1960)

Borchers, O., C. Busch, A. Sokolichin, G. Eigenberger, "Applicability of the standard k-ε turbulence model to the dynamic simulation of bubble columns. Part II: Comparison of detailed experiments and flow simulations," *Chem. Eng. Sci.*, **54**, 5927 (1999).

Brandt, A., "Multilevel adaptive technique (MLAT) for fast numerical solutions to boundary value problems," *Lecture Notes in Physics 18*, Springer-Verlag, Berlin (1972).

Brandt, A., "Multilevel adaptive solutions to boundary value problems," *Math. Comp.*, **31**, 333 (1977).

Brandt, A., "On multigrid solution of high Reynolds incompressible entering flows," *J. Com. Phys.*, 151 (1992).

Chan, H., and J. R, Fair, "Prediction of point efficiencies on sieve trays," *Ind. Eng. Chem. Proc. Des. Dev.*, **23**, 814 & 820 (1984).

Chen, G. X. and K. T. Chuang, "Prediction of Point Efficiency for Sieve Trays in Distillation," *Ind. Eng. Chem. Res.*, **32**, 701 (1993).

Chung, T. J., *Computational Fluid Dynamics*, Cambridge University Press, Cambridge (2002).

Colwell, C. J., "Clear liquid height and froth density on sieve trays," *Ind. Eng. Chem. Proc. Des. Dev.*, **20**, 298 (1979).

Courant, R., E. Isaacson, and M. Rees, "On the Solution of Non-linear Hyperbolic Differential Equations by Finite Differences," *Comm. Pure Appl. Math.*, **5**, 243 (1952).

Crowe, C., M. Sommerfield, and Y. Tsuji, *Multiphase Flows with Droplets and Particles*, CRC Press, Boca Raton (1998).

Fair, J. R., W. R. Trutna, and A. F. Seibert, "A New, Ultracapacity Tray for Distillation Columns," *Chem. Eng. Res. Des.*, **77**, 619 (1999).

Favre, A., "Equations des Gaz Turbulents Compressibles," *Journal de Mecanique*, **4**, 361 (1965)

Ferziger, J. H., and M. Perić, *Computational Methods for Fluid Dynamics*, Springer-Verlag, Berlin (1996).

Fischer, C. H., and J. L. Quarini, "Three-dimensional heterogeneous modelling of distillation tray hydraulics," Paper presented at the AIChE Annual Meeting, 15-20 November 1998, Miami Beach, USA.

Garcia, J. A., and J. R. Fair, "A Fundamental Model for the Prediction of Distillation Sieve Tray Efficiency. 1. Database Development," *Ind. Eng. Chem. Res.*, **39**, 1809 (2000a).

Garcia, J. A., and J. R. Fair, "A Fundamental Model for the Prediction of Distillation Sieve Tray Efficiency. 2. Model Development and Validation," *Ind. Eng. Chem. Res.*, **39**, 1818 (2000b).

Gidaspow, D., *Multiphase Flow and Fluidization: Continuum and Kinetic Theory Descriptions*, Academic Press, Inc., Boston (1994).

Jakobsen, H. A., B. H. Sannæs, S. Grevskott, and H.F. Svendsen, "Modelling of Bubble Driven Vertical Flows," *Ind. Eng. Chem. Res.*, **36**, 4052 (1997).

Jones, W. P., and B. E. Launder, "The prediction of laminarization with a two-equation model of turbulence," *Int. J. Heat Mass Transfer*, **15**, 301 (1972)

Kister, H. Z., *Distillation Operation*, McGraw-Hill, New York (1990).

Kister, H. Z., *Distillation Design*, McGraw-Hill, New York (1992).

Korchinsky, W. J., " Liquid Mixing in Distillation Trays: Simultaneous Measurement of the Diffusion Coefficient and Point Efficiency," *Trans. Inst. Chem. Engrs.*, **72**, 472 (1994).

Korchinsky, W. J., M. R. Eshani, and T. Plaka, " Sieve Plate Efficiencies: 0.6 m Diameter Column," *Trans. Inst. Chem. Engrs.*, **72**, 465 (1994).

Krishna, R., M. I. Urseanu, J. M. van Baten, and J. Ellenberger, "Rise velocity of a swarm of large gas bubbles in liquids," *Chem. Eng. Sci.*, **54**, 171 (1999a).

Krishna, R., and J. M. van Baten, "Modelling Sieve Tray Hydraulics using Computational Fluid Dynamics," *Chem. Eng. Res. Des., Trans. Inst. Chem. Engrs.*, **81**, 27 (2003).

Krishna, R., J. M. van Baten, J. Ellenberger, A. P. Higler, and R. Taylor, "CFD simulations of sieve tray hydrodynamics," *Chem. Eng. Res. Des., Trans. Inst. Chem. Engrs.*, **77**, 639 (1999b).

Krishnamurthy, R, and R. Taylor, "A Nonequilibrium Stage Model of Multicomponent Separation Processes. Part I: Model Description and Method of Solution," *AIChE Journal,* **31**, 449 (1985a)

Krishnamurthy, R, and R. Taylor, "A Nonequilibrium Stage Model of Multicomponent Separation Processes. Part II: Comparison with Experiment," *AIChE Journal,* **31**, 456 (1985b)

Lakehal, D., "On the modelling of multiphase turbulent flows for environmental and hydrodynamic applications," *Int. J. Multiphase Flow,* **28**, 823 (2002)

Launder, B. E., and B. I. Sharma, "Application of the energy-dissipation model of turbulence to the calculation of flow near a spinning disc," *Lett. Heat Mass Transfer*, **1**, 131 (1974)

Leonard, B. P., "A stable and accurate convection modelling procedure based on quadratic upwind interpolation," *Comput. Meth. Appl. Mech. Engrg*, **19**, 59 (1979)

Libby, Paul A., *Introduction to Turbulence*, Taylor & Francis, Washington (1998).

Liu, C. J., X. G. Yuan, K. T. Yu, and X. J. Zhu, "A fluid-dynamic model for flow pattern on a distillation tray," *Chem. Eng. Sci.*, **55**, 2287 (1999).

Lockett, M. J., *Distillation Tray Fundamentals*, Cambridge University Press, Cambridge (1986).

Lockett, M. J, and A. Safekourdi, "The effect of liquid flow pattern on distillation plate efficiency," *Chemical Engineering. Journal*, **11**, 117 (1976).

Mehta, B., K. T. Chuang, and K. Nandakumar, "Model for Liquid Phase Flow on Sieve Trays," *Chem. Eng. Res. Des., Trans. Inst. Chem. Engrs.*, **76**, 843 (1998).

Nutter, D. E., "The MVG™ Tray at FRI," *Chem. Eng. Res. Des.*, **77**, 493 (1999).

Patankar, Suhas V., *Numerical Heat Transfer and Fluid Flow*, McGraw-Hill, New York (1980)

Plaka, T., M. R. Eshani, and W. J. Korchinsky, "Determination of Individual Phase Transfer Units, N_G and N_L, for a 0.6 m Diameter Distillation Column Sieve Plate: Methylcyclohexane-Toluene System," *Chem. Eng. Res. Des.*, **67**, 316 (1989).

Pope, S. B., *Turbulent Flows*, Cambridge University Press, Cambridge (2000).

Porter, K. E., M. J. Lockett, and C. T. Lim, "The Effect of Liquid Channelling on Distillation Plate Efficiency," *Trans. Inst. Chem. Engrs.*, **50**, 91 (1972).

Prado, M., and J. R. Fair, "Fundamental Model for the Prediction of Sieve Tray Efficiency," *Ind. Eng. Chem. Res.*, **29**, 1031 (1990).

Reynolds, O., "On the Dynamical Theory of Incompressible Viscous Fluids and the Determination of the Criterion," *Philosophical Transactions of the Royal Society of London, Series A*, **186**, 123 (1895)

Salas, M. D., J. N. Hefner, and L. Sakell, *Modelling Complex Turbulent Flows*, Kluwer Academic Publishers, Boston (1999).

Sohlo, J. J., and S. Kinnunen, "Dispersion and Flow Phenomena on a Sieve Plate," *Trans. Inst. Chem. Engrs.*, **55**, 71 (1977).

Solari, R. B., and R. L. Bell, "Fluid Flow Patterns and Velocity Distribution on Commercial-Scale Sieve Trays," *AIChE Journal*, **32**, 640 (1986).

Solari, R. B., and R. L. Bell, "The Effect of Transverse Eddy Dispersion on Distillation Efficiency," AIChE 84th National Meeting, Atlanta, Paper 46f (1978).

Solari, R. B., E. Saez, I. D'apollo, and A. Bellet, "Velocity Distribution and Liquid Flow Patterns on Industrial Sieve Trays," *Chem. Eng. Commun.*, **13**, 369 (1982).

Spalding, D. B., "A Novel Finite-Difference Formulation for Differential Expressions Involving both First and Second Derivatives," *Int. J. Num. Methods Eng.*, **4**, 551 (1972).

Stichlmair, J., *Bodenkolonne*, Verlag Chemie (1978)

Stichlmair, J., and J. R. Fair, *Distillation: Principles and Practices*, Wiley, New York (1998)

Tannehill, J. C., D. A. Anderson, and R. H. Pletcher, *Computaional Fluid Mechanics and Heat Transfer*, Taylor & Francis, 2nd ed., Washington DC (1997)

Taylor, R., and R. Krishna, *Multicomponent Mass Transfer*, Wiley, New York (1993).

Thompson, J. F., Z. U. A. Warsi, and C. W. Mastin, *Numerical Grid Generation: Foundations and Applications*, Elsevier, New York (1985).

Thompson, J. F., B. K. Soni, and N. P. Weatherill, *Handbook of Grid Generation*, CRC Press (1998).

Van Baten, J. M., and R. Krishna, "Modelling Sieve Tray Hydraulics using Computational Fluid Dynamics," *Chemical Engineering Journal*, **77**, 143 (2000).

Van Doormal, J. P., and G. D. Raithby, "Enhancements of the SIMPLE method for predicting incompressible fluid flows," *Numer. Heat Transfer*, **7**, 147 (1984).

Van Leer, B., "Towards the Ultimate Conservation Difference Scheme, V: A second order sequel to Godunov's method," *J. Comput. Phys.*, **32**, 101 (1979)

Van Wachem, B. J. M., and A. E. Almstedt, "Methods for multiphase computational fluid dynamics," *Chemical Engineering Journal*, **96**, 81 (2003).

Versteeg, H. K., and W. Malalasekera, *An Introduction to Computational Fluid Dynamics: The Finite Volume Method*, Longman, Harlow (1995)

Weiler, D. W., W. V. Delniki, and B. L. England, "Flow Hydraulics of Large Diameter Trays," *Chem. Eng. Progress*, **69**, 67 (1973).

Wesseling, P., *Principles of Computational Fluid Dynamics*, Springer, Berlin (2001)

Wilcox, David C., *Turbulence Modelling for CFD*, DCW Industries, Inc., La Cañada, California (1993).

Yanagi, T., and B. D. Scott, "Effect of Liquid Mixing on Sieve Trays," *Chem. Eng. Progress*, **69**, 75 (1973).

Zuiderweg, F. J., "Sieve Trays- A View on the State of the Art," *Chem. Eng. Sci.*, **37**, 1441 (1982).

Zuiderweg, F. J., "Influence of two-phase flow regimes on the separation performance of sieve trays," *International Chemical Engineering*, **26**, 1 (1986).

Appendix A CFX-4.4 Code

CFX-4.4 Sample Command File

```
/*************************************************************************/
/*     3-D 2-PHASE FLOW SIEVE TRAY SIMULATION                            */
/*************************************************************************/
>>CFX4
  >>SET LIMITS
    LARGE
    TOTAL REAL WORK SPACE 90000000
    MAXIMUM NUMBER OF BLOCKS 100
    MAXIMUM NUMBER OF PATCHES 1000
    MAXIMUM NUMBER OF INTER BLOCK BOUNDARIES 200
  >>OPTIONS
    THREE DIMENSIONS
    BODY FITTED GRID
    TURBULENT FLOW
    INCOMPRESSIBLE FLOW
    BUOYANT FLOW
    TRANSIENT FLOW
    USER SCALAR EQUATIONS 7
    NUMBER OF PHASES 2
  >>USER FORTRAN
    USRBCS
    USRIPT
    USRTPL
    USRTRN
  >>VARIABLE NAMES
    U VELOCITY 'U VELOCITY'
    V VELOCITY 'V VELOCITY'
    W VELOCITY 'W VELOCITY'
    PRESSURE 'PRESSURE'
    VOLUME FRACTION 'VOLUME FRACTION'
    DENSITY 'DENSITY'
    VISCOSITY 'VISCOSITY'
    USER SCALAR1 'YPLUS'
    USER SCALAR2 'U VELOCITY LOG RES'
    USER SCALAR3 'V VELOCITY LOG RES'
    USER SCALAR4 'W VELOCITY LOG RES'
    USER SCALAR5 'PRESSURE LOG RES'
    USER SCALAR6 'K LOG RES'
    USER SCALAR7 'EPSILON LOG RES'
>>MODEL TOPOLOGY
  >>INPUT TOPOLOGY
    READ GEOMETRY FILE
>>MODEL DATA
  >>AMBIENT VARIABLES
    PHASE NAME 'PHASE1'
    VOLUME FRACTION 9.3000E-01
  >>AMBIENT VARIABLES
    PHASE NAME 'PHASE2'
    VOLUME FRACTION 7.0000E-02
```

```
>>DIFFERENCING SCHEME
  ALL EQUATIONS 'HYBRID'
  VOLUME FRACTION 'MIN-MOD'
  K 'HYBRID'
  EPSILON 'HYBRID'
  YPLUS 'NO MATRIX'
  U VELOCITY LOG RES 'NO MATRIX'
  V VELOCITY LOG RES 'NO MATRIX'
  W VELOCITY LOG RES 'NO MATRIX'
  PRESSURE LOG RES 'NO MATRIX'
  K LOG RES 'NO MATRIX'
  EPSILON LOG RES 'NO MATRIX'
>>SET INITIAL GUESS
  >>INPUT FROM FILE
    READ DUMP FILE
    LAST DATA GROUP
>>TITLE
  PROBLEM TITLE '3D TWO-PHASE SIEVE TRAY DISTILLATION SIMULATION'
>>WALL TREATMENTS
  PHASE NAME 'PHASE1'
  NO SLIP
>>WALL TREATMENTS
  PHASE NAME 'PHASE2'
  SLIP
>>PHYSICAL PROPERTIES
  >>BUOYANCY PARAMETERS
    GRAVITY VECTOR 0.000000E+00 -9.800000E+00 0.000000E+00
    BUOYANCY REFERENCE DENSITY 4.9995E+02
  >>FLUID PARAMETERS
    PHASE NAME 'PHASE1'
    VISCOSITY 1.0170E-03
    DENSITY 9.9780E+02
  >>FLUID PARAMETERS
    PHASE NAME 'PHASE2'
    VISCOSITY 1.8120E-05
    DENSITY 1.2080E+00
  >>MULTIPHASE PARAMETERS
    >>PHASE DESCRIPTION
      PHASE NAME 'PHASE1'
      LIQUID
      CONTINUOUS
      MINIMUM VOLUME FRACTION 1.0000E-08
      MODIFY EMPTY CELL VELOCITY 1.0000E-08
    >>PHASE DESCRIPTION
      PHASE NAME 'PHASE2'
      GAS
      DISPERSE
      MEAN DIAMETER 1.0000E-02
      MINIMUM VOLUME FRACTION 1.0000E-08
      MODIFY EMPTY CELL VELOCITY 1.0000E-08
    >>MULTIPHASE MODELS
      >>MOMENTUM
        INTER PHASE TRANSFER
        SINCE
        IPSAC
      >>TURBULENCE
        INTER PHASE TRANSFER
```

```
        SINCE
      >>INTER PHASE TRANSFER MODELS
        >>MOMENTUM
          FIRST PHASE NAME 'PHASE1'
          SECOND PHASE NAME 'PHASE2'
          SURFACE TENSION COEFFICIENT 7.2000E-02
          >>PARTICLE DRAG MODEL
            FLOW REGIME 'AUTOMATIC'
    >>TRANSIENT PARAMETERS
      >>FIXED TIME STEPPING
      '   TIME STEPS 5000*1.0E-03
        BACKWARD DIFFERENCE
    >>TURBULENCE PARAMETERS
      >>TURBULENCE MODEL
        PHASE NAME 'PHASE1'
        TURBULENCE MODEL 'K-EPSILON'
      >>TURBULENCE MODEL
        PHASE NAME 'PHASE2'
        TURBULENCE MODEL 'LAMINAR'
>>SOLVER DATA
  >>PROGRAM CONTROL
    MAXIMUM NUMBER OF ITERATIONS 30
    MASS SOURCE TOLERANCE 5.0E-03
  >>DEFERRED CORRECTION
    K START 0
    K END 15
    EPSILON START 31
    EPSILON END 31
  >>EQUATION SOLVERS
    PRESSURE 'BLOCK STONE'
    K 'BLOCK STONE'
    EPSILON 'BLOCK STONE'
  >>REDUCTION FACTORS
    ALL PHASES
    U VELOCITY 1.5000E-01
    V VELOCITY 1.2500E-01
    W VELOCITY 1.5000E-01
    PRESSURE 1.0000E-03
    VOLUME FRACTION 1.0000E-02
    K 1.0000E-01
    EPSILON 1.0000E-01
  >>SWEEPS INFORMATION
    >>MAXIMUM NUMBER
      ALL PHASES
      U VELOCITY 10
      V VELOCITY 10
      W VELOCITY 10
      PRESSURE 70
      VOLUME FRACTION 30
      K 15
      EPSILON 15
  >>UNDER RELAXATION FACTORS
    ALL PHASES
    U VELOCITY 1.500E-01
    V VELOCITY 1.250E-01
    W VELOCITY 1.500E-01
    PRESSURE 5.000E-01
```

```
    VOLUME FRACTION 4.0000E-01
    VISCOSITY 4.0000E-01
    K 3.0000E-01
    EPSILON 3.0000E-01
>>CREATE GRID
  >>INPUT GRID
    READ GRID FILE
>>MODEL BOUNDARY CONDITIONS
  >>INLET BOUNDARIES
    PHASE NAME 'PHASE1'
    PATCH NAME 'LIQUID INLET'
    TURBULENCE INTENSITY 3.7000E-02
    DISSIPATION LENGTH SCALE 7.3100E-02
  >>MASS FLOW BOUNDARIES
    >>FLUX
      PHASE NAME 'PHASE1'
      FLUXES 1.000000E+00 0.000000E+00
      FRACTIONAL MASS FLOW SPECIFIED
    >>FLUX
      PHASE NAME 'PHASE2'
      FLUXES 0.000000E+00 1.000000E+00
      FRACTIONAL MASS FLOW SPECIFIED
>>OUTPUT OPTIONS
  >>DUMP FILE OPTIONS
    ALL PHASES
    TIME INTERVAL 1.0E+00
    INITIAL GUESS
    FINAL SOLUTION
    ALL VARIABLES
    ALL USER SCALARS
  >>LINE GRAPH DATA
    EACH TIME STEP
    FILE NAME 'LOG_RESIDUALS'
    XYZ 0.765 0.055 0.055
    U VELOCITY LOG RES
    V VELOCITY LOG RES
    W VELOCITY LOG RES
    PRESSURE LOG RES
    K LOG RES
    EPSILON LOG RES
>>STOP
```

```
      SUBROUTINE USRBCS(VARBCS,VARAMB,A,B,C,ACND,BCND,CCND,IWGVEL,
     +                  NDVWAL,FLOUT,NLABEL,NSTART,NEND,NCST,NCEN,U,V,W,
     +                   P,VFRAC,DEN,VIS,TE,ED,RS,T,H,RF,SCAL,XP,YP,ZP,
     +                   VOL,AREA,VPOR,ARPOR,WFACT,IPT,IBLK,IPVERT,
     +                   IPNODN,IPFACN,IPNODF,IPNODB,IPFACB,WORK,IWORK,
     +                   CWORK)
C
C***********************************************************************
C
C  USER ROUTINE TO SET REALS AT BOUNDARIES.
C
C   >>> IMPORTANT                                                    <<<
C   >>>                                                             <<<
C   >>> USERS MAY ONLY ADD OR ALTER PARTS OF THE SUBROUTINE WITHIN  <<<
C   >>> THE DESIGNATED USER AREAS                                   <<<
C
C***********************************************************************
C
C  THIS SUBROUTINE IS CALLED BY THE FOLLOWING SUBROUTINE
C    CUSR  SRLIST
C
C***********************************************************************
C   CREATED
C      30/11/88 ADB
C   MODIFIED
C      08/09/90 ADB  RESTRUCTURED FOR USER-FRIENDLINESS.
C      10/08/91 IRH  FURTHER RESTRUCTURING ADD ACND BCND CCND
C      22/09/91 IRH  CHANGE ICALL TO IUCALL + ADD /SPARM/
C      10/03/92 PHA  UPDATE CALLED BY COMMENT, ADD RF ARGUMENT,
C                    CHANGE LAST DIMENSION OF RS TO 6 AND IVERS TO 2
C      03/06/92 PHA  ADD PRECISION FLAG AND CHANGE IVERS TO 3
C      30/06/92 NSW  INCLUDE FLAG FOR CALLING BY ITERATION
C                    INSERT EXTRA COMMENTS
C      03/08/92 NSW  MODIFY DIMENSION STATEMENTS FOR VAX
C      21/12/92 CSH  INCREASE IVERS TO 4
C      02/08/93 NSW  INCORRECT AND MISLEADING COMMENT REMOVED
C      05/11/93 NSW  INDICATE USE OF FLOUT IN MULTIPHASE FLOWS
C      23/11/93 CSH  EXPLICITLY DIMENSION IPVERT ETC.
C      01/02/94 NSW  SET VARIABLE POINTERS IN WALL EXAMPLE.
C                    CHANGE FLOW3D TO CFDS-FLOW3D.
C                    MODIFY MULTIPHASE MASS FLOW BOUNDARY TREATMENT.
C      03/03/94 FHW  CORRECTION OF SPELLING MISTAKE
C      02/07/94 BAS  SLIDING GRIDS - ADD NEW ARGUMENT IWGVEL
C                    TO ALLOW VARIANTS OF TRANSIENT-GRID WALL BC
C                    CHANGE VERSION NUMBER TO 5
C      09/08/94 NSW  CORRECT SPELLING
C                    MOVE 'IF(IUSED.EQ.0) RETURN' OUT OF USER AREA
C      19/12/94 NSW  CHANGE FOR CFX-F3D
C      02/02/95 NSW  CHANGE COMMON /IMFBMP/
C      02/06/97 NSW  MAKE EXAMPLE MORE LOGICAL
C      02/07/97 NSW  UPDATE FOR CFX-4
```

```
C      08/09/98 NSW  CORRECT SIZE OF WALL ARRAY IN COMMENT
C      22/05/00 NSW  INITIALISE IUBCSF
C
C*************************************************************************
C
C   SUBROUTINE ARGUMENTS
C
C     VARBCS - REAL BOUNDARY CONDITIONS
C     VARAMB - AMBIENT VALUE OF VARIABLES
C     A      - COEFFICIENT IN WALL BOUNDARY CONDITION
C     B      - COEFFICIENT IN WALL BOUNDARY CONDITION
C     C      - COEFFICIENT IN WALL BOUNDARY CONDITION
C     ACND   - COEFFICIENT IN CONDUCTING WALL BOUNDARY CONDITION
C     BCND   - COEFFICIENT IN CONDUCTING WALL BOUNDARY CONDITION
C     CCND   - COEFFICIENT IN CONDUCTING WALL BOUNDARY CONDITION
C     IWGVEL - USAGE OF INPUT VELOCITIES(0 = AS IS,1 = ADD GRID MOTION)
C     NDVWAL - FIRST DIMENSION OF ARRAY IWGVEL
C     FLOUT  - MASS FLOW/FRACTIONAL MASS FLOW
C     NLABEL - NUMBER OF DISTINCT OUTLETS
C     NSTART - ARRAY POINTER
C     NEND   - ARRAY POINTER
C     NCST   - ARRAY POINTER
C     NCEN   - ARRAY POINTER
C     U      - U COMPONENT OF VELOCITY
C     V      - V COMPONENT OF VELOCITY
C     W      - W COMPONENT OF VELOCITY
C     P      - PRESSURE
C     VFRAC  - VOLUME FRACTION
C     DEN    - DENSITY OF FLUID
C     VIS    - VISCOSITY OF FLUID
C     TE     - TURBULENT KINETIC ENERGY
C     ED     - EPSILON
C     RS     - REYNOLD STRESSES
C     T      - TEMPERATURE
C     H      - ENTHALPY
C     RF     - REYNOLD FLUXES
C     SCAL   - SCALARS (THE FIRST 'NCONC' OF THESE ARE MASS FRACTIONS)
C     XP     - X COORDINATES OF CELL CENTRES
C     YP     - Y COORDINATES OF CELL CENTRES
C     ZP     - Z COORDINATES OF CELL CENTRES
C     VOL    - VOLUME OF CELLS
C     AREA   - AREA OF CELLS
C     VPOR   - POROUS VOLUME
C     ARPOR  - POROUS AREA
C     WFACT  - WEIGHT FACTORS
C
C     IPT    - 1D POINTER ARRAY
C     IBLK   - BLOCK SIZE INFORMATION
C     IPVERT - POINTER FROM CELL CENTERS TO 8 NEIGHBOURING VERTICES
C     IPNODN - POINTER FROM CELL CENTERS TO 6 NEIGHBOURING CELLS
C     IPFACN - POINTER FROM CELL CENTERS TO 6 NEIGHBOURING FACES
C     IPNODF - POINTER FROM CELL FACES TO 2 NEIGHBOURING CELL CENTERS
C     IPNODB - POINTER FROM BOUNDARY CENTERS TO CELL CENTERS
C     IPFACB - POINTER TO NODES FROM BOUNDARY FACES
C
C     WORK   - REAL WORKSPACE ARRAY
C     IWORK  - INTEGER WORKSPACE ARRAY
```

```
C     CWORK  - CHARACTER WORKSPACE ARRAY
C
C   SUBROUTINE ARGUMENTS PRECEDED WITH A '*' ARE ARGUMENTS THAT MUST
C   BE SET  BY THE USER IN THIS ROUTINE.
C
C   NOTE THAT OTHER DATA MAY BE OBTAINED FROM CFX-4 USING THE
C   ROUTINE GETADD; FOR FURTHER DETAILS SEE THE VERSION 4
C   USER MANUAL.
C
C*************************************************************************
      DOUBLE PRECISION VARBCS
      DOUBLE PRECISION VARAMB
      DOUBLE PRECISION A
      DOUBLE PRECISION B
      DOUBLE PRECISION C
      DOUBLE PRECISION ACND
      DOUBLE PRECISION BCND
      DOUBLE PRECISION CCND
      DOUBLE PRECISION FLOUT
      DOUBLE PRECISION U
      DOUBLE PRECISION V
      DOUBLE PRECISION W
      DOUBLE PRECISION P
      DOUBLE PRECISION VFRAC
      DOUBLE PRECISION DEN
      DOUBLE PRECISION VIS
      DOUBLE PRECISION TE
      DOUBLE PRECISION ED
      DOUBLE PRECISION RS
      DOUBLE PRECISION T
      DOUBLE PRECISION H
      DOUBLE PRECISION RF
      DOUBLE PRECISION SCAL
      DOUBLE PRECISION XP
      DOUBLE PRECISION YP
      DOUBLE PRECISION ZP
      DOUBLE PRECISION VOL
      DOUBLE PRECISION AREA
      DOUBLE PRECISION VPOR
      DOUBLE PRECISION ARPOR
      DOUBLE PRECISION WFACT
      DOUBLE PRECISION WORK
      DOUBLE PRECISION SMALL
      DOUBLE PRECISION SORMAX
      DOUBLE PRECISION TIME
      DOUBLE PRECISION DT
      DOUBLE PRECISION DTINVF
      DOUBLE PRECISION TPARM
      LOGICAL LDEN,LVIS,LTURB,LTEMP,LBUOY,LSCAL,LCOMP,LRECT,LCYN,LAXIS,
     +        LPOROS,LTRANS
C
      CHARACTER*(*) CWORK
C
C+++++++++++++++++ USER AREA 1 ++++++++++++++++++++++++++++++++++++++
C---- AREA FOR USERS EXPLICITLY DECLARED VARIABLES
C
      DOUBLE PRECISION usrPI,usrDC,usrAC,usrxL,usrLw,usrTH,usrAS1,
```

```
     +                usrAT,usrAS2,usrAB,usrNH,usrFs,usrdnV,usrVs,
     +                usrhap,usrACL,usrQL,usrmbv,usritv,V2VVEL,
     +                V2VMIN,V2VMAX
C
C
C+++++++++++++++++ END OF USER AREA 1 +++++++++++++++++++++++++++++++
C
      COMMON /ALL/NBLOCK,NCELL,NBDRY,NNODE,NFACE,NVERT,NDIM,
     +      /ALLWRK/NRWS,NIWS,NCWS,IWRFRE,IWIFRE,IWCFRE,/ADDIMS/NPHASE,
     +       NSCAL,NVAR,NPROP,NDVAR,NDPROP,NDXNN,NDGEOM,NDCOEF,NILIST,
     +       NRLIST,NTOPOL,/BCSOUT/IFLOUT,/CHKUSR/IVERS,IUCALL,IUSED,
     +       /DEVICE/NREAD,NWRITE,NRDISK,NWDISK,/IDUM/ILEN,JLEN,
     +       /IMFBMP/IMFBMP,JMFBMP,/LOGIC/LDEN,LVIS,LTURB,LTEMP,LBUOY,
     +       LSCAL,LCOMP,LRECT,LCYN,LAXIS,LPOROS,LTRANS,/MLTGRD/MLEVEL,
     +       NLEVEL,ILEVEL,/SGLDBL/IFLGPR,ICHKPR,/SPARM/SMALL,SORMAX,
     +       NITER,INDPRI,MAXIT,NODREF,NODMON,/TRANSI/NSTEP,KSTEP,MF,
     +       INCORE,/TRANSR/TIME,DT,DTINVF,TPARM,/UBCSFL/IUBCSF
C
C+++++++++++++++++ USER AREA 2 +++++++++++++++++++++++++++++++++++++
C---- AREA FOR USERS TO DECLARE THEIR OWN COMMON BLOCKS
C     THESE SHOULD START WITH THE CHARACTERS 'UC' TO ENSURE
C     NO CONFLICT WITH NON-USER COMMON BLOCKS
C
C+++++++++++++++++ END OF USER AREA 2 +++++++++++++++++++++++++++++++
C
      DIMENSION VARBCS(NVAR,NPHASE,NCELL+1:NNODE),VARAMB(NVAR,NPHASE),
     +          A(4+NSCAL,NPHASE,NSTART:*),B(4+NSCAL,NPHASE,NSTART:*),
     +          C(4+NSCAL,NPHASE,NSTART:*),FLOUT(*),ACND(NCST:*),
     +          BCND(NCST:*),CCND(NCST:*),IWGVEL(NDVWAL,NPHASE)
C
      DIMENSION U(NNODE,NPHASE),V(NNODE,NPHASE),W(NNODE,NPHASE),
     +          P(NNODE,NPHASE),VFRAC(NNODE,NPHASE),DEN(NNODE,NPHASE),
     +          VIS(NNODE,NPHASE),TE(NNODE,NPHASE),ED(NNODE,NPHASE),
     +          RS(NNODE,NPHASE,6),T(NNODE,NPHASE),H(NNODE,NPHASE),
     +          RF(NNODE,NPHASE,4),SCAL(NNODE,NPHASE,NSCAL)
C
      DIMENSION XP(NNODE),YP(NNODE),ZP(NNODE),VOL(NCELL),AREA(NFACE,3),
     +          VPOR(NCELL),ARPOR(NFACE,3),WFACT(NFACE),IPT(*),
     +          IBLK(5,NBLOCK),IPVERT(NCELL,8),IPNODN(NCELL,6),
     +          IPFACN(NCELL,6),IPNODF(NFACE,4),IPNODB(NBDRY,4),
     +          IPFACB(NBDRY),IWORK(*),WORK(*),CWORK(*)
C
C+++++++++++++++++ USER AREA 3 +++++++++++++++++++++++++++++++++++++
C---- AREA FOR USERS TO DIMENSION THEIR ARRAYS
C
C---- AREA FOR USERS TO DEFINE DATA STATEMENTS
C
C+++++++++++++++++ END OF USER AREA 3 +++++++++++++++++++++++++++++++
C
C---- STATEMENT FUNCTION FOR ADDRESSING
      IP(I,J,K) = IPT((K-1)*ILEN*JLEN+ (J-1)*ILEN+I)
C
C----VERSION NUMBER OF USER ROUTINE AND PRECISION FLAG
C
      IVERS = 5
      ICHKPR = 2
C
```

```
C+++++++++++++++++ USER AREA 4 ++++++++++++++++++++++++++++++++++++++++
C---- TO USE THIS USER ROUTINE FIRST SET IUSED=1
C     AND SET IUBCSF FLAG:
C     BOUNDARY CONDITIONS NOT CHANGING                          IUBCSF=0
C     BOUNDARY CONDITIONS CHANGING WITH ITERATION               IUBCSF=1
C     BOUNDARY CONDITIONS CHANGING WITH TIME                    IUBCSF=2
C     BOUNDARY CONDITIONS CHANGING WITH TIME AND ITERATION      IUBCSF=3
C
      IUSED = 1
      IUBCSF = 0
C
C+++++++++++++++++ END OF USER AREA 4 +++++++++++++++++++++++++++++++++
C
      IF (IUSED.EQ.0) RETURN
C
C---- FRONTEND CHECKING OF USER ROUTINE
      IF (IUCALL.EQ.0) RETURN
C
C+++++++++++++++++ USER AREA 5 ++++++++++++++++++++++++++++++++++++++++
C
C
C SET INDIVIDUAL CELL INLET VELOCITIES
C
C
      usrPI = 3.1415926535898
      usrDC = 1.220000
      usrAC = (usrPI/4.0)*usrDC**2.0
      usrxL = 0.762000
      usrLw = SQRT(usrDC**2.0-usrxL**2.0)
      usrTH = 4.0*(180.0/usrPI)*DACOS(usrxL/usrDC)
      usrAS1 = (usrTH/360.0)*usrPI*(usrDC/2.0)**2.0
      usrAT = 4.0*(0.5*(0.5*usrxL*0.5*usrLw))
      usrAS2 = usrAC-usrAS1
      usrAB = usrAS2+usrAT
      usrNH = 45.000
      usrFS = 0.462
      usrdnV = 1.208
      usrVs = usrFs/SQRT(usrdnV)
C
C  SET VAPOR INLET VELOCITY UNIFORMLY
C
C FIND THE VARIABLE NUMBERS FOR THE QUANTITIES VELOCITY, VOLUME
C FRACTION WHICH HAVE TO BE SET AT THE INLET. (IU,IV,IW,IVF)
C
      CALL GETVAR('USRBCS','U     ',IU)
      CALL GETVAR('USRBCS','V     ',IV)
      CALL GETVAR('USRBCS','W     ',IW)
      CALL GETVAR('USRBCS','VFRAC ',IVF)
C
C      CALL GETVAR('USRBCS','ED    ',IE)
C      CALL GETVAR('USRBCS','TE    ',IK)
C
C   USE IPALL TO FIND ADDRESSES OF BOUNDARY NODES ON PATCH PRESS1
C
      CALL IPALL('VAPOR INLET','INLET','PATCH','CENTRES',
     +           IPT,NPT,CWORK,IWORK)
C
```

```
C  LOOP OVER ALL PHASES
C
      V2VMIN = 9999999.9
      V2VMAX = -999999.9
C
      DO 10 IPHASE=1,NPHASE
C
C  LOOP OVER ALL BOUNDARY NODES AND SET U, V, W and VFRAC
C
       DO 100 I=1,NPT
C
C  USE ARRAY IPT TO GET ADDRESS
C
        INODE = IPT(I)
        IBDRY = INODE - NCELL
        IFACE = IPFACB(IBDRY)
        IF (IPHASE .EQ. 2) THEN
          VARBCS(IU,IPHASE,INODE) = 0.D0
          V2VVEL = usrAB*usrVs/(2.0*usrNH)*
     +             1.0/(DABS(AREA(IFACE,2)))
          VARBCS(IV,IPHASE,INODE) = V2VVEL
          V2VMIN = MIN(V2VMIN,V2VVEL)
          V2VMAX = MAX(V2VMAX,V2VVEL)
          VARBCS(IW,IPHASE,INODE) = 0.D0
          VARBCS(IVF,IPHASE,INODE) = 1.D0
        ELSE IF (IPHASE .EQ. 1) THEN
          VARBCS(IU,IPHASE,INODE) = 0.D0
          VARBCS(IV,IPHASE,INODE) = 0.D0
          VARBCS(IW,IPHASE,INODE) = 0.D0
          VARBCS(IVF,IPHASE,INODE) = 0.D0
        END IF
 100   CONTINUE
C
 10   CONTINUE
C
C
C SET PARABOLIC LIQUID INLET VELOCITY PROFILE
C
C
      usrhap = 0.038
      usrACL = usrhap*usrLw
      usrQL = 0.0178
      usrmbv = 1.50*usrQL/usrACL
      usritv = 1.0
C
C   USE IPALL TO FIND ADDRESSES OF BOUNDARY NODES ON PATCH PRESS1
C
      CALL IPALL('LIQUID INLET','INLET','PATCH','CENTRES',
     +           IPT,NPT,CWORK,IWORK)
C
C  LOOP OVER ALL PHASES
C
      DO 110 IPHASE=1,NPHASE
C
C  LOOP OVER ALL BOUNDARY NODES AND SET U, V, W and VFRAC
C
       DO 120 I=1,NPT
```

```
C
C  USE ARRAY IPT TO GET ADDRESS
C
        INODE = IPT(I)
        IF (IPHASE .EQ. 1) THEN
          VARBCS(IU,IPHASE,INODE) = usrmbv*
     +              (usritv-(2.0*ZP(INODE)/usrLw)**2.0)
          VARBCS(IV,IPHASE,INODE) = 0.D0
          VARBCS(IW,IPHASE,INODE) = 0.D0
          VARBCS(IVF,IPHASE,INODE) = 1.D0
        ELSE IF (IPHASE .EQ. 2) THEN
          VARBCS(IU,IPHASE,INODE) = 0.D0
          VARBCS(IV,IPHASE,INODE) = 0.D0
          VARBCS(IW,IPHASE,INODE) = 0.D0
          VARBCS(IVF,IPHASE,INODE) = 0.D0
        END IF
 120   CONTINUE
C
 110   CONTINUE
C
C PRINT SOME RESULTS FOR CHECKING
C
       ISEQF = 0
C
      IF (KSTEP .LE. 1)  THEN
        CALL FILCON('USRBCS','boundary.dat','OPEN','FORMATTED','NEW',
     +              IDATBC,ISEQF,IOST,IERR)
        WRITE(IDATBC,410) usrVs*usrAB/(2.0*usrNH),usrmbv,V2VMIN,V2VMAX
      END IF
C
 410  FORMAT(4F16.10)
C
C+++++++++++++++++ USER AREA 7 ++++++++++++++++++++++++++++++++++++++
C
C----- DEFINE FLOW AT OUTLETS (MASS FLOW BOUNDARIES)
C
C+++++++++++++++++ END OF USER AREA 7 +++++++++++++++++++++++++++++++
C
      RETURN
C
      END



      SUBROUTINE USRIPT(IEQN,CNAME,CALIAS,PHI,CAB,DPDIAM,U,V,W,P,VFRAC,
     +                  DEN,VIS,TE,ED,RS,T,H,RF,SCAL,XP,YP,ZP,VOL,AREA,
     +                  VPOR,ARPOR,WFACT,IPT,IBLK,IPVERT,IPNODN,IPFACN,
     +                  IPNODF,IPNODB,IPFACB,WORK,IWORK,CWORK)
C
C**********************************************************************
C
C   THIS SUBROUTINE COMPUTES INTERPHASE EXCHANGE COEFFICIENTS.
C
C   >>> IMPORTANT                                                  <<<
C   >>>                                                            <<<
C   >>> USERS MAY ONLY ADD OR ALTER PARTS OF THE SUBROUTINE WITHIN  <<<
```

```
C   >>> THE DESIGNATED USER AREAS                                        <<<
C
C*************************************************************************
C
C   THIS SUBROUTINE IS CALLED BY THE FOLLOWING SUBROUTINE
C      CUSR  CALCAB
C
C*************************************************************************
C   CREATED
C     01/05/91 ADB  BASED ON ROUTINE IPMOMT FROM MPHASE 1.3.
C   MODIFIED
C     05/08/91 IRH  NEW STRUCTURE
C     05/09/91 IRH  CHANGE ICALL TO IUCALL
C     27/11/91 ADB  REMOVE COMMENTING OUT OF EXAMPLES
C     28/01/92 PHA  UPDATE CALLED BY COMMENT, ADD RF ARGUMENT,
C                   CHANGE LAST DIMENSION OF RS TO 6 AND IVERS TO 2
C     03/06/92 PHA  ADD PRECISION FLAG AND CHANGE IVERS TO 3
C     01/07/92 NSW  VAX CORRECTIONS
C     23/11/93 CSH  EXPLICITLY DIMENSION IPVERT ETC.
C     03/02/94 PHA  CHANGE FLOW3D TO CFDS-FLOW3D
C     23/03/94 FHW  EXAMPLES COMMENTED OUT
C     09/08/94 NSW  CORRECT SPELLING
C                   MOVE 'IF(IUSED.EQ.0) RETURN' OUT OF USER AREA
C                   INCLUDE COMMENT ON SLIP VELOCITY
C     19/12/94 NSW  CHANGE FOR CFX-F3D
C     02/07/97 NSW  UPDATE FOR CFX-4
C     29/07/99 SML  ADD DPDIAM TO ARGUMENT LIST,
C                   CHANGE EXAMPLES TO GALILEAN INVARIANT FORMULA
C                   CORRECT CALLING ROUTINE LIST
C     10/08/99 NSW  REMOVE REDUNDANT COMMENT AND CORRECT ALIGNMENT
C
C*************************************************************************
C
C   SUBROUTINE ARGUMENTS
C
C      IEQN   - EQUATION NUMBER
C      CNAME  - EQUATION NAME
C      CALIAS - ALIAS OF EQUATION NAME
C      PHI    - VARIABLE CNAME
C   *  CAB    - INTERPHASE EXCHANGE COEFFICIENT
C      DPDIAM - PARTICLE DIAMETER
C      U      - U COMPONENT OF VELOCITY
C      V      - V COMPONENT OF VELOCITY
C      W      - W COMPONENT OF VELOCITY
C      P      - PRESSURE
C      VFRAC  - VOLUME FRACTION
C      DEN    - DENSITY OF FLUID
C      VIS    - VISCOSITY OF FLUID
C      TE     - TURBULENT KINETIC ENERGY
C      ED     - EPSILON
C      RS     - REYNOLD STRESSES
C      T      - TEMPERATURE
C      H      - ENTHALPY
C      RF     - REYNOLD FLUXES
C      SCAL   - SCALARS (THE FIRST 'NCONC' OF THESE ARE MASS FRACTIONS)
C      XP     - X COORDINATES OF CELL CENTRES
C      YP     - Y COORDINATES OF CELL CENTRES
```

```
C     ZP     - Z COORDINATES OF CELL CENTRES
C     VOL    - VOLUME OF CELLS
C     AREA   - AREA OF CELLS
C     VPOR   - POROUS VOLUME
C     ARPOR  - POROUS AREA
C     WFACT  - WEIGHT FACTORS
C
C     IPT    - 1D POINTER ARRAY
C     IBLK   - BLOCK SIZE INFORMATION
C     IPVERT - POINTER FROM CELL CENTERS TO 8 NEIGHBOURING VERTICES
C     IPNODN - POINTER FROM CELL CENTERS TO 6 NEIGHBOURING CELLS
C     IPFACN - POINTER FROM CELL CENTERS TO 6 NEIGHBOURING FACES
C     IPNODF - POINTER FROM CELL FACES TO 2 NEIGHBOURING CELL CENTERS
C     IPNODB - POINTER FROM BOUNDARY CENTERS TO CELL CENTERS
C     IPFACB - POINTER FROM BOUNDARY CENTERS TO BOUNDARY FACESS
C
C     WORK   - REAL WORKSPACE ARRAY
C     IWORK  - INTEGER WORKSPACE ARRAY
C     CWORK  - CHARACTER WORKSPACE ARRAY
C
C   SUBROUTINE ARGUMENTS PRECEDED WITH A '*' ARE ARGUMENTS THAT MUST
C   BE SET  BY THE USER IN THIS ROUTINE.
C
C   NOTE THAT OTHER DATA MAY BE OBTAINED FROM CFX-4 USING THE
C   ROUTINE GETADD, FOR FURTHER DETAILS SEE THE VERSION 4
C   USER MANUAL.
C
C*************************************************************************
C
      DOUBLE PRECISION PHI
      DOUBLE PRECISION CAB
      DOUBLE PRECISION DPDIAM
      DOUBLE PRECISION U
      DOUBLE PRECISION V
      DOUBLE PRECISION W
      DOUBLE PRECISION P
      DOUBLE PRECISION VFRAC
      DOUBLE PRECISION DEN
      DOUBLE PRECISION VIS
      DOUBLE PRECISION TE
      DOUBLE PRECISION ED
      DOUBLE PRECISION RS
      DOUBLE PRECISION T
      DOUBLE PRECISION H
      DOUBLE PRECISION RF
      DOUBLE PRECISION SCAL
      DOUBLE PRECISION XP
      DOUBLE PRECISION YP
      DOUBLE PRECISION ZP
      DOUBLE PRECISION VOL
      DOUBLE PRECISION AREA
      DOUBLE PRECISION VPOR
      DOUBLE PRECISION ARPOR
      DOUBLE PRECISION WFACT
      DOUBLE PRECISION WORK
      LOGICAL LDEN,LVIS,LTURB,LTEMP,LBUOY,LSCAL,LCOMP,LRECT,LCYN,LAXIS,
     +        LPOROS,LTRANS
```

```
C
      CHARACTER*(*) CWORK
      CHARACTER CNAME*6,CALIAS*24
C
C+++++++++++++++++ USER AREA 1 +++++++++++++++++++++++++++++++++++++
C---- AREA FOR USERS EXPLICITLY DECLARED VARIABLES
C
        DOUBLE PRECISION  uG,rhoL,rhoG,BLVF,BGVF,TU,TV,TW,
     .+                   SLIP,USK1,USK2,usrFs,usDRGX,usDRGY,
     +                    usDRGZ
C
C+++++++++++++++++ END OF USER AREA 1 +++++++++++++++++++++++++++++++
C
      COMMON /ALL/NBLOCK,NCELL,NBDRY,NNODE,NFACE,NVERT,NDIM,
     +       /ADDIMS/NPHASE,NSCAL,NVAR,NPROP,NDVAR,NDPROP,NDXNN,NDGEOM,
     +       NDCOEF,NILIST,NRLIST,NTOPOL,/ADDMPH/NAB,NCOMPT,NCOMB,
     +       NSCUSR,/CHKUSR/IVERS,IUCALL,IUSED,/DEVICE/NREAD,NWRITE,
     +      NRDISK,NWDISK,/IDUM/ILEN,JLEN,/LOGIC/LDEN,LVIS,LTURB,LTEMP,
     +       LBUOY,LSCAL,LCOMP,LRECT,LCYN,LAXIS,LPOROS,LTRANS,
     +       /MLTGRD/MLEVEL,NLEVEL,ILEVEL,/SGLDBL/IFLGPR,ICHKPR
C
C+++++++++++++++++ USER AREA 2 +++++++++++++++++++++++++++++++++++++
C---- AREA FOR USERS TO DECLARE THEIR OWN COMMON BLOCKS
C     THESE SHOULD START WITH THE CHARACTERS 'UC' TO ENSURE
C     NO CONFLICT WITH NON-USER COMMON BLOCKS
C

C+++++++++++++++++ END OF USER AREA 2 +++++++++++++++++++++++++++++++
C
      DIMENSION PHI(NNODE),CAB(NCELL,*),DPDIAM(NCELL,NPHASE),
     +          U(NNODE,NPHASE),V(NNODE,NPHASE),W(NNODE,NPHASE),
     +          P(NNODE,NPHASE),VFRAC(NNODE,NPHASE),DEN(NNODE,NPHASE),
     +          VIS(NNODE,NPHASE),TE(NNODE,NPHASE),ED(NNODE,NPHASE),
     +          RS(NNODE,NPHASE,6),T(NNODE,NPHASE),H(NNODE,NPHASE),
     +          RF(NNODE,NPHASE,4),SCAL(NNODE,NPHASE,NSCAL)
      DIMENSION XP(NNODE),YP(NNODE),ZP(NNODE),VOL(NCELL),AREA(NFACE,3),
     +          VPOR(NCELL),ARPOR(NFACE,3),WFACT(NFACE),IPT(*),
     +          IBLK(5,NBLOCK),IPVERT(NCELL,8),IPNODN(NCELL,6),
     +          IPFACN(NCELL,6),IPNODF(NFACE,4),IPNODB(NBDRY,4),
     +          IPFACB(NBDRY),IWORK(*),WORK(*),CWORK(*)
C
C+++++++++++++++++ USER AREA 3 +++++++++++++++++++++++++++++++++++++
C---- AREA FOR USERS TO DIMENSION THEIR ARRAYS
C
C---- AREA FOR USERS TO DEFINE DATA STATEMENTS
C
C+++++++++++++++++ END OF USER AREA 3 +++++++++++++++++++++++++++++++
C
C---- STATEMENT FUNCTION FOR ADDRESSING
      IP(I,J,K) = IPT((K-1)*ILEN*JLEN+ (J-1)*ILEN+I)
C
C----VERSION NUMBER OF USER ROUTINE AND PRECISION FLAG
C
      IVERS = 4
      ICHKPR = 2
C
C+++++++++++++++++ USER AREA 4 +++++++++++++++++++++++++++++++++++++
```

```
C---- TO USE THIS USER ROUTINE FIRST SET IUSED=1
C
      IUSED = 1
C
C+++++++++++++++++ END OF USER AREA 4 +++++++++++++++++++++++++++++++
C
      IF (IUSED.EQ.0) RETURN
C
C---- FRONTEND CHECKING OF USER ROUTINE
      IF (IUCALL.EQ.0) RETURN
C
C+++++++++++++++++ USER AREA 5 +++++++++++++++++++++++++++++++++++++
C
C----USE IPALL TO FIND 1D ADDRESSES OF ALL CELL CENTRES
C
       CALL IPALL  ('*','*','BLOCK','CENTRES',IPT,NPT,CWORK,IWORK)
C
       rhoL = 997.8
       rhoG = 1.208
       usrFs = 0.462
       uG = usrFs/SQRT(rhoG)
C
C
C
       IA  = 1
       IB  = 2
       IAB = 1
C
C
C--------------Calculate Bennett et al. Volume Fraction
C
           BLVF=EXP(-12.55*(uG*SQRT(rhoG/(rhoL-rhoG)))**0.91)
C
           BGVF=1.0-BLVF
C
C------- CALCULATE SLIP VELOCITY
C
       IF (CNAME(1:2).EQ.'U ' .OR. CNAME(1:2).EQ.'V '
     +    .OR. CNAME(1:2).EQ.'W ') THEN
C
C----LOOP OVER ALL INTERIOR CELLS
C
          DO 110 I = 1,NPT
C
C----USE ARRAY IPT TO GET ADDRESS
C
             INODE=IPT(I)
             TU=(U(INODE,IA)-U(INODE,IB))
             TV=(V(INODE,IA)-V(INODE,IB))
             TW=(W(INODE,IA)-W(INODE,IB))
             SLIP=SQRT(TU**2.0 + TV**2.0 +TW**2.0)
C------------ CALCULATE CAB
             USK1=((uG/BGVF)**2.0)*BLVF
             USK2=(9.80655/USK1)*SLIP
             CAB(INODE,IAB)=VFRAC(INODE,IB)*VFRAC(INODE,IA)
     +           *( DEN(INODE,IA)-DEN(INODE,IB) )*USK2*VOL(INODE)
C
```

```
  110     CONTINUE
C
        ENDIF
C
C+++++++++++++++++ END OF USER AREA 5 +++++++++++++++++++++++++++++++++
C
      RETURN
C
      END


      SUBROUTINE USRTPL(NBLOCK,NPATCH,NGLUE,NDBLK,CBLK,INFPCH,CPATCH,
     +                  INFGLU,IBBPP,IBBPD,WORK,IWORK,CWORK)
C
C*****************************************************************************
C
C   USER SUBROUTINE TO ADD GRID TOPOLOGY
C   NAMELY BLOCKS, PATCHES AND INTER-BLOCK BOUNDARIES.
C
C   >>> IMPORTANT                                                          <<<
C   >>>                                                                   <<<
C   >>> USERS MAY ONLY ADD OR ALTER PARTS OF THE SUBROUTINE WITHIN        <<<
C   >>> THE DESIGNATED USER AREAS                                         <<<
C
C*****************************************************************************
C
C   CALLED BY SUBROUTINE
C     CUSR  GETTPL
C
C*****************************************************************************
C   CREATED
C      28/08/91  IRH
C   MODIFIED
C      05/09/91  IRH  CHANGE ICALL TO IUCALL
C      29/11/91  PHA  UPDATE CALLED BY COMMENT
C      03/06/92  PHA  ADD PRECISION FLAG AND CHANGE IVERS TO 2
C      10/02/93  NSW  CORRECT CALL TO GLUE IN EXAMPLE
C      24/01/94  IRH  CORRECT COMMENTS
C      22/08/94  NSW  MOVE 'IF(IUSED.EQ.0) RETURN' OUT OF USER AREA
C      29/09/94  BAS  NEW ARGUMENT LIST + EXAMPLE FOR UNMATCHED GRIDS
C      26/03/96  NSW  CORRECT COMMENTS ABOUT USRPCH
C
C*****************************************************************************
C
C   SUBROUTINE ARGUMENTS
C
C     NBLOCK - TOTAL NUMBER OF BLOCKS
C     NPATCH - TOTAL NUMBER OF PATCHES
C     NGLUE  - TOTAL NUMBER OF GLUING OPERATIONS
C     NDBLK  - BLOCK SIZE ARRAY
C     CBLK   - BLOCK NAME
C     INFPCH - INTEGER PATCH DATA
C     CPATCH - PATCH NAME
C     INFGLU - INTEGER GLUE DATA
C     IBBPP  - UNMATCHED-GRID GLUE DATA (PATCH POINTERS)
```

```
C      IBBPD  - UNMATCHED-GRID GLUE DATA (PATCH DATA)
C
C      WORK   - REAL WORKSPACE ARRAY
C      IWORK  - INTEGER WORKSPACE ARRAY
C      CWORK  - CHARACTER WORKSPACE ARRAY
C
C   SUBROUTINE ARGUMENTS PRECEDED WITH A '*' ARE ARGUMENTS THAT MUST
C   BE SET  BY THE USER IN THIS ROUTINE.
C
C*********************************************************************
C
      DOUBLE PRECISION WORK
      DOUBLE PRECISION XCYCLE
      CHARACTER*(*) CBLK,CPATCH,CWORK
C
C+++++++++++++++++ USER AREA 1 ++++++++++++++++++++++++++++++++++++++++
C---- AREA FOR USERS EXPLICITLY DECLARED VARIABLES
C
C     THESE FOLLOWING CHARACTER VARIABLES ARE USED

      CHARACTER*32  CNAME,CBLOCK
      CHARACTER*6  CTYPE

C
C+++++++++++++++++ END OF USER AREA 1 +++++++++++++++++++++++++++++++++
C
      COMMON /ALLWRK/NRWS,NIWS,NCWS,IWRFRE,IWIFRE,IWCFRE,
     +       /BBCYCL/XCYCLE(3),/BBDIM/MBB,MBBPAT,MBBNOD,MBBNBR,MBB1,
     +       MBB2,MBB3,MBB4,MBB5,MBB6,MBB7,MBB8,MBB9,MBB10,MBB11,MBB12,
     +       MBB13,MBB14,MBB15,MBB16,MBB17,MBB18,MBB19,MBB20,
     +       /CHKUSR/IVERS,IUCALL,IUSED,/DEVICE/NREAD,NWRITE,NRDISK,
     +       NWDISK,/LIMTPL/NBLMAX,NPCMAX,NGLMAX,/SGLDBL/IFLGPR,ICHKPR
C
C+++++++++++++++++ USER AREA 2 ++++++++++++++++++++++++++++++++++++++++
C---- AREA FOR USERS TO DECLARE THEIR OWN COMMON BLOCKS
C     THESE SHOULD START WITH THE CHARACTERS 'UC' TO ENSURE
C     NO CONFLICT WITH NON-USER COMMON BLOCKS
C
C+++++++++++++++++ END OF USER AREA 2 +++++++++++++++++++++++++++++++++
C
C
      DIMENSION WORK(NRWS),IWORK(NIWS),CWORK(NCWS),NDBLK(3,*),CBLK(*),
     +          INFPCH(9,*),CPATCH(2,*),INFGLU(5,*),IBBPP(MBB1,MBB2),
     +          IBBPD(MBB3)
C
C+++++++++++++++++ USER AREA 3 ++++++++++++++++++++++++++++++++++++++++
C---- AREA FOR USERS TO DIMENSION THEIR ARRAYS
C
C     THESE FOLLOWING ARRAYS ARE USED IN THE USER EXAMPLES
C     PARAMETER (MNAME1=10,MNAME2=10)
C     DIMENSION CLIST1(MNAME1), CLIST2(MNAME2)
C
C---- AREA FOR USERS TO DEFINE DATA STATEMENTS
C
C+++++++++++++++++ END OF USER AREA 3 +++++++++++++++++++++++++++++++++
C
C----VERSION NUMBER OF USER ROUTINE AND PRECISION FLAG
```

```
C
      IVERS = 3
      ICHKPR = 2
C
C+++++++++++++++++ USER AREA 4 ++++++++++++++++++++++++++++++++++++++++++
C---- TO USE THIS USER ROUTINE FIRST SET IUSED=1
C
      IUSED = 1
C
C+++++++++++++++++ END OF USER AREA 4 ++++++++++++++++++++++++++++++++++
C
      IF (IUSED.EQ.0) RETURN
C
C---- FRONTEND CHECKING OF USER ROUTINE
      IF (IUCALL.EQ.0) RETURN
C
C+++++++++++++++++ USER AREA 5 ++++++++++++++++++++++++++++++++++++++++++
C
C+++++++++++++++++ USER AREA 6 ++++++++++++++++++++++++++++++++++++++++++
C
C
C  CREATING VAPOR INLET HOLES IN BLOCK 1
       LABEL  = 2
       CTYPE  = 'INLET '
       CNAME  = 'VAPOR INLET'
       CBLOCK = 'BLOCK-NUMBER-1'
C
C-- UTILITY ROUTINE ADDS INLET HOLE PATCHES TO LOW J FACE
C
       DO 50 K=1,5
C
        IF (MOD(K,2).EQ.0) THEN
C
C FIRST ROW OF HOLES
C
         DO 150 I=1,7
           CALL PATCH (CTYPE,CNAME,CBLOCK
     +             ,LABEL,4*I+2,4*I+2,1,1,4*K-2,4*K-2,5,
     +             NBLOCK,NPATCH,NDBLK,CBLK,INFPCH,CPATCH)
 150     CONTINUE
C
        ELSE
C
C SECOND ROW OF HOLES
C
         DO 250 I=1,8
           CALL PATCH (CTYPE,CNAME,CBLOCK
     +             ,LABEL,4*I,4*I,1,1,4*K-2,4*K-2,5,
     +             NBLOCK,NPATCH,NDBLK,CBLK,INFPCH,CPATCH)
 250     CONTINUE
C
        END IF
C
 50   CONTINUE
C
C
C  CREATING VAPOR INLET HOLES IN BLOCK 2
```

```
      LABEL  = 2
      CTYPE  = 'INLET '
      CNAME  = 'VAPOR INLET'
      CBLOCK = 'BLOCK-NUMBER-2'
C
C-- UTILITY ROUTINE ADDS INLET HOLE PATCHES TO LOW J FACE
C
      DO 350 K=1,1
C
       IF (MOD(K,2).EQ.0) THEN
C
C FIRST ROW OF HOLES
C
        DO 450 I=1,8
          CALL PATCH (CTYPE,CNAME,CBLOCK
     +            ,LABEL,4*I,4*I,1,1,4*K-2,4*K-2,5,
     +            NBLOCK,NPATCH,NDBLK,CBLK,INFPCH,CPATCH)
 450    CONTINUE
C
       ELSE
C
C SECOND ROW OF HOLES
C
        DO 550 I=1,7
          CALL PATCH (CTYPE,CNAME,CBLOCK
     +            ,LABEL,4*I+2,4*I+2,1,1,4*K-2,4*K-2,5,
     +            NBLOCK,NPATCH,NDBLK,CBLK,INFPCH,CPATCH)
 550    CONTINUE
C
       END IF
C
 350   CONTINUE
C
C  CREATING VAPOR OUTLET HOLES IN BLOCK 1
       LABEL  = 2
       CTYPE  = 'OUTLET'
       CNAME  = 'VAPOR OUTLET'
       CBLOCK = 'BLOCK-NUMBER-1'
C
C-- UTILITY ROUTINE ADDS OUTLET HOLE PATCHES TO HIGH J FACE
C
      DO 650 K=1,5
C
       IF (MOD(K,2).EQ.0) THEN
C
C FIRST ROW OF HOLES
C
        DO 750 I=1,7
          CALL PATCH (CTYPE,CNAME,CBLOCK
     +            ,LABEL,4*I+2,4*I+2,24,24,4*K-2,4*K-2,2,
     +            NBLOCK,NPATCH,NDBLK,CBLK,INFPCH,CPATCH)
 750    CONTINUE
       ELSE
C
C SECOND ROW OF HOLES
C
        DO 850 I=1,8
```

```
          CALL PATCH (CTYPE,CNAME,CBLOCK
     +             ,LABEL,4*I,4*I,24,24,4*K-2,4*K-2,2,
     +             NBLOCK,NPATCH,NDBLK,CBLK,INFPCH,CPATCH)
 850     CONTINUE
C
        END IF
C
 650    CONTINUE
C
C
C
C  CREATING VAPOR OUTLET HOLES IN BLOCK 2
        LABEL  = 2
        CTYPE  = 'OUTLET'
        CNAME  = 'VAPOR OUTLET'
        CBLOCK = 'BLOCK-NUMBER-2'
C
C-- UTILITY ROUTINE ADDS OUTLET HOLE PATCHES TO HIGH J FACE
C
       DO 950 K=1,1
C
        IF (MOD(K,2).EQ.0) THEN
C
C FIRST ROW OF HOLES
C
         DO 1050 I=1,8
           CALL PATCH (CTYPE,CNAME,CBLOCK
     +             ,LABEL,4*I,4*I,24,24,4*K-2,4*K-2,2,
     +             NBLOCK,NPATCH,NDBLK,CBLK,INFPCH,CPATCH)
 1050     CONTINUE
         ELSE
C
C SECOND ROW OF HOLES
C
         DO 1150 I=1,7
           CALL PATCH (CTYPE,CNAME,CBLOCK
     +             ,LABEL,4*I+2,4*I+2,24,24,4*K-2,4*K-2,2,
     +             NBLOCK,NPATCH,NDBLK,CBLK,INFPCH,CPATCH)
 1150     CONTINUE
C
        END IF
C
 950    CONTINUE
C
C+++++++++++++++++ END OF USER AREA 6 +++++++++++++++++++++++++++++++++++
C
C
        RETURN
C
        END


        SUBROUTINE USRTRN(U,V,W,P,VFRAC,DEN,VIS,TE,ED,RS,T,H,RF,SCAL,XP,
     +                    YP,ZP,VOL,AREA,VPOR,ARPOR,WFACT,CONV,IPT,IBLK,
     +                    IPVERT,IPNODN,IPFACN,IPNODF,IPNODB,IPFACB,WORK,
     +                    IWORK,CWORK)
```

```
C
C*********************************************************************
C
C   USER SUBROUTINE TO ALLOW USERS TO MODIFY OR MONITOR THE SOLUTION AT
C   THE END OF EACH TIME STEP
C   THIS SUBROUTINE IS CALLED BEFORE THE START OF THE RUN AS WELL AS AT
C   THE END OF EACH TIME STEP
C
C   >>> IMPORTANT                                                    <<<
C   >>>                                                             <<<
C   >>> USERS MAY ONLY ADD OR ALTER PARTS OF THE SUBROUTINE WITHIN  <<<
C   >>> THE DESIGNATED USER AREAS                                   <<<
C
C*********************************************************************
C
C   THIS SUBROUTINE IS CALLED BY THE FOLLOWING SUBROUTINES
C      CUSR  TRNMOD
C
C*********************************************************************
*
C   CREATED
C      27/04/90  ADB
C   MODIFIED
C      05/08/91  IRH  NEW STRUCTURE
C      01/10/91  DSC  REDUCE COMMENT LINE GOING OVER COLUMN 72.
C      29/11/91  PHA  UPDATE CALLED BY COMMENT, ADD RF ARGUMENT,
C                     CHANGE LAST DIMENSION OF RS TO 6 AND IVERS TO 2
C      05/06/92  PHA  ADD PRECISION FLAG AND CHANGE IVERS TO 3
C      03/07/92  DSC  CORRECT COMMON MLTGRD.
C      23/11/93  CSH  EXPLICITLY DIMENSION IPVERT ETC.
C      03/02/94  PHA  CHANGE FLOW3D TO CFDS-FLOW3D
C      22/08/94  NSW  MOVE 'IF(IUSED.EQ.0) RETURN' OUT OF USER AREA
C      19/12/94  NSW  CHANGE FOR CFX-F3D
C      02/07/97  NSW  UPDATE FOR CFX-4
C      02/07/99  NSW  INCLUDE NEW EXAMPLE FOR CALCULATING FLUX OF A
C                     SCALAR AT A PRESSURE BOUNDARY
C
C*********************************************************************
*
C
C   SUBROUTINE ARGUMENTS
C
C     U       - U COMPONENT OF VELOCITY
C     V       - V COMPONENT OF VELOCITY
C     W       - W COMPONENT OF VELOCITY
C     P       - PRESSURE
C     VFRAC   - VOLUME FRACTION
C     DEN     - DENSITY OF FLUID
C     VIS     - VISCOSITY OF FLUID
C     TE      - TURBULENT KINETIC ENERGY
C     ED      - EPSILON
C     RS      - REYNOLD STRESSES
C     T       - TEMPERATURE
C     H       - ENTHALPY
C     RF      - REYNOLD FLUXES
C     SCAL    - SCALARS (THE FIRST 'NCONC' OF THESE ARE MASS FRACTIONS)
C     XP      - X COORDINATES OF CELL CENTRES
```

```
C      YP      - Y COORDINATES OF CELL CENTRES
C      ZP      - Z COORDINATES OF CELL CENTRES
C      VOL     - VOLUME OF CELLS
C      AREA    - AREA OF CELLS
C      VPOR    - POROUS VOLUME
C      ARPOR   - POROUS AREA
C      WFACT   - WEIGHT FACTORS
C      CONV    - CONVECTION COEFFICIENTS
C
C      IPT     - 1D POINTER ARRAY
C      IBLK    - BLOCK SIZE INFORMATION
C      IPVERT - POINTER FROM CELL CENTERS TO 8 NEIGHBOURING VERTICES
C      IPNODN - POINTER FROM CELL CENTERS TO 6 NEIGHBOURING CELLS
C      IPFACN - POINTER FROM CELL CENTERS TO 6 NEIGHBOURING FACES
C      IPNODF - POINTER FROM CELL FACES TO 2 NEIGHBOURING CELL CENTERS
C      IPNODB - POINTER FROM BOUNDARY CENTERS TO CELL CENTERS
C      IPFACB - POINTER FROM BOUNDARY CENTERS TO BOUNDARY FACESS
C
C      WORK    - REAL WORKSPACE ARRAY
C      IWORK   - INTEGER WORKSPACE ARRAY
C      CWORK   - CHARACTER WORKSPACE ARRAY
C
C    SUBROUTINE ARGUMENTS PRECEDED WITH A '*' ARE ARGUMENTS THAT MUST
C    BE SET  BY THE USER IN THIS ROUTINE.
C
C    NOTE THAT OTHER DATA MAY BE OBTAINED FROM CFX-4 USING THE
C    ROUTINE GETADD, FOR FURTHER DETAILS SEE THE VERSION 4
C    USER MANUAL.
C
C*************************************************************************
C
C
      DOUBLE PRECISION U
      DOUBLE PRECISION V
      DOUBLE PRECISION W
      DOUBLE PRECISION P
      DOUBLE PRECISION VFRAC
      DOUBLE PRECISION DEN
      DOUBLE PRECISION VIS
      DOUBLE PRECISION TE
      DOUBLE PRECISION ED
      DOUBLE PRECISION RS
      DOUBLE PRECISION T
      DOUBLE PRECISION H
      DOUBLE PRECISION RF
      DOUBLE PRECISION SCAL
      DOUBLE PRECISION XP
      DOUBLE PRECISION YP
      DOUBLE PRECISION ZP
      DOUBLE PRECISION VOL
      DOUBLE PRECISION AREA
      DOUBLE PRECISION VPOR
      DOUBLE PRECISION ARPOR
      DOUBLE PRECISION WFACT
      DOUBLE PRECISION CONV
      DOUBLE PRECISION WORK
      DOUBLE PRECISION SMALL
```

```
      DOUBLE PRECISION SORMAX
      DOUBLE PRECISION DTUSR
      DOUBLE PRECISION TIME
      DOUBLE PRECISION DT
      DOUBLE PRECISION DTINVF
      DOUBLE PRECISION TPARM
      DOUBLE PRECISION SGNWL
      LOGICAL LDEN,LVIS,LTURB,LTEMP,LBUOY,LSCAL,LCOMP,LRECT,LCYN,LAXIS,
     +        LPOROS,LTRANS
C
      CHARACTER*(*) CWORK
C
C+++++++++++++++++ USER AREA 1 ++++++++++++++++++++++++++++++++++++++++
C---- AREA FOR USERS EXPLICITLY DECLARED VARIABLES
C
      DOUBLE PRECISION  SUMHld,SUMTVL,SUMFHT,SUMTAR,SUMALP,SUMAVT
      DOUBLE PRECISION  AVGHLD,CLRLHT,AVGFHT,ALPCAL,ALPEST,usrTs
C
C+++++++++++++++++ END OF USER AREA 1 ++++++++++++++++++++++++++++++++++
C
      COMMON /ALL/NBLOCK,NCELL,NBDRY,NNODE,NFACE,NVERT,NDIM,
     +
/ALLWRK/NRWS,NIWS,NCWS,IWRFRE,IWIFRE,IWCFRE,/ADDIMS/NPHASE,
     +        NSCAL,NVAR,NPROP,NDVAR,NDPROP,NDXNN,NDGEOM,NDCOEF,NILIST,
     +        NRLIST,NTOPOL,/CHKUSR/IVERS,IUCALL,IUSED,/CONC/NCONC,
     +        /DEVICE/NREAD,NWRITE,NRDISK,NWDISK,/IDUM/ILEN,JLEN,
     +        /LOGIC/LDEN,LVIS,LTURB,LTEMP,LBUOY,LSCAL,LCOMP,LRECT,LCYN,
     +        LAXIS,LPOROS,LTRANS,/MLTGRD/MLEVEL,NLEVEL,ILEVEL,
     +        /SGLDBL/IFLGPR,ICHKPR,/SPARM/SMALL,SORMAX,NITER,INDPRI,
     +        MAXIT,NODREF,NODMON,/TIMUSR/DTUSR,/TRANSI/NSTEP,KSTEP,MF,
     +        INCORE,/TRANSR/TIME,DT,DTINVF,TPARM
C
C+++++++++++++++++ USER AREA 2 ++++++++++++++++++++++++++++++++++++++++
C---- AREA FOR USERS TO DECLARE THEIR OWN COMMON BLOCKS
C     THESE SHOULD START WITH THE CHARACTERS 'UC' TO ENSURE
C     NO CONFLICT WITH NON-USER COMMON BLOCKS
C
C+++++++++++++++++ END OF USER AREA 2 ++++++++++++++++++++++++++++++++++
C
      DIMENSION U(NNODE,NPHASE),V(NNODE,NPHASE),W(NNODE,NPHASE),
     +          P(NNODE,NPHASE),VFRAC(NNODE,NPHASE),DEN(NNODE,NPHASE),
     +          VIS(NNODE,NPHASE),TE(NNODE,NPHASE),ED(NNODE,NPHASE),
     +          RS(NNODE,NPHASE,6),T(NNODE,NPHASE),H(NNODE,NPHASE),
     +          RF(NNODE,NPHASE,4),SCAL(NNODE,NPHASE,NSCAL)
      DIMENSION XP(NNODE),YP(NNODE),ZP(NNODE),VOL(NCELL),AREA(NFACE,3),
     +          VPOR(NCELL),ARPOR(NFACE,3),WFACT(NFACE),
     +          CONV(NFACE,NPHASE),IPT(*),IBLK(5,NBLOCK),
     +          IPVERT(NCELL,8),IPNODN(NCELL,6),IPFACN(NCELL,6),
     +          IPNODF(NFACE,4),IPNODB(NBDRY,4),IPFACB(NBDRY),IWORK(*),
     +          WORK(*),CWORK(*)
      DIMENSION SGNWL(6)
C
C+++++++++++++++++ USER AREA 3 ++++++++++++++++++++++++++++++++++++++++
C---- AREA FOR USERS TO DIMENSION THEIR ARRAYS
C
C---- AREA FOR USERS TO DEFINE DATA STATEMENTS
C
```

```
C
      DATA usrTs  /0.61/
C
C
C+++++++++++++++++ END OF USER AREA 3 +++++++++++++++++++++++++++++++++
C
      DATA SGNWL/1.0D0,1.0D0,1.0D0,-1.0D0,-1.0D0,-1.0D0/
C
C---- STATEMENT FUNCTION FOR ADDRESSING
      IP(I,J,K) = IPT((K-1)*ILEN*JLEN+ (J-1)*ILEN+I)
C
C----VERSION NUMBER OF USER ROUTINE AND PRECISION FLAG
C
      IVERS = 3
      ICHKPR = 2
C
C+++++++++++++++++ USER AREA 4 +++++++++++++++++++++++++++++++++++++++++
C---- TO USE THIS USER ROUTINE FIRST SET IUSED=1
C
      IUSED = 1
C
C+++++++++++++++++ END OF USER AREA 4 +++++++++++++++++++++++++++++++++
C
      IF (IUSED.EQ.0) RETURN
C
C---- FRONTEND CHECKING OF USER ROUTINE
      IF (IUCALL.EQ.0) RETURN
C
C+++++++++++++++++ USER AREA 5 +++++++++++++++++++++++++++++++++++++++++
C
C----- AVERAGE LIQUID HOLDUP,ALHOLD, AS FUNCTION OF TIME
C
       SUMHld = 0.0
       SUMTVL = 0.0
       SUMFHT = 0.0
       SUMTAR = 0.0
       SUMALP = 0.0
       SUMAVT = 0.0
C
       CALL IPALL('*','*','BLOCK','CENTERS',IPT,NPT,CWORK,IWORK)
C
      DO 400 I=1,NPT
         INODE=IPT(I)
         IF (XP(INODE) .LT. 0.762) THEN
           SUMHld = SUMHld+VFRAC(INODE,1)*VOL(INODE)
           SUMTVL = SUMTVL+VOL(INODE)
           IF ( (ABS(VFRAC(INODE,1)-0.10) .LE. 1.0E-02) .AND.
     +          (YP(INODE) .GE. 0.038) ) THEN
               IFACE = IPFACN(INODE,2)
               SUMFHT = SUMFHT + YP(INODE)*ABS(AREA(IFACE,2))
               SUMTAR = SUMTAR+ABS(AREA(IFACE,2))
           END IF
           IF (VFRAC(INODE,1) .GE. 0.10) THEN
               SUMALP = SUMALP+VFRAC(INODE,1)*VOL(INODE)
               SUMAVT = SUMAVT+VOL(INODE)
           END IF
         END IF
```

```
 400  CONTINUE
C
        AVGHLD = SUMHld/(SUMTVL+1.0D-12)
        CLRLHT = AVGHLD*usrTs
        AVGFHT = SUMFHT/(SUMTAR+1.0D-12)
        ALPCAL = CLRLHT/(AVGFHT+1.0D-12)
        ALPEST = SUMALP/(SUMAVT+1.0D-12)
C
C
       ISEQF = 0
C
       IF (KSTEP .LE. 1) THEN
        CALL FILCON('USRTRN','PHIhL.dat','OPEN','FORMATTED','NEW',
     +              IDAThL,ISEQF,IOST,IERR)
       ELSE
C
       CALL FILCON('USRTRN','PHIhL.dat','GET','FORMATTED','OLD',
     +              IDAThL,ISEQF,IOST,IERR)
       END IF
C
       WRITE(IDAThL,410) TIME,AVGHLD,CLRLHT,AVGFHT,ALPCAL,ALPEST
 410  FORMAT(F12.6,5F14.8)
C
C
C
C+++++++++++++++++ END OF USER AREA 5 +++++++++++++++++++++++++++++++++++
C
      RETURN
C
      END
```

Appendix B CFX-5.4 Code

CFX-5.4 Sample Command File

```
+--------------------------------------------------------------------+
|                          Command File                              |
+--------------------------------------------------------------------+

LIBRARY :
 MATERIAL : air
  Option = Pure Substance
  PROPERTIES :
   Option = General Fluid
   Density = 1.208 [kg m^-3]
   Dynamic Viscosity = 1.812E-5 [kg m^-1 s^-1]
   Specific Heat Capacity = 1.E3 [J kg^-1 K^-1]
   Thermal Conductivity = 2.428E-2 [W m^-1 K^-1]
   Thermal Expansivity = 3.67E-3 [K^-1]
  END
 END
 MATERIAL : water
  Option = Pure Substance
  PROPERTIES :
   Option = General Fluid
   Density = 9.98E2 [kg m^-3]
   Dynamic Viscosity = 1.017E-3 [kg m^-1 s^-1]
   Specific Heat Capacity = 4.19E3 [J kg^-1 K^-1]
   Thermal Conductivity = 5.91E-1 [W m^-1 K^-1]
   Thermal Expansivity = 2.1E-4 [K^-1]
  END
 END
 CEL :
  EXPRESSIONS :
   DC = 1.22 [ m ]
   xleng = 0.76200002 [ m ]
   Ts = 0.61000001 [ m ]
   hw = 0.050000001 [ m ]
   hap = 0.037999999 [ m ]
   dh = 0.025 [ m ]
   Lw = sqrt(DC^2.0-xleng^2.0)
   NHoles = 45.0 [ ]
   AH = 3.14159265359/4.0*2.0*NHoles*dh^2.0
   AT = 3.14159265358979/4.0*DC^2.0
   thetaW = (180.0/3.14159265358979)*acos(xleng/DC)
   AT1 = 0.5*(xleng/2.0*Lw/2.0)
   AS2 = (180.0-2.0*thetaW)/360.0*3.14159265358979*(DC/2.0)^2.0
   AB = 2.0*(AS2+2.0*AT1)
   AS1 = thetaW/360.0*3.14159265358979*(DC/2.0)^2.0
   ADC = 2.0*(AS1-AT1)
   ACL = hap*Lw
   Fs = 0.462 [ kg^0.5 m^-0.5 s^-1 ]
```

```
    QL = 0.0178 [ m^3 s^-1 ]
    Vs = Fs/sqrt(1.208[kg m^-3])
    zL = sqrt((DC/2.0)^2.0-(x-xleng/2.0)^2.0)+1.0e-10[m]
    ULmaxPar = 3.0*QL/(2.0*ACL)
    ULin = ULmaxPar*(1.0-(z/zL)^2.0)
    UWater = 0.90*ULmaxPar*(1.0-(z/zL)^2.0)
    VAirin = Vs*AB/AH
    eLB = 0.764431716751605 [ ]
    eGB = 1-eLB
    how = 0.09838302 [ m ]
    hL = 0.0730270719469728 [ m ]
    hF = 0.148383019502 [ ]
    hLdc = 0.276344224162347 [ m ]
    hFdc = 0.55268842 [ m ]
    rL = 0.8 [ ]
    rLdc = 0.99 [ ]
    stepx = step(1.0-x/xleng)
    stepy = step(1.0-y/hL)
    stepydc = step(y/(hLdc-Ts)-1.0)
    stepypn = step(y/Ts)
    VFL1 = (1.0-stepy)*stepx*stepypn*hL*(1.0-rL)/(Ts-hL)
    VFL2 = stepy*stepx*stepypn*rL
    VFL3 = (1.0-stepx)*stepypn*eLB*0.5*hL*(1.0-rL)/(Ts-hL)
    VFL4 = (1.0-stepx)*(1.0-stepypn)*(1.0-stepydc)*hLdc*(1.0-rLdc)/(Ts-hLdc)
    VFL5 = (1.0-stepx)*(1.0-stepypn)*stepydc*rLdc
    VFwater = VFL1+VFL2+VFL3+VFL4+VFL5
    VFair = 1.0-VFwater
    UL1 = 0.75*stepx*stepypn*UWater
    UL2 = -0.75*(1.0-stepx)*(1.0-stepypn)*stepydc*UWater
    ULinitial = UL1+UL2
    dB = 0.01 [ m ]
    KrshGrp = (eGB/Vs)^2.0/eLB
    DragCoef = (4.0/3.0)*KrshGrp*dB*g*(water.vf)*(997.8-1.208)/997.8
  END
 END
END
FLOW :
 SOLUTION UNITS :
  Mass Units = [kg]
  Length Units = [m]
  Time Units = [s]
  Temperature Units = [K]
 END
 SIMULATION TYPE :
  Option = Steady State
 END
 DOMAIN : cfdgeos1
  Coord Frame = Coord 0
  Fluids List = air, water
  DOMAIN MODELS :
   DOMAIN MOTION :
    Option = Stationary
   END
   BUOYANCY MODEL :
    Option = Buoyant
    Gravity X Component = 0.00 [m s^-2]
```

```
  Gravity Y Component = -9.8066 [m s^-2]
  Gravity Z Component = 0.00 [m s^-2]
  Buoyancy Reference Density = 5.E2 [kg m^-3]
 END
 REFERENCE PRESSURE :
  Reference Pressure = 1.0133E5 [Pa]
 END
END
FLUID MODELS :
 HEAT TRANSFER MODEL :
  Option = None
 END
END
FLUID : air
 FLUID MODELS :
  TURBULENCE MODEL :
   Option = Laminar
  END
  MORPHOLOGY :
   Option = Dispersed Fluid
   Mean Diameter = 1.E-2 [m]
  END
 END
END
FLUID : water
 FLUID MODELS :
  TURBULENCE MODEL :
   Option = k epsilon
  END
  MORPHOLOGY :
   Option = Continuous Fluid
  END
 END
END
FLUID PAIR : air | water
 Option = Particle Model
 Surface Tension Coefficient = 7.2E-2 [N m^-1]
 MOMENTUM TRANSFER :
  DRAG FORCE :
   Option = Drag Coefficient
   Drag Coefficient = DragCoef
  END
 END
END
SUBDOMAIN : subregion
 Coord Frame = Coord 0
END
BOUNDARY : Liquid Inlet
 Boundary Type = INLET
 Coord Frame = Coord 0
 BOUNDARY CONDITIONS :
  FLOW REGIME :
   Option = Subsonic
  END
  MASS AND MOMENTUM :
   Option = Fluid Velocity
```

```
  END
 END
 FLUID : air
  BOUNDARY CONDITIONS :
   VELOCITY :
    Option = Normal Speed
    Normal Speed = 0.00 [m s^-1]
   END
   VOLUME FRACTION :
    Option = Value
    Volume Fraction = 0.00
   END
  END
 END
 FLUID : water
  BOUNDARY CONDITIONS :
   VELOCITY :
    Option = Normal Speed
    Normal Speed = ULin
   END
   TURBULENCE :
    Option = Default Intensity and Autocompute Length Scale
   END
   VOLUME FRACTION :
    Option = Value
    Volume Fraction = 1.
   END
  END
 END
END
BOUNDARY : Vapor Inlet
 Boundary Type = INLET
 Coord Frame = Coord 0
 BOUNDARY CONDITIONS :
  FLOW REGIME :
   Option = Subsonic
  END
  MASS AND MOMENTUM :
   Option = Fluid Velocity
  END
 END
 FLUID : air
  BOUNDARY CONDITIONS :
   VELOCITY :
    Option = Normal Speed
    Normal Speed = VAirin
   END
   VOLUME FRACTION :
    Option = Value
    Volume Fraction = 1.
   END
  END
 END
 FLUID : water
  BOUNDARY CONDITIONS :
   VELOCITY :
```

```
      Option = Normal Speed
      Normal Speed = 0.00 [m s^-1]
    END
    TURBULENCE :
      Option = Default Intensity and Autocompute Length Scale
    END
    VOLUME FRACTION :
      Option = Value
      Volume Fraction = 0.00
    END
  END
 END
END
BOUNDARY : Liquid Outlet
 Boundary Type = OUTLET
 Coord Frame = Coord 0
 BOUNDARY CONDITIONS :
  FLOW REGIME :
    Option = Subsonic
  END
  MASS AND MOMENTUM :
    Option = Fluid Velocity
  END
 END
 FLUID : air
  BOUNDARY CONDITIONS :
   VELOCITY :
     Option = Normal Speed
     Normal Speed = 0.00 [m s^-1]
   END
  END
 END
 FLUID : water
  BOUNDARY CONDITIONS :
   VELOCITY :
     Option = Normal Speed
     Normal Speed = ULin
   END
  END
 END
END
BOUNDARY : Vapor Outlet
 Boundary Type = OUTLET
 Coord Frame = Coord 0
 BOUNDARY CONDITIONS :
  FLOW REGIME :
    Option = Subsonic
  END
  MASS AND MOMENTUM :
    Option = Fluid Velocity
  END
 END
 FLUID : air
  BOUNDARY CONDITIONS :
   VELOCITY :
     Option = Normal Speed
```

```
      Normal Speed = VAirin
     END
    END
   END
   FLUID : water
    BOUNDARY CONDITIONS :
     VELOCITY :
      Option = Normal Speed
      Normal Speed = 0.00 [m s^-1]
     END
    END
   END
  END
  BOUNDARY : Weir1
   Boundary Type = WALL
   Coord Frame = Coord 0
   BOUNDARY CONDITIONS :
    WALL ROUGHNESS :
     Option = Smooth Wall
    END
   END
   FLUID : air
    BOUNDARY CONDITIONS :
     WALL INFLUENCE ON FLOW :
      Option = Free Slip
     END
    END
   END
   FLUID : water
    BOUNDARY CONDITIONS :
     WALL INFLUENCE ON FLOW :
      Option = No Slip
     END
    END
   END
  END
  BOUNDARY : Weir2
   Boundary Type = WALL
   Coord Frame = Coord 0
   BOUNDARY CONDITIONS :
    WALL ROUGHNESS :
     Option = Smooth Wall
    END
   END
   FLUID : air
    BOUNDARY CONDITIONS :
     WALL INFLUENCE ON FLOW :
      Option = Free Slip
     END
    END
   END
   FLUID : water
    BOUNDARY CONDITIONS :
     WALL INFLUENCE ON FLOW :
      Option = No Slip
     END
```

```
  END
 END
END
BOUNDARY : Center Plane
 Boundary Type = SYMMETRY
 Coord Frame = Coord 0
END
BOUNDARY : Default
 Boundary Type = WALL
 Coord Frame = Coord 0
 FLUID : air
  BOUNDARY CONDITIONS :
   WALL INFLUENCE ON FLOW :
    Option = No Slip
   END
  END
 END
 FLUID : water
  BOUNDARY CONDITIONS :
   WALL INFLUENCE ON FLOW :
    Option = No Slip
   END
  END
 END
END
INITIALISATION :
 Option = Automatic
 Coord Frame = Coord 0
 INITIAL CONDITIONS :
  STATIC PRESSURE :
   Option = Automatic with Value
   Relative Pressure = 0.00 [Pa]
  END
 END
 FLUID : air
  INITIAL CONDITIONS :
   CARTESIAN VELOCITY COMPONENTS :
    Option = Automatic with Value
    U = 0.00 [m s^-1]
    V = Vs
    W = 0.00 [m s^-1]
   END
   VOLUME FRACTION :
    Option = Automatic with Value
    Volume Fraction = VFair
   END
  END
 END
 FLUID : water
  INITIAL CONDITIONS :
   K :
    Option = Automatic with Value
    k = 1.E-4 [m^2 s^-2]
   END
   EPSILON :
    Option = Automatic with Value
```

```
      Epsilon = 1.E-4 [m^2 s^-3]
     END
     CARTESIAN VELOCITY COMPONENTS :
      Option = Automatic with Value
      U = ULinitial
      V = -5.E-2 [m s^-1]
      W = 0.00 [m s^-1]
     END
     VOLUME FRACTION :
      Option = Automatic with Value
      Volume Fraction = VFwater
     END
    END
   END
  END
 END
 SOLVER CONTROL :
  CONVERGENCE CONTROL :
   Maximum Number of Iterations = 1000
   Timescale Control = Auto Timescale
   Maximum Timescale = 1.E-2 [s]
  END
  CONVERGENCE CRITERIA :
   Residual Type = RMS
   Residual Target = 1.E-3
  END
  ADVECTION SCHEME :
   Option = Upwind
  END
 END
END
COMMAND FILE :
 Version = 5.4
END
```